Important Notice

UNIVERSITY OF CALGARY

Depth imaging with reflection statics derived from model-based moveout

by

Dennis Kent Ellison

A THESIS

SUBMITTED TO THE FACULTY OF GRADUATE STUDIES

IN PARTIAL FULFILLMENT OF THE REQUIREMENTS FOR THE

DEGREE OF MASTER OF SCIENCE

GRADUATE PROGRAM IN GEOLOGY AND GEOPHYSICS

CALGARY, ALBERTA

OCTOBER, 2018

Abstract

In land reflection seismic data analysis, reflection static corrections are analytical solutions for resolving timing differences between measured and theoretical arrival times of seismic waves. These static corrections can make a substantial difference in the absence of detailed near-surface information and are dependent on assumptions associated with the normal moveout (NMO) theory. NMO is an analytical solution based on the assumption that the moveout in seismic data can be approximated by an hyperbola. This assumption is valid when the moveout pattern is near-hyperbolic but fails when it is not. Scenarios where moveout is not hyperbolic include situations: when the topography is not flat; when strong lateral velocity variations are present; when there are strong variations in velocity magnitudes and seismic weathering thickness across the data.

A moveout velocity field can be created using raytraced traveltimes from the velocity model instead of NMO. These traveltimes are calculated from each source and receiver and can be applied to the respective traces at the corresponding offset. This model-based moveout (MMO) correction is coupled to depth migration and allows for asymmetric non-hyperbolic moveout commonly associated with strong lateral velocity variations in the subsurface. These MMO derived static corrections can render sharper depth migrated images and lead to stronger geologic representation of the depth imaging velocity model.

Acknowledgements

I would be grossly negligent if I did not first thank my wife, Chelsea. She is truly my perfect companion She is my joy when I am sad, my center when I am deviant, and my strength when I am weak. It was her support, encouragement, and inspiration that allowed me to initially pursue and then continue my graduate work as I had commenced. I must also thank my children, Willem and Everly, for their energy, curiosity, and unfailing love to constantly remind me of the important things in life.

I must thank Rob Vestrum, Greg Cameron, and Jon Gittins. It was through their technical background and insights that have allowed me to pursue and complete this graduate work. At times I feel that the only thing that I have done is bring their ideas to paper. Marc Langlois, for his incredible computer, technical, and problem-solving skills, if not for him I would still be lost in computer code.

Thanks to Kris Innanen, my academic supervisor, who took a risk with me and was willing to oversee a project of personal interest and to ensure that it met academic standards. His gift for distilling to abstract & complex into something that is tangible & concrete is beyond compare and has allowed me to articulate key components of my work to others.

Thanks to Daniel Trad and Sam Gray, for the weekly meetings we had to work through and understand the theories associated with static corrections. Sam's unyielding and tenacious curiosity has encouraged me to seek even stronger for understanding. Bernie Law for sharing his knowledge and his humble example that I will always strive to emulate. My office mates, Andy Iverson, Adriana Gordon, and Michelle Montano for their friendship, laughter, and tranquillity. And Laura Baird, for her ability to make an office feel like a home, will forever be appreciated.

I would also like to thank the countless individuals I have spoken within academia and industry. Their guidance, mentorship, and advice have helped me personally and with this thesis.

Table of Contents

List of Tables

List of Figures

ix

x

List of Symbols, Abbreviations and Nomenclature

δ	Near-Offset Anisotropy Parameter
ε	Far-Offset Anisotropy Parameter
τ_{MMO}	MMO corrected Traveltime
τ_r	Receiver Traveltime
τ_s	Source Traveltime
A	Source Straight Ray Intersection Point
AGC	Automatic Gain Correction
B	Receiver Straight Ray Intersection Point
C	Source Minimum Time Intersection Point
C_k	Structure Static
CDP	Common Depth Point
CPML	Convolutional Perfectly Matched Layers
D	Receiver Minimum Time Intersection Point
F	Frequency
Hz	Hertz
km	Kilometer
m	Meter
m/s	Meters per Second
ms	Millisecond
M_k	Residual NMO
MBS	Model-Based Stack
MMO	Model-Based Moveout
NMO	Normal Moveout
PSDM	Prestack Depth Migration
PSTM	Prestack Time Migration
R	Receiver at Surface
R'	Receiver at Datum
R_i	Receiver Static
RMS	Root-Mean-Squared
s	Second
S	Source at Surface
S'	Source at Datum
S_j	Source Static
θ	Angle of Incidence
T_{ijk}	Total Static Shift in Time
t_0	Zero-Offset Time
t_{NMO}	NMO corrected Time for Offset X
TVSW	Time-Variant Spectral Whitening
V_x	Velocity Variable x
V_{NMO}	Normal Moveout Velocity
V_{RMS}	Root-Mean-Squared Velocity

Chapter 1: Introduction

The goal of seismic processing is to generate an image of the Earth's subsurface. Seismic energy propagation from a source through the Earth and back to a sensor can be approximated using analytical solutions. The impact of the near-surface layer is difficult to constrain but can be approximated with first-break arrival times. These first break arrival times are used to estimate the near-surface velocity structure and generate a model used to determine refraction statics (Yilmaz, 2001). However, seismic arrival times can still be affected by localized irregularities that are beyond the temporal and spatial resolution of the data. Because these localized irregularities are beyond the seismic resolution of the near-surface velocity model, small timing errors are passed through to the refraction statics solution. Idealized shot gathers have perfect hyperbolic moveout (Cox, 1999) and any variation from this hyperbolic curve can be corrected by shifting either the source or receiver trace. Reflections statics are commonly attributed to near-surface irregularities which are not captured in the near-surface velocity model and resulting refractions statics. Both refraction and reflection statics corrections allow for a closer approximation of the energy propagation using an analytical solution.

Assumptions about the subsurface such as lateral velocity homogeneity or flat geometry, allow for analytical solutions to be constructed and applied. However, they are not universally appropriate. For example, foothills datasets can have strong lateral velocity variations that will violate NMO assumptions. These strong lateral velocity variations are compensated for by applying larger static corrections to the seismic data. These larger static corrections are not associated with undetermined near-surface effects but are an attempt to accommodate the assumptions of NMO theory. Traditionally, these NMO derived reflection static corrections are applied to input traces for depth migration. This method has been accepted as traces with these corrections generally generate more coherent images in depth migration than without these corrections. However, the approach tends to cause depth velocity models to deviate from their geologic representation, having introduced artefacts into the static correction solution for the sole purpose of compensating for assumptions in NMO theory. When there are strong lateral velocity variations in the near-surface and subsurface, normal moveout introduces anomalies in static

corrections in consequence of theory error. Using raypath traveltime tomography, a model-based stack can be generated by applying source and receiver traveltimes to the respective traces (Sherwood, et al., 1976; Sherwood, Chen, & Wood, 1986; Landa, Thore, & Reshef, 1993). Statics derived from the model-based stack, yield trace shifts coupled to depth migration (Tjan, Larner, & Audebert, 1994; Larner & Tjan, 1995).

1.1 Near-Surface Layer

The near-surface low-velocity layer is often referred to as the weathering layer. However, the term "weathering" differs to a small degree when speaking to geologists and geophysicists and can be separated into *seismic weathering* and *geological weathering*. Using Sheriff's (2002) definition of seismic weathering, this is "a near-surface, low-velocity layer, usually the portion where air rather than water fills the pore spaces of rocks and unconsolidated earth." This low-velocity layer is defined by how seismic waves travel through the Earth's near-surface. Often this low-velocity layer is a sharp boundary, but it can also be gradational. Sometimes the sharp boundary at the base of weathering is caused by a rapid change in rock properties and is commonly associated with the water table, where the pore space is filled with water rather than air. As for geologic weathering, this refers to the physical decomposition of rocks.

Sheriff's definition of seismic weathering removes the direct tie to geologic phenomena and is more of a characterization of the behaviour of seismic waves as they propagate down from and back up to the surface of the earth. As much as the velocity of this low-velocity layer can vary, so can its thickness (Figure 1-1).

The assumptions made when modelling the near-surface of the Earth are an attempt to quantify variations in low-velocity layer thickness and the high-frequency velocity changes with the intent to improve the quality of the final migrated image. As a result, there are many potential geologic and technology related issues in acquiring seismic data that make it difficult to image the subsurface accurately. Near-surface models that create static corrections are constantly being tested, updated, and improved to increase the ability to image the subsurface of the earth.

3

For example, if the velocity of the low-velocity layer, v_1, is much slower relative to the sub-weathering layer velocity, v_2—for a large range on incidence angles in the sub-weathering layer, θ_2, the angle of incidence in the low-velocity layer, θ_1, is near vertical (which is understood to be within 15° of vertical (Cox, 1999)) according to Snell's law (Equation 1-1). This assumption breaks down when high-velocity layers are at the surface.

$$\frac{sin(\theta_1)}{sin(\theta_2)} = \frac{v_1}{v_2}$$

(1-1)
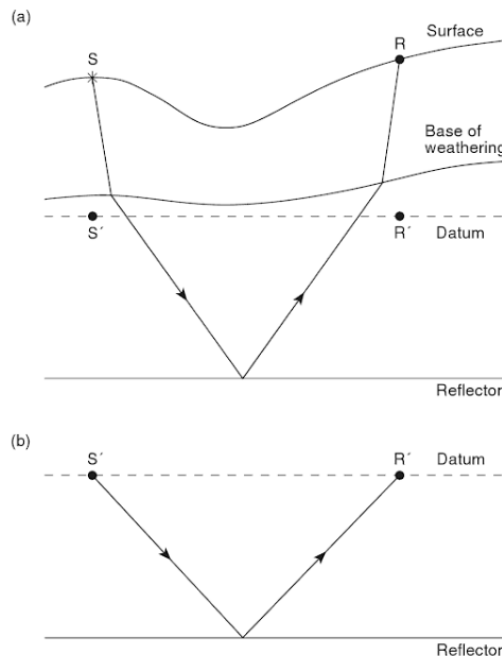
Figure 1-1 Ray-path schematic from source to receiver and potential datum static correction. (a) Acquired source (S)-receiver (R) ray-path from surface. (b) Source (S)-receiver (R) ray-path corrected to datum, after Cox (1999).

1.2 Moveout

Moveout, in simplest terms, describes the time it takes for energy to travel from a source to a subsurface boundary and then up to a receiver as compared to a zero-offset reflection. Cecil Green wrote one of the first papers that discusses the theory and application of normal moveout

(Green, 1938). This moveout will not be seen on a single trace, which is a record of the motion of a single geophone over time, but an array of traces. This array will be a series of geophones, desirably separated by equal increments and commonly identical in length on either side of the source. These traces from the most distant geophone on one side to the most distant geophone on the other side will make up a shot gather – an array of geophones whose energy comes from the same shot. When these geophones measure the energy that is reflected from a subsurface boundary it has a certain appearance. Often idealized flat-layered earth is used to derive an analytical solution for moveout (Figure 1-2a). However, the subsurface is significantly different from an idealized flat-layered earth with homogeneous velocity (Figure 1-2b).
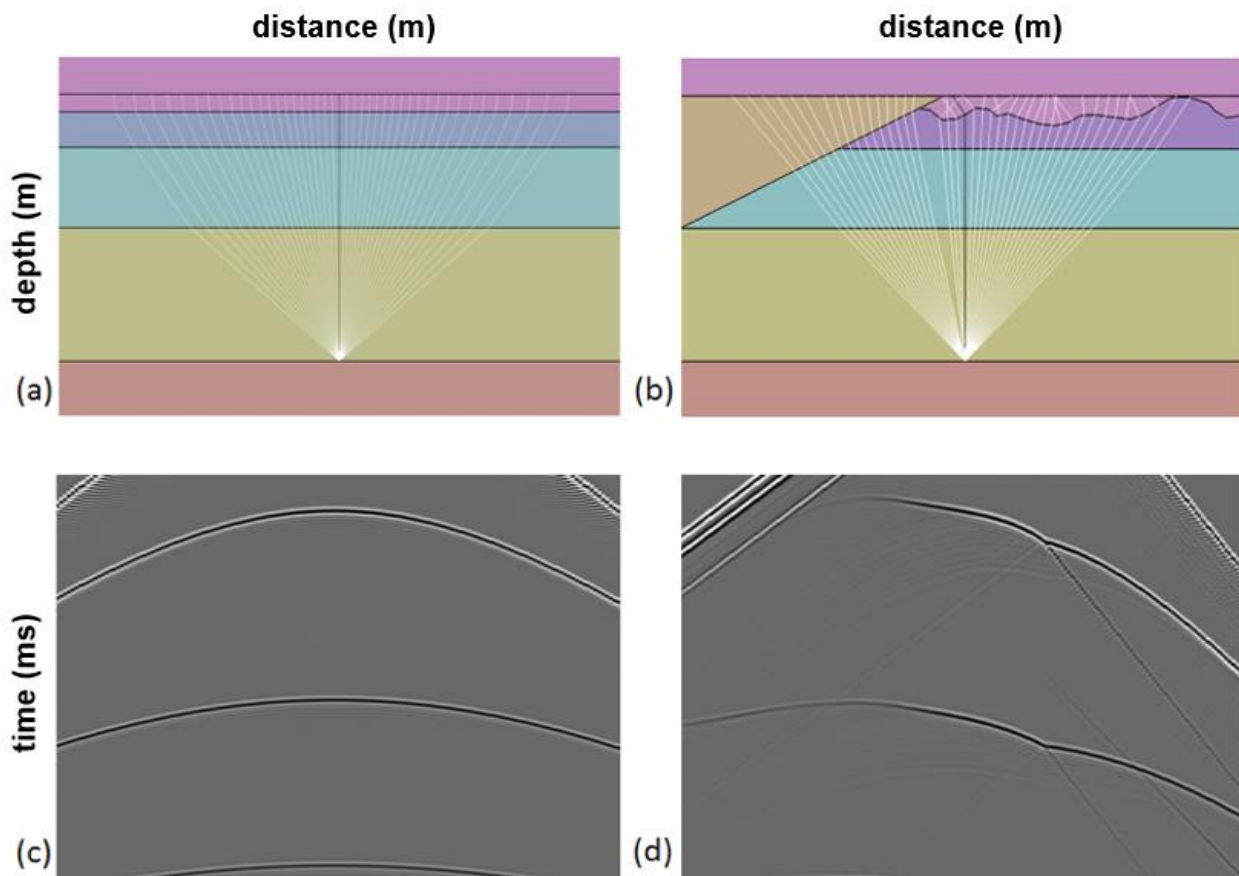
Figure 1-2 Ray fan schematic: (a) near-vertical rays at the near-surface when velocities are slower in the near surface and when seismic weathering is flat, and (b) non-vertical rays in the near-surface when velocities are faster than the layer below and when seismic weathering is complicated. (c) is the representative hyperbolic moveout for flat geometries similar to (a), (d) is the representative non-hyperbolic move-out from complex geological environments similar to (b).

An approach was presented three different ways by Landa (1993), Schmid (1995), and Newrick (2004), where they use the raytraced traveltimes derived from a depth velocity model and applied to raw traces as a model-based moveout (MMO) correction. Landa used MMO to create a model-based stack (MBS) as an efficient tool for structural inversion problems. He also remarked that the MMO corrected traces may be used for new reflection static corrections. Schmid gave some insight into the value of using traveltimes to replicate non-hyperbolic moveout. He also highlights that statics derived from MMO corrected data were successful in revealing new structural details, yet there were no published images with the comparisons. Newrick commented on how she applied MMO but does not discuss the value to the data.

1.2.1 Normal moveout.

For a flat homogeneous layered subsurface (Figure 1-2a), the geophones closest to the source will capture the reflected energy signal first, and the geophones that are further away will capture the energy later. On a shot gather the reflected energy on an array of traces will have the shape of a symmetric hyperbola – approximated by a parabola at small offsets, and by a line at far offsets with the limbs pointing downwards and away from the apex (Figure 1-2c).

During seismic signal processing, it is necessary to apply an appropriate moveout correction to flatten the reflected energy. Flattening this energy is necessary for the subsequent processing steps, to grasp a better visualization of the subsurface layers. The next processing step is called stacking, the summation of the energy across an offset gather for each shot location. If the energy on the shot gather is not flat, the energy signature will be weaker on the stack because there will destructive interference of the coherent signal that is not at the same time across each trace on the gather. In the idealized flat-layered earth with laterally homogeneous velocity and small offsets relative to the depth target (Taner, Koehler, & Alhilali, 1974), moveout would be easy to determine using analytical approaches, such as the 2-term NMO equation presented by Dix (1955):

$$t_{NMO} = \sqrt{t_0^2 + \frac{X^2}{V_{RMS}^2}} \qquad (1\text{-}2)$$

where X is the full-offset, V_{RMS} is the root-mean-square of layer velocities above the reflector, t_0 is the zero-offset time, and t_{NMO} is the moveout corrected time.

1.2.2 Model-based moveout.

The premise of MMO is that the moveout velocity field can be approximated by raytracing through the depth velocity model. In Kirchhoff depth migration, traveltimes are calculated from each source and receiver location prior to migration as one-way seismic energy propagating though the earth. Together, these source and receiver traveltimes are assumed to approach the true travel paths of seismic energy that created the data for each trace from the energy down from the source to the reflector and up to the receiver. In sections where the depth velocity model is flat and laterally homogenous, the MMO will be hyperbolic. The sections that have lateral velocity variation, MMO will have non-hyperbolic moveout.

The novelty of MMO is in how the moveout velocity field is calculated. Instead of using the NMO velocity correction that has the assumption of lateral velocity homogeneity, a moveout velocity field can be determined directly from the depth velocity model using the source and receiver traveltimes. Equation 1-2 in hernetly assumes that the velocities at the zero-offset location are laterally continuous and constant, that for all *X*, the V_{RMS} is the same. Equation 1-3 shows how the MMO is calculated; notice that is wholly dependent on the traveltimes from the source and receiver locations. MMO for each trace is the sum of the respective and symmetric source and receiver traveltimes. Therefore, lateral velocity heterogeneity can be accommodated for through the depth velocity model as measured by these respective traveltimes. Two assumptions here are important to note: reciprocity and symmetry. The reciprocity assumption of source and receiver positions assumes that the effect of downward and upward traveling waves are equal (Knopoff & Gangi, 1959; Taner, Koehler, & Alhilali, 1974). The symmetry assumption of the contributing energy to a trace assumes that it came from a source and receiver are equally distant apart from the midpoint yet on opposite sides.

$$\tau_{MMO} = \tau_s + \tau_r \qquad\qquad (1\text{-}3)$$

A common practice in depth imaging is to smooth the velocity model before the traveltimes are calculated. This smoothing reduces the potential erroneous source and receiver traveltimes created by the traveltime algorithm breaking down in areas of rapid and large changes in the velocity model. This smoothing is a source of uncertainty with the source and receiver traveltimes and accordingly, with MMO.

Once the reflection statics from the MMO stack have been calculated, they are applied to the depth input gathers and migrated with the same velocity field used to determine MMO. Therefore, each velocity model update requires a new MMO velocity determined by the traveltimes which are used to derive new reflection statics that are coupled to the updated velocity model.

The MMO applied to the pre-stack gathers is derived from the depth velocity model. This moveout takes advantage of depth imaging's ability to capture the raypath as it moves through the subsurface which is ignored when using NMO for reflection static corrections (Figure 1-2b). Figure 1-2d illustrates the non-symmetric and non-hyperbolic nature of shot gathers below the leading edge of the velocity contrast. The velocity on either side of the leading edge is different and the resulting moveout cannot be flattened with the NMO equation because it uses   a single velocity term that inherently assumes lateral velocity homogeneity. This assumption causes theory error and is compensated in the reflection static calculations.

1.3 Reflection Static Corrections

Land seismic surveys commonly require statics corrections to reduce or remove the effects of the low-velocity layer by assuming vertical time shifts on reflection data (Figure 1-1). These time-invariant shifts or static corrections are often referred as statics. Sheriff (2002) defines statics as, "corrections applied to seismic data to compensate for the effects of variations in elevation, weathering thickness, weathering velocity, or reference datum."

These statics are a calculated time shift that will compensate for the uncertainties of the seismic weathering layer. The assumption is that the near-surface model is underdetermined

which causes small inaccuracies in the seismic data. Continuing from Sheriff's definition of static corrections:

"[Reflection statics] assume that patterns of irregularity that most events have in common result from near-surface variations and hence static-correction trace shifts should be such as to minimize such irregularities. Most automatic statics-determination programs employ statistical methods to achieve the minimization." — Sheriff (2002).

Reflection statics are calculated because often the lack of detailed near-surface information leads to inaccuracies (Cox, 1999). In preparation of reflection statics, an NMO velocity field is applied to correct for moveout and stack the data. NMO velocity is approximated by a hyperbola and assumes lateral homogeneity (Figure 1-2c). The hyperbolic assumption is violated when the topography is not flat, strong lateral heterogeneity of velocity is present, and when there are variations in the seismic weathering thickness and velocities (Figure 1-2d). (Marsden, 1993).

Generally, the static corrections from the time processing flow are applied to the traces for depth migration. Improvements have focussed on corrections specific to the time migration image and relatively little research, and resources have been allocated to the development, enhancement, and application of near-surface modelling and weathering corrections specific to the depth migration image (Fomel & Kazinnik, 2013; Koren & Ravve, 2018).

Reflection static corrections (Equation 1-3), have four components to determine the total time shift on the stacked trace. R_i is the receiver static at the ith receiver position, S_j is the source static at the jth source position, C_k = time shift for the kth common depth point (CDP) gather, this is sometimes called the structure static, M_k is the residual NMO component at kth CDP gather, and (j-i) is the source-receiver distance (Taner, Koehler, & Alhilali, 1974).

$$T_{ijk} = R_i + S_j + C_k + M_k(j - i)^2 \qquad (1\text{-}3)$$

The C_k parameter identifies trends in the data determine if incorrect event times are part of the actual data and not removed through a static correction. The M_k parameter optimizes the

moveout velocity to minimize the amount of statics shift that could have been applied due to a velocity estimation error.

1.4 Thesis Objectives

The objective of this thesis is to formulate, apply, and test a methodology that derives static corrections that are coupled to depth imaging. This work applies conventional time and depth processing workflows on synthetic datasets and a test field dataset. In comparing the final image results, the only differences are the method in which moveout is applied, NMO vs MMO.

Chapter 2 provides the background and scenario where NMO theory fails. The presence of strong lateral velocity variation cannot be replicated with the symmetric and analytical NMO equation. Using a synthetic velocity model that has no near-surface low-velocity layer, no topography and a known velocity structure, there should be no need for static corrections. However static shifts are generated to compensate for NMO's inability to compensate for strong lateral velocity variation.

Chapter 3 compares the results of NMO corrected data and MMO corrected data on two synthetic datasets. An idealized wedge velocity model and a subset of the BP 1994 Statics Benchmark Model. Each case compares and illustrates the impact of the moveout correction used on the final depth image.

Chapter 4 is an overview of the time processing steps of the field dataset. This dataset was taken through to the prestack time migration (PSTM) image to ensure that the static corrections applied enhanced the final image.

Chapter 5 describes the interpretive depth processing workflow. The final image stacks with statics derived from NMO corrected data and statics derived MMO corrected data are compared. A preliminary investigation in applying the tomographic near-surface velocity model to the depth velocity model is presented.

Chapter 6 summarizes the work presented in this thesis and comments on the value of using statics coupled to depth imaging.

1.5 Data

1.5.1 Wedge model.
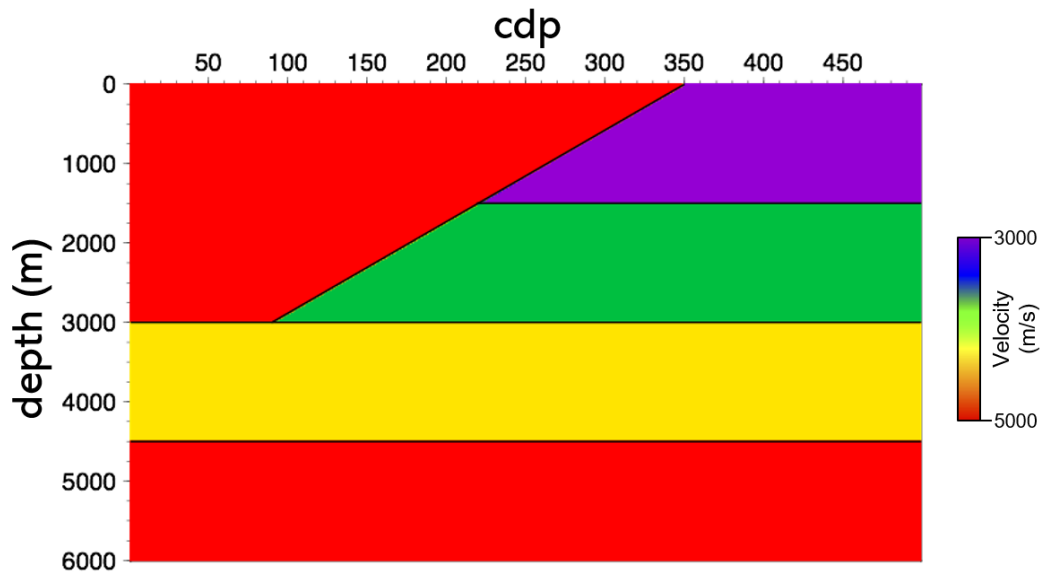
Figure 1-3 Wedge thrust model.

The wedge thrust velocity model (Figure 1-3) is a 20 m x 20 m grid that is 10 km long requiring no statics because of no low-velocity layer and no elevation change. The intent was to determine the effectiveness of normal NMO and MMO on a synthetic thrust environment with strong lateral velocity variation.

Using Acceleware's acoustic modelling software AxWave, I shot every second receiver station using a 30 Hz source Ricker wavelet. The acquisition geometry for the wedge thrust model was 80 m source spacing and 40 m receiver spacing equating a max fold of 63, while the BP 94 model was 40m source spacing and a 10 m receiver spacing producing a max fold of 126.

1.5.2 1994 BP statics benchmark model.

The 1994 BP statics benchmark model (BP 94) is a 5 m x 5 m grid that is 60 km line in total length. I focussed on the 20 km on the right end of the line shown in Figure 1-4. The BP 94 velocity model not only contains low-velocity layers, but this section of the synthetic model is

also a suitable example for classic complex foothills environments. This modelling was shot every fourth receiver station using a 30 Hz source Ricker wavelet.
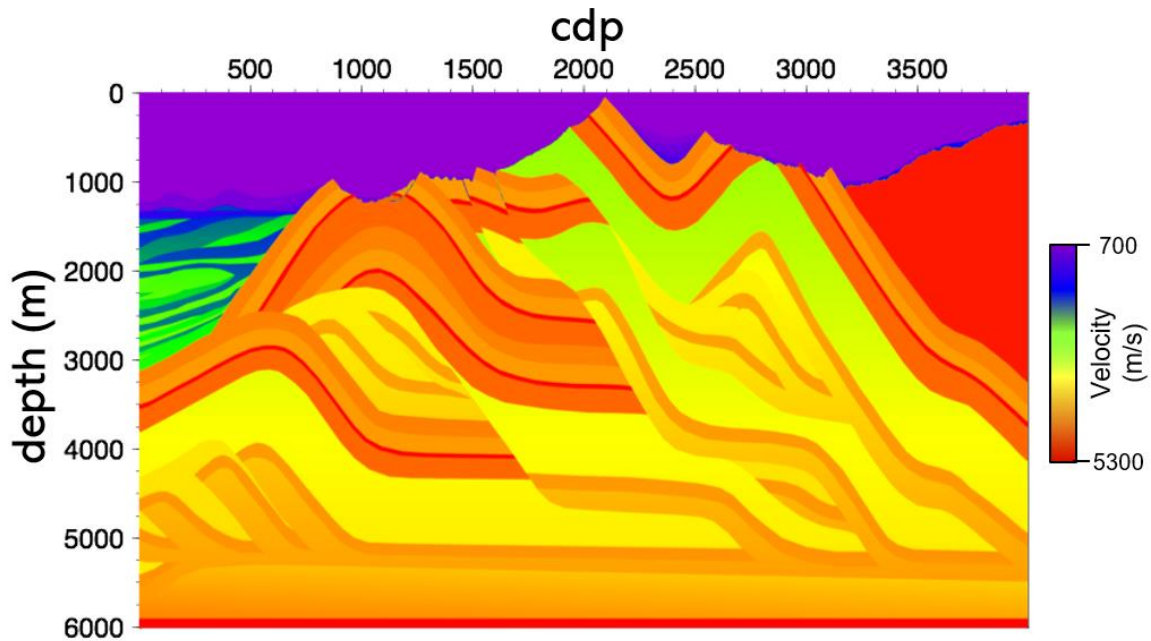
Figure 1-4 1994 BP statics benchmark model, created by O'Brien (1994).

1.5.3 Canadian foothills dataset.

The foothills field dataset is from the Canadian foothills and was publicly released in 1995 at the SEG AGM Workshop #6 in Houston as a foothills imaging benchmark for data processing (Stork, Welsh, & Skuce, 1995). This dataset is known as the 'Husky Structural Dataset' and has a lot of geologic complexity and excellent signal quality. At the workshop, the presenters provided many insights and expertise imaging the foothills dataset.

1.6 Software

Acceleware's AxWave software was used extensively to generate the synthetic velocity models. SeisSpace was used for time processing and conditioning the input traces or depth migration. Techco's VELANAL software allowed for user-friendly, interpretive velocity analysis. Thrust Belt Imaging's proprietary software written in python and SeismicUnix was used for depth imaging. GeoTomo's TomoPlus software was used to calculate the tomographic near-surface velocity model and refraction statics. MATLAB was used for data analysis and

regression. Python, Unix and SeismicUnix, were used the most in the handling of the seismic data.

Chapter 2: Normal Moveout Theory Error

2.1 Introduction

This chapter shows how NMO theory error may be quantified by exploring the impact of the offset distance used to determine the NMO velocity and the magnitude of velocity variation. The offset and velocity are variables that determine the appropriate NMO correction. Poor convergence on an appropriate NMO velocity field will result in greater static correction to compensate to flatten the data. The Wedge Thrust Model (Figure 1-3) is used to examine the limits of NMO theory. This model is suitable because it has no topographic relief and has no near-surface weathering layer. Because of these two features, no static corrections should be necessary and the consequence of applying NMO in a strong velocity variation scenario can be evaluated.

2.2 Theory

In Cecil Green's paper (1938), he discusses the theory and application normal moveout. Even though he presented the simple and generally used form for moveout (Equation 2-1), others still recognized the theory error with lateral velocity variations (Widess, 1952). Dix (1955) discussed how deeper layers with higher velocities will not have straight raypaths from source to reflector to receiver (Figure 2-1) if NMO velocities are used. Instead, the root-mean-square (RMS) velocities can be used in place of NMO velocities (Equation 2-2) to more closely approximate the timing of the seismic waves not only to the reflector of interest, but also the reflectors above the target. Dix also presented higher order right-hand terms to equation 2-2 that allow for greater accuracy to the velocity in layers above the target reflection.

$$t_{NMO} = \sqrt{t_0^2 + \frac{X^2}{V_{NMO}^2}} \quad \text{(2-1)} \qquad t_{NMO} = \sqrt{t_0^2 + \frac{X^2}{V_{RMS}^2}} \quad \text{(2-2)}$$

14
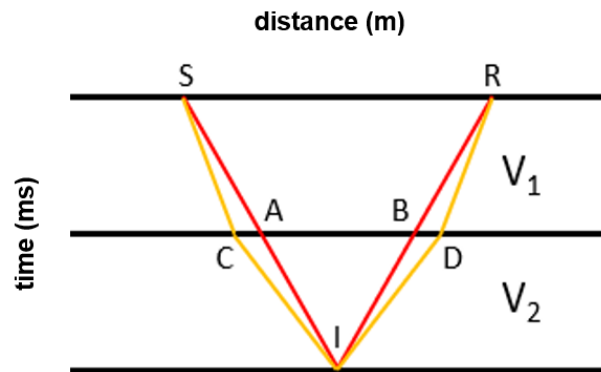
Figure 2-1 Two-layer schematic for increasing velocities. Rays from source (S) to receiver (R) from reflection point (I), Straight raypath will travel thought points A and B on the V_1-V_2 boundary. Minimum time paths will travel through points C and D on the same boundary, after Dix (1955)

However, Taner and Koehler (1969) record that equation 2-2 is still accurate within two percentage points without the higher order terms when the offset is small relative to depth of the target, which is generally sufficient for applied seismic purposes. Also, in this paper, Taner and Koehler proposed the semblance plot, which is a hyperbolic stack that generates stronger energy at more appropriate velocities for moveout determination.

Once the appropriate NMO is determined, the assumption is that any remaining anomalies which limit reflector coherency are associated with velocity variations too insignificant to be resolved by a more detailed NMO velocity but large enough to impact the stack.

Basic assumptions of NMO are reciprocity, symmetry, and that the velocity is laterally homogeneous. Reciprocity is the assumptions that raypaths from the source to the receiver are the same raypaths if the source and receivers had switched positions. Symmetry is that the subsurface image point is in the middle of the source and receiver distance. Lateral velocity homogeneity is an embedded assumption in equation 2-2 as there is a single velocity term, V_{RMS}, for the distance between the source and receiver, X.

These three assumptions are related to the potential error that can be generated. Figure 2-2 is an adaptation to Figure 2-1. The red lines show how if one side of the raypath travels through a

velocity different than the other side, and if the subsurface image point is fixed, that the source location will need to be adjusted. The source location will need to move to the right if the $V_3 <$ V_1 and to the left if $V_3 > V_1$. Reciprocity is maintained, but symmetry and the ability to correct for NMO with a single velocity becomes compromised.

In applied seismic exploration, it is accepted that NMO will not fully correct for the all the subsurface variations encountered but is a good approximation when the model assumptions are valid. Static corrections are then used to make up for the limitations of NMO applications to enhance the subsurface image.
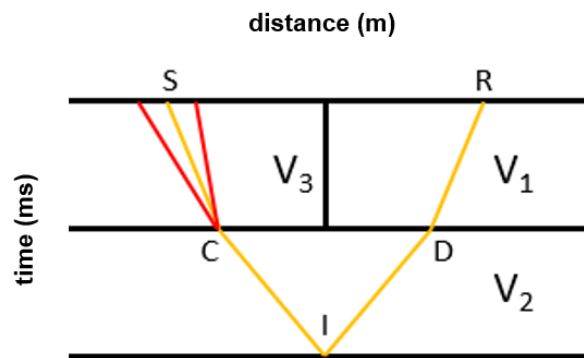
Figure 2-2 Two-layer schematic for increasing velocities and laterally varying velocity in the first layer. Raypaths from source (S) to receiver (R) from reflection point (I). The red rays show the source position change needed to image (I) if the top layer velocity changes laterally. If $V_3 < V_1$ the source will need to move to the right, if $V_3 > V_1$ the source will need to move to the left.

2.3 Velocity Modelling

The wedge thrust model was used to generate the synthetic data to test the impact of offset distance on NMO velocity determination in the presence of strong lateral velocity variation. Although a velocity variation from 3000 m/s to 5000 m/s may seem extreme, it is common in areas where a rigid carbonate layers are thrust to the surface and overlay softer, more ductile lithology. This wedge thrust velocity model requires no static corrections. As there is no low-velocity layer and no elevation change any static generated will be solely due to theory error associated with NMO. The synthetic acquisition parameters of this model are detailed in Section 1.5 of Chapter 1. Four different velocities in the hanging wall of the wedge model were chosen

to investigate impact of lateral velocity variation on the NMO correction. The hanging wall velocities used are 5000 m/s, 4000 m/s, 3600 m/s, and 3300 m/s. The relative change between the first layer of the footwall and the hanging wall velocity is 67%, 33%, 20%, and 10% respectively.

2.4 Offset Testing

To investigate the impact that the offset range has on the NMO velocity optimized to correct for moveout, I used four half-offset windows, 0.5 km, 1.5 km, 3 km, and 5 km (Figure 2-4). The average NMO velocities chosen for the longer offset windows will have a greater variance in the presence of strong lateral velocity variations. I ran constant velocity panels (

Panel	Velocity (m/s)	Panel	Velocity (m/s)	Panel	Velocity (m/s)	Panel	Velocity (m/s)	Panel	Velocity (m/s)
1	1800	11	2300	21	3100	31	4100	41	5200
2	1850	12	2350	22	3200	32	4200	42	5400
3	1900	13	2400	23	3300	33	4300	43	5600
4	1950	14	2450	24	3400	34	4400	44	5800
5	2000	15	2500	25	3500	35	4500	45	6000
6	2050	16	2600	26	3600	36	4600		
7	2100	17	2700	27	3700	37	4700		
8	2150	18	2800	28	3800	38	4800		
9	2200	19	2900	29	3900	39	4900		
10	2250	20	3000	30	4000	40	5000		

Table 2-1) and used VELANAL to pick the V_{RMS} for each stack Figure 2-3 VELANAL panel example. Green lines are control lines where stacking velocities can be fixed.Figure 2-3). VELANAL loads multiple stacks at with various velocities (

Panel	Velocity (m/s)	Panel	Velocity (m/s)	Panel	Velocity (m/s)	Panel	Velocity (m/s)	Panel	Velocity (m/s)
1	1800	11	2300	21	3100	31	4100	41	5200
2	1850	12	2350	22	3200	32	4200	42	5400
3	1900	13	2400	23	3300	33	4300	43	5600
4	1950	14	2450	24	3400	34	4400	44	5800
5	2000	15	2500	25	3500	35	4500	45	6000
6	2050	16	2600	26	3600	36	4600		
7	2100	17	2700	27	3700	37	4700		

8	2150	18	2800	28	3800	38	4800		
9	2200	19	2900	29	3900	39	4900		
10	2250	20	3000	30	4000	40	5000		

Table 2-1), and these stacks can be scanned through to identify the optimal stacking velocity based on visual coherency and the sharpness of the reflector along the velocity control lines. These velocity control lines, green lines in Figure 2-3, are every 10th CDP. At a desired time down the seismic section, a control point can be added to lock in the desired velocity for a target reflector. The velocity field is linearly interpolated, first vertically along the velocity control lines between points, then horizontally between velocity controls. This aggregate velocity field is used to stack the data in preparation for static calculations.

Panel	Velocity (m/s)	Panel	Velocity (m/s)	Panel	Velocity (m/s)	Panel	Velocity (m/s)	Panel	Velocity (m/s)
1	1800	11	2300	21	3100	31	4100	41	5200
2	1850	12	2350	22	3200	32	4200	42	5400
3	1900	13	2400	23	3300	33	4300	43	5600
4	1950	14	2450	24	3400	34	4400	44	5800
5	2000	15	2500	25	3500	35	4500	45	6000
6	2050	16	2600	26	3600	36	4600		
7	2100	17	2700	27	3700	37	4700		
8	2150	18	2800	28	3800	38	4800		
9	2200	19	2900	29	3900	39	4900		
10	2250	20	3000	30	4000	40	5000		

Table 2-1 Values used to create constant velocity panels for velocity analysis for each wedge model. These values are used to create stacking velocities and time migration velocities.
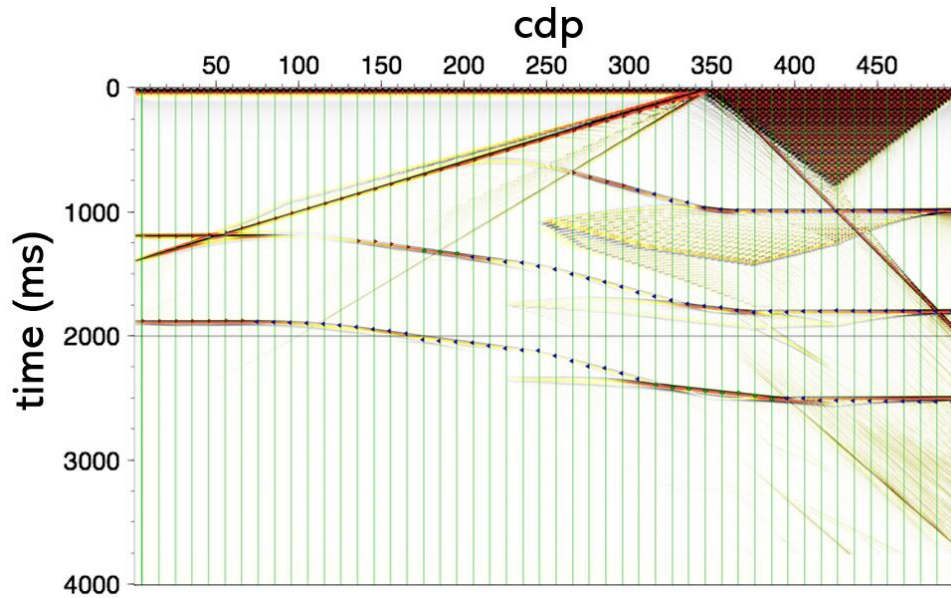
Figure 2-3 VELANAL panel example. Green lines are control lines where stacking velocities can be fixed. Blue left pointing arrows indicate where picked velocities are slower than the current constant velocity stack. Red right pointing arrows indicate where picked velocities are faster than the current constant velocity stack.
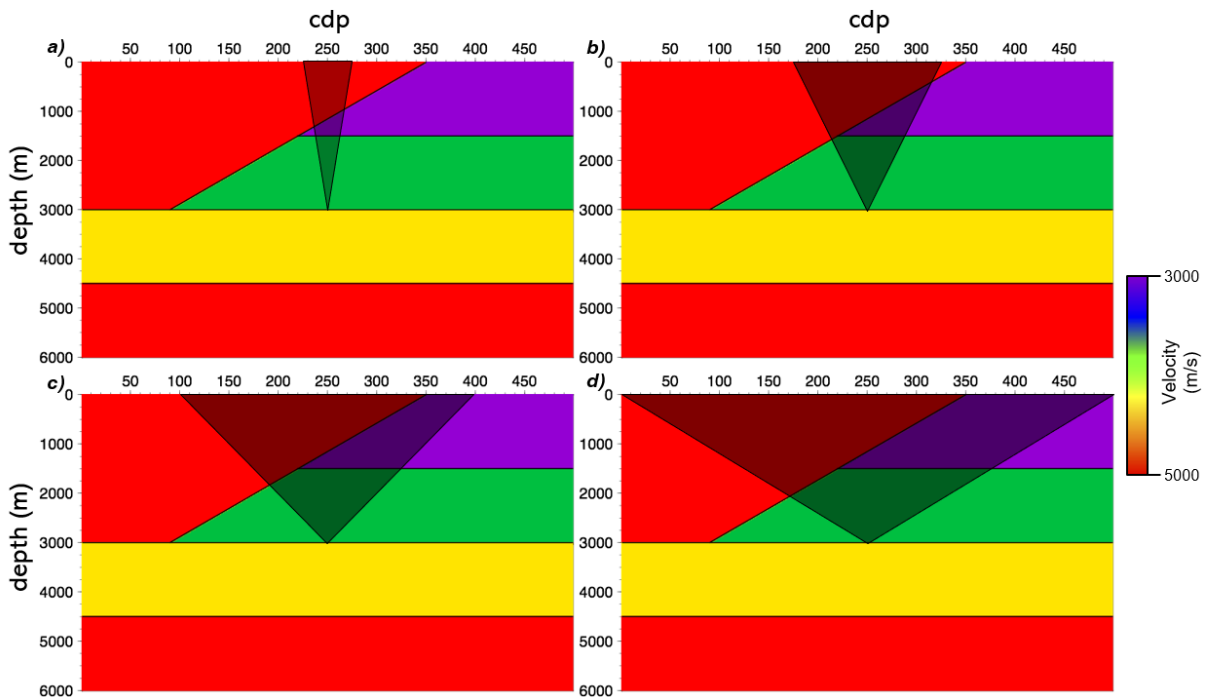
Figure 2-4 Schematic illustrating the testing of offset sensitivity of NMO centred at CDP 250. (a) 0-0.5 km, (b) 0-1.5 km, (c) 0-3 km, and (d) 0-5 km. The wider offset windows encounter greater velocity variation that narrow offset windows.

2.4.1 Offset stacks and velocities.

A qualitative review of the offset stacks (Figure 2-5) show that limiting the offsets allows for a more coherent image going into reflection static corrections calculations, see the respective variations on the stacks with the red rectangles. Figure 2-4c and Figure 2-4d are showing how NMO is having difficulty correcting for the moveout with a single velocity below CDP 300.
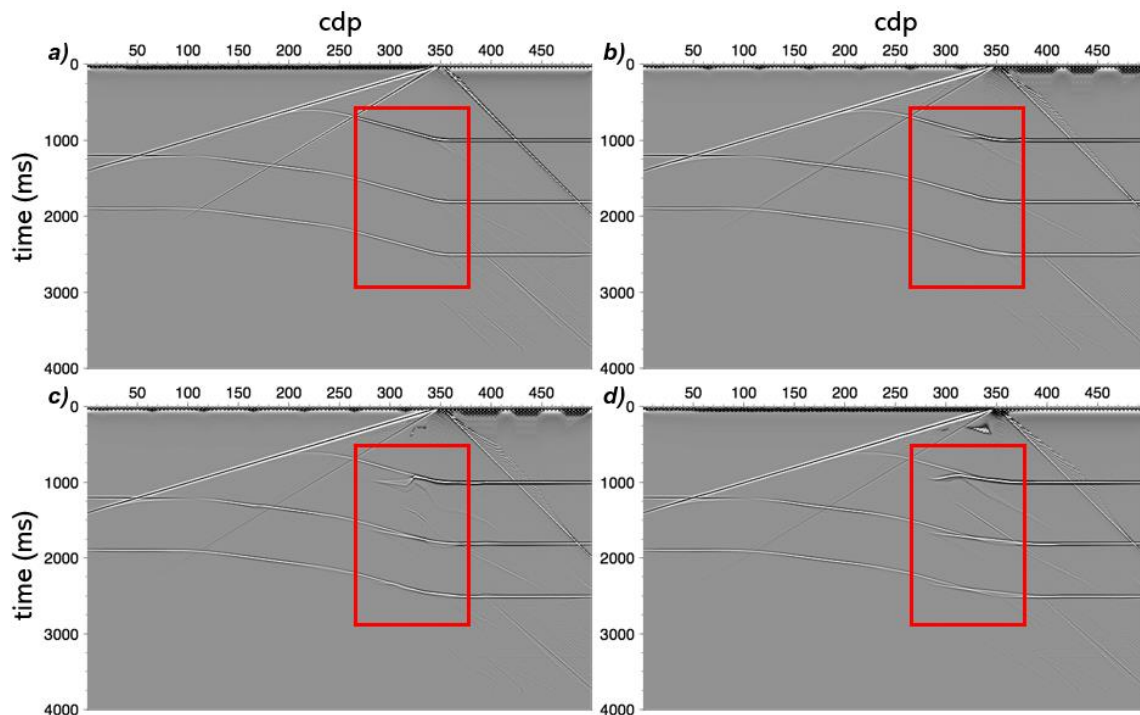
Figure 2-5 Stacks prior to static corrections with same velocity model but varying offsets. The largest see the variations on the stacks are within the red rectangles. (a) offset, 0-0.5 km, (b) offset, 0-1.5 km, (c) offset, 0-3 km (d) offset 0-5 km, full offset.

Figure 2-6 has the respective stacks but with static corrections applied (discussed in more detail in section 2.6). It is interesting to note that for the stacks with 3 and 5 km offsets, the static corrections enhanced the part of the data that is erroneous due to the lateral velocity variation, see the respective variations on the stacks with the red rectangles.
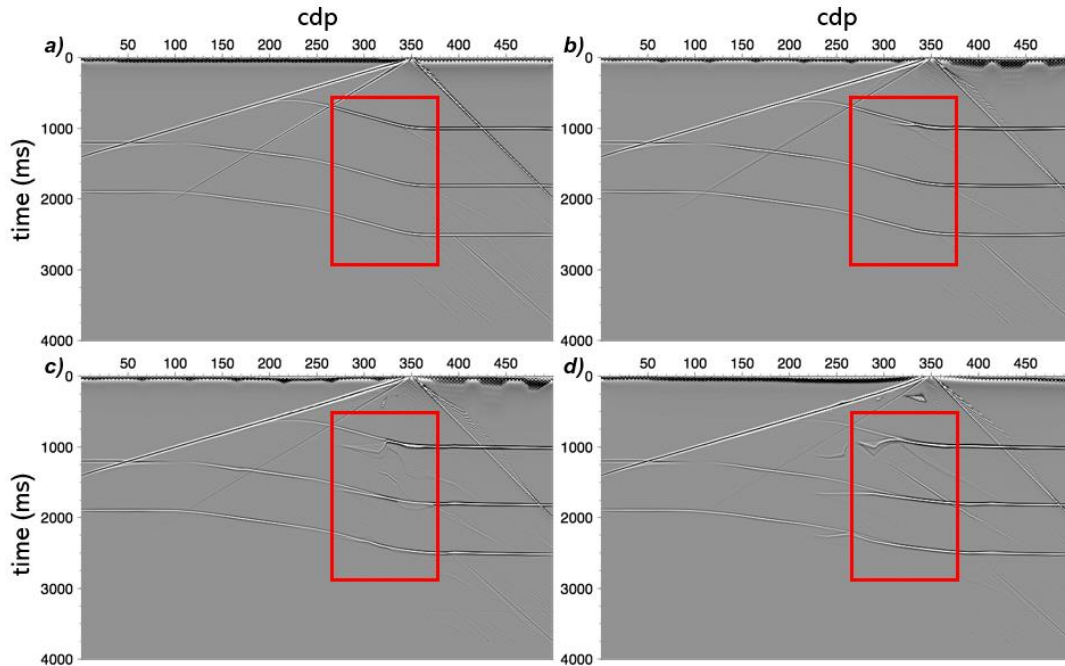
Figure 2-6 Stacks after static corrections with same velocity model but varying offsets. The largest see the variations on the stacks are within the red rectangles. (a) offset, 0-0.5 km, (b) offset, 0-1.5 km, (c) offset, 0-3 km (d) offset 0-5 km, full offset.
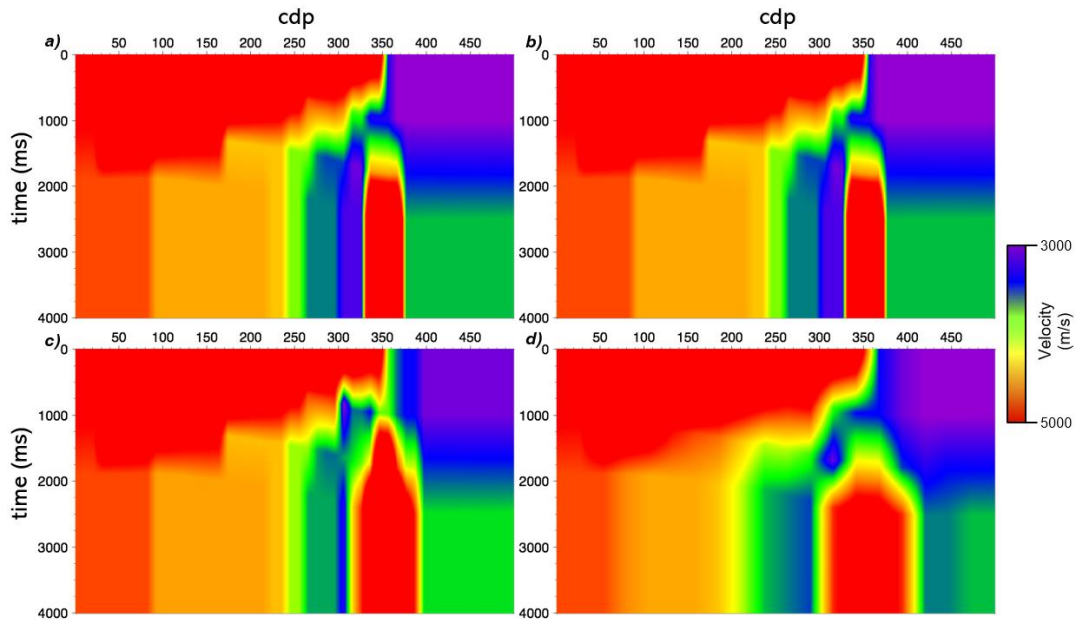
Figure 2-7 Interval velocities for each offset range. RMS velocities were picked using VELANAL and then converted to interval velocities for comparison with the geologic representation of the synthetic wedge model. (a) offset, 0-0.5 km, (b) offset, 0-1.5 km, (c) offset, 0-3 km (d) offset 0-5 km, full offset.

2.5 Velocity Testing

These models (Figure 2-8) were used to test the impact of the strength of the lateral velocity heterogeneity needed to break the NMO assumption. The hanging wall velocities are: 5000 m/s; 4000 m/s; 3600 m/s; and 3300 m/s. The relative change between the first layer of the footwall and the hangingwall velocity is 67%, 33%, 20%, and 10% respectively. The full offset (5 km) is constant between each of these models.

The stacks prior to static corrections that had the 3300 m/s hangingwall (Figure 2-8a) and the 3600 m/s hangingwall (Figure 2-8b) show that the NMO assumptions are holding sufficient well and are not creating any artificial reflection in the image. Figure 2-8c begins to show the NMO assumption breaking down with a 33% velocity variation in hangingwall from the first layer in the footwall (inside red rectangle). Figure 2-8d having a strong variation in velocities breaks down even more (inside red rectangle).
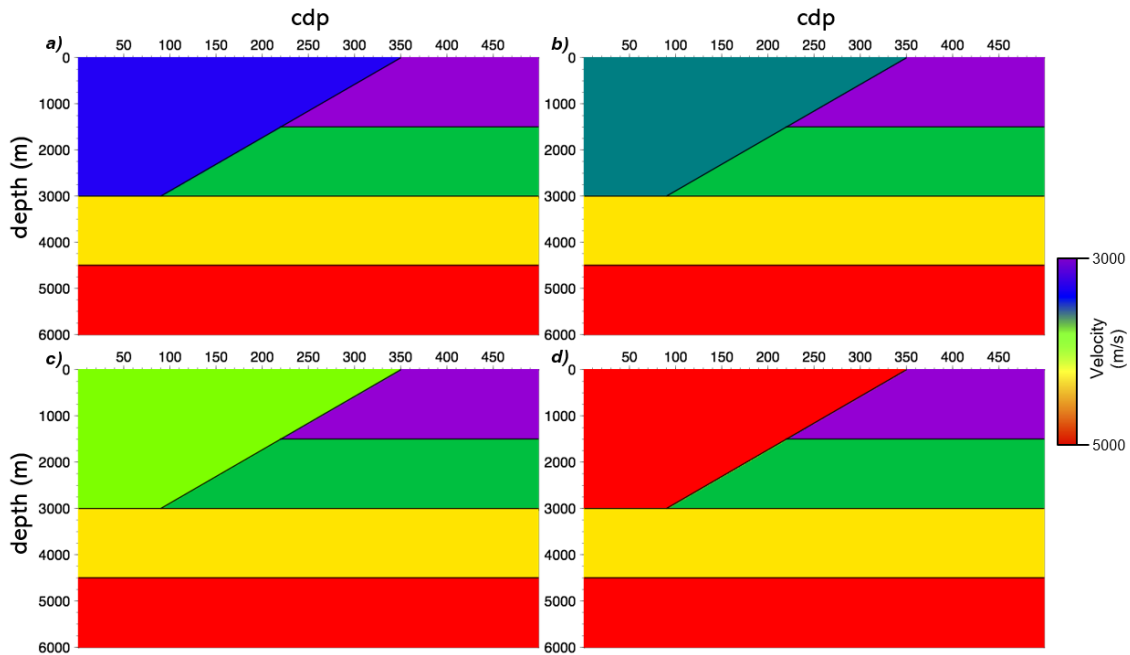
Figure 2-8 Velocity models used to test lateral velocity variation sensitivity with NMO.

2.5.1 Stacks and velocities.

The stacks in Figure 2-9 are prior to static corrections and the stacks Figure 2-10 have static corrections applied. Figure 2-10c and Figure 2-10d show the enhanced reflections that are associated with the static corrections, but this is where the NMO assumptions breaks down and create false reflectors are not representative of the geology. Figure 2-10a and Figure 2-10b indicates that an NMO correction will not introduce any extra or anomalous reflectors if the velocity variation is 20% or less. This suggest the feasibility of NMO in applied seismology as perfect solution is difficult to determine or to know what aspect of a seismic processing workflow has the biggest potential in the presence of noise and an unknown geologic velocity. This potential means that a strong lateral variation in velocity is between 20% and 33% relative lateral difference in velocity.
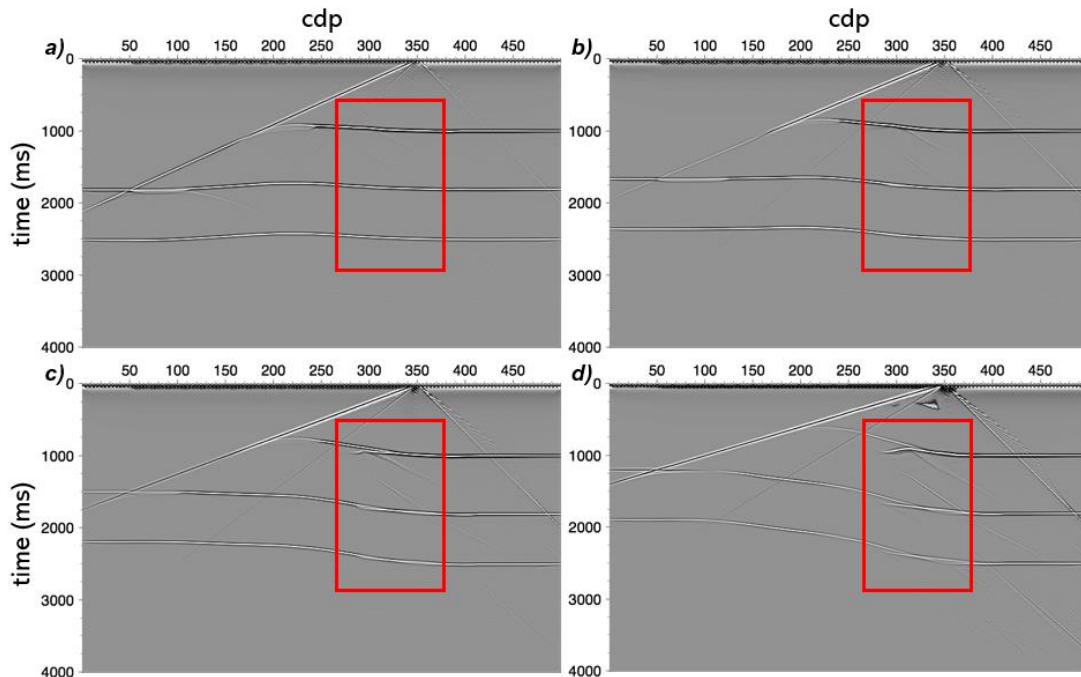
Figure 2-9 Stacks prior to static corrections with full offset but varying velocity models. The largest see the variations on the stacks are within the red rectangles. Hanging wall velocity, (a) 3300 m/s, (b) 3600 m/s, (c) 4000 m/s (d) 5000 m/s
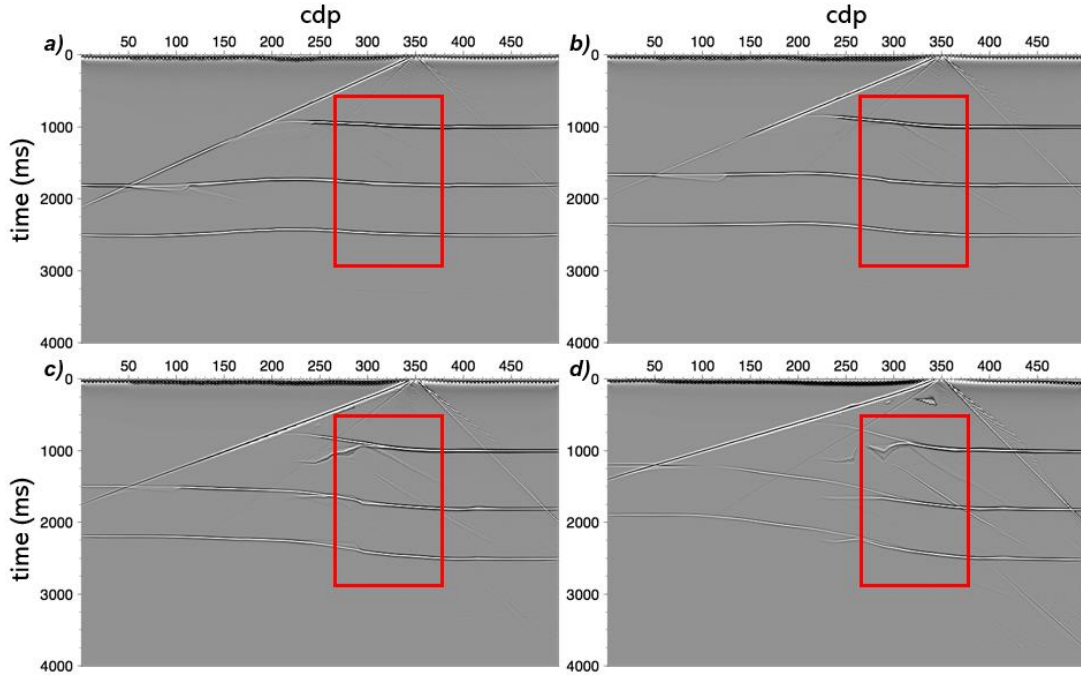
Figure 2-10 Stacks after static corrections applied with full offset but varying velocity models. The largest see the variations on the stacks are within the red rectangles. Hanging wall velocities, (a) 3300 m/s, (b) 3600 m/s, (c) 4000 m/s (d) 5000 m/s.
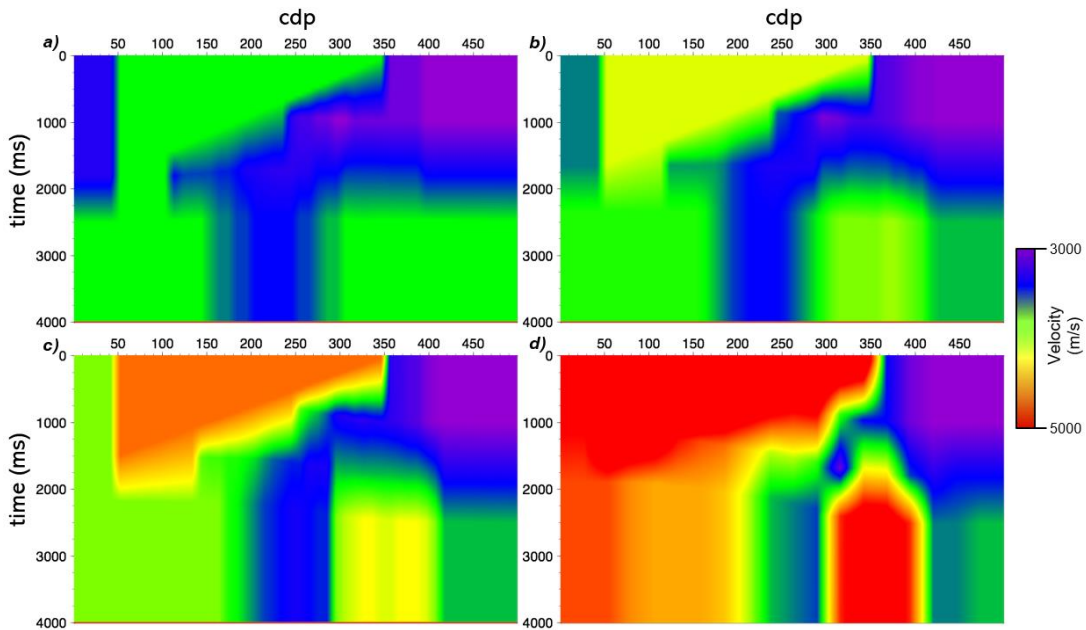
Figure 2-11 Interval velocities for each offset iteration of hanging wall velocity. RMS velocities were picked using VELANAL and then converted to interval velocities for comparison with the geologic representation of the synthetic wedge model. Hanging wall velocity, (a) 3300 m/s, (b) 3600 m/s, (c) 4000 m/s (d) 5000 m/s

The RMS velocities are more stable for Figure 2-11a and Figure 2-11b. Figure 2-11c is starting to show stronger complexity at CDP 350 and 2 s. Figure 9d shows a lot of strain in the stacking velocities to compensate for the 66% velocity variation between the hangingwall and the first layer of the footwall. It is also present in these velocity figures the higher stacking velocity required for dipping layers (Dix, 1955; Taner & Koehler, 1969)

2.6 Static Corrections Evaluation

The reflection static corrections were calculated as described in section 1.3 of Chapter 1. The velocity models employed in this NMO testing are flat with no low-velocity layers. As such it is reasonable to assume that any value for a static correction can be attributed to theory error in the NMO correction process. Although equation 1-3 has four terms that are involved in static corrections, only two of them are applied to the data, the receiver static (R_j) and source static (S_i). The structure term C_k and residual NMO term M_k are not applied to the data. Also, since the S_i and R_j are effectively the same shift along the length of the model (Figure 2-12) I will compare the source static portion of the correction determined from the data. The correlation window was only applied the bottom reflector in each of the stacks. The window placement needed to change when being used on the models with varying velocity.
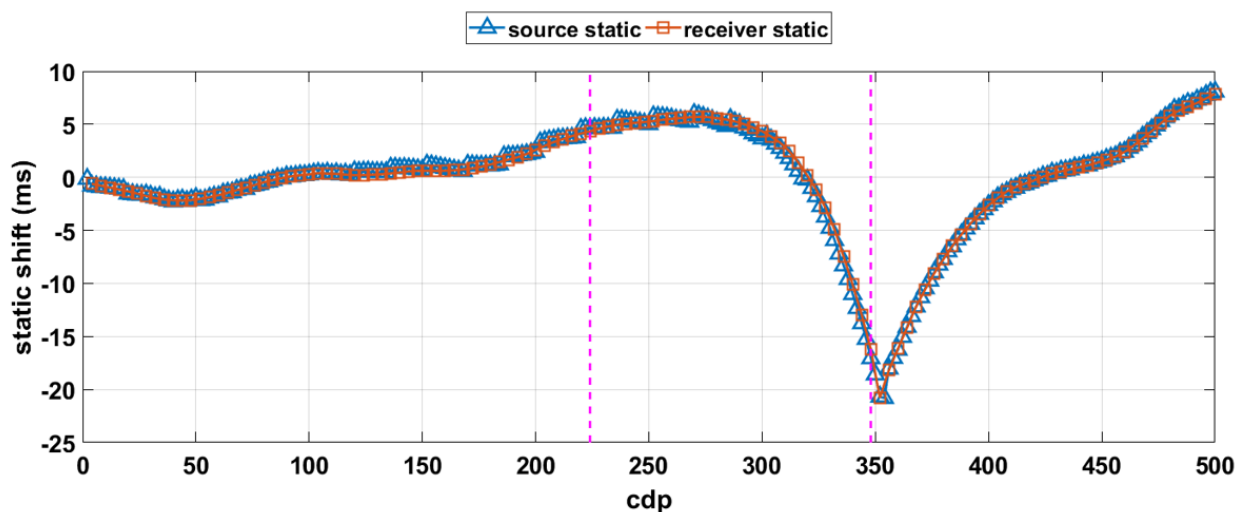
Figure 2-12 Static corrections comparison. The line with squares represents the statics shift for the sources, the line with the triangles represent the statics shift for receivers. The vertical dashed lines represent the leading edge of the velocity contrasts in the model.

25

2.6.1 Offset comparison.

Figure 2-13 shows the static corrections needed to increase to maintain the reflector coherency with each increasing offset test. The velocity model is common between each offset test. Around 7000 m as depicted by the dashed line, the magnitude of the impact does increase with the range of offsets used, and it is a definite feature in the static corrections. The 0.5 km offset test required the least amount of static corrections to enhance the coherency, and they are largely negligible away from the leading edge of the thrust at the top of the model. However, the target that was in the correlation window was 4.5 km deep. Although these acquisition parameters are not ideal for field data and limit the confidence in picking an accurate RMS velocity, it does illustrate the point that the length offsets in the data impact as the optimal velocity can be different from the near offsets to the far offsets.

The results for the static corrections for the 1.5 km offset test are like the 0.5 km offset test except for the increase in statics shift around CDP 225. This static shift is near another leading edge of a velocity contrast that is associated with the second layer in the footwall (Figure 2-4) indicated by the dashed line.
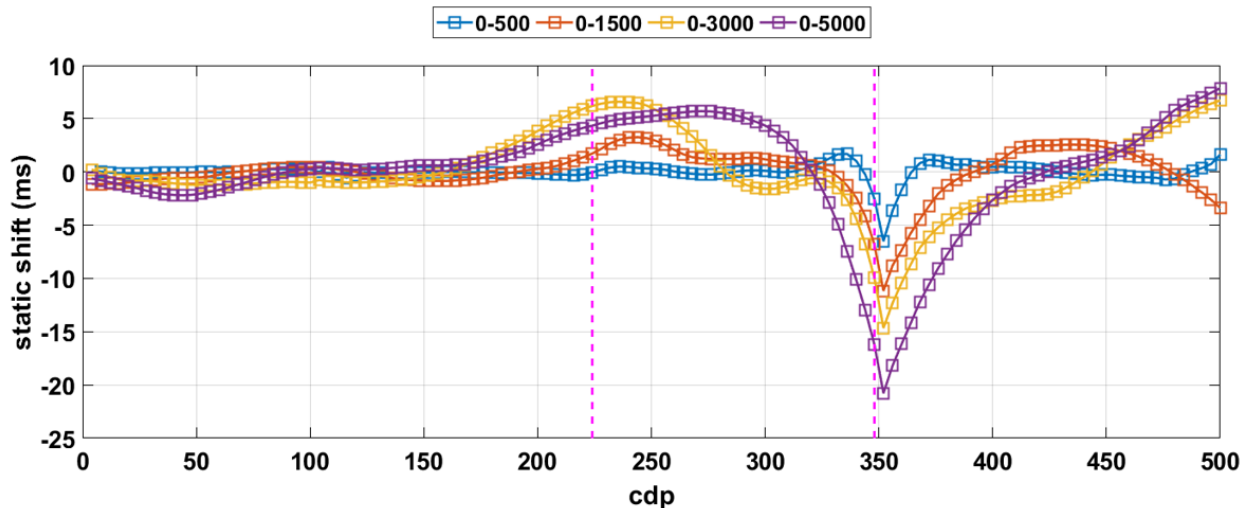
Figure 2-13 Static corrections on the stacks testing the impact of offset for the NMO equation. The vertical dashed lines represent the leading edge of the velocity contrasts in the model.

The static corrections associated with the 3 km offset are even larger. This makes sense that more static corrections are required to correct for the longer offsets because the single V_{RMS} would be more noticeably incorrect at farther offsets. The 5 km results have one big sweep of positive static corrections that appear to compensate for the negative statics shift associated with the leading edge of the thrust at the near surface. However, after reviewing the previous solutions with the different offsets, the magnitude of the positive static corrections between sources 40 – 80 is a result of an additive effect due to the length of the offset included, and the two velocity contrasts from the top two layers in the footwall adjacent to the high-velocity thrust. The left plot in Figure 2-15 has a plot of the static corrections magnitude relative to the offset used to determine the V_{RMS}.

2.6.2 Velocity comparison.

Figure 2-14 shows the source static corrections needed to increase the reflector coherency with each variation of velocity in the thrust. The offset range of 5 km is common between each velocity variation test. The two dashed lines near 4500 m and 7000 m indicate the leading edge of the velocity contrasts. The magnitude of the static shifts is correlated with the scale of the velocity contrast in the model. The maximum value of these static corrections also correlates with the spatial location of the velocity variation in the subsurface.
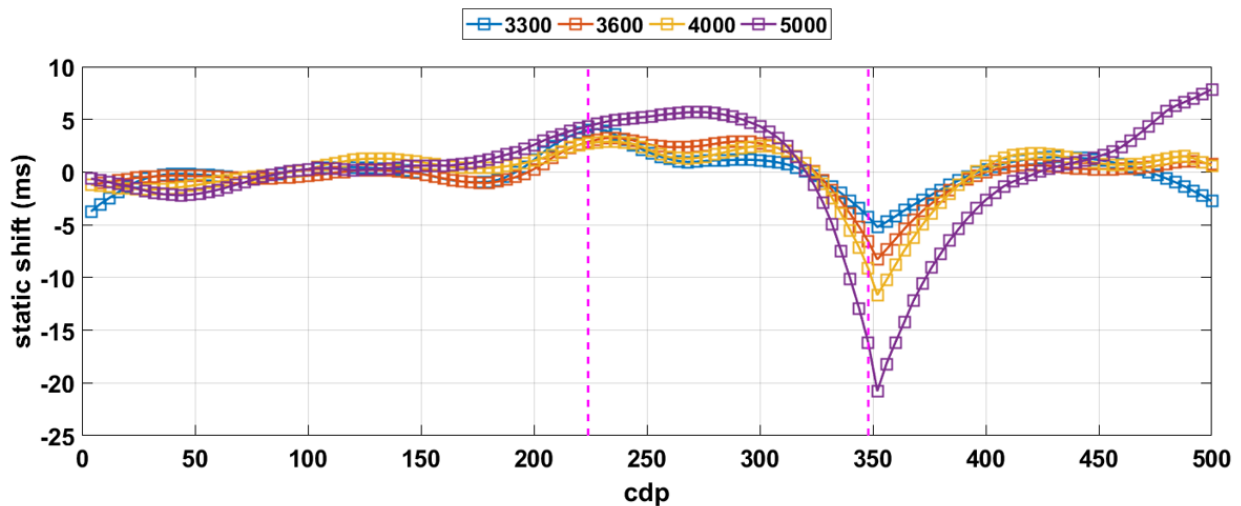
Figure 2-14 Static corrections testing the magnitude of velocity variation for the NMO equation. The vertical dashed lines represent the leading edge of the velocity contrasts in the model.

The velocity test with 3300 m/s in the overthrust has 10% change with respect to the first layer in the footwall and 11% change with the second layer. This being the smallest velocity contrast evaluated, it also required the least amount of static corrections to enhance the coherency. Both locations of the lateral variations in velocity model are seen in the source static corrections needed to increase the stack's coherency. The 3600 m/s and 4000 m/s velocity tests had similar static corrections for the deeper velocity contrast. The relative changes in velocity are 3% and 8% respectively. The static corrections for the leading edge of the velocity contrast in the first layer increased with the magnitude of the relative change of the velocity variation, 20% and 33% respectively. The 5000 m/s velocity test had the largest static corrections with a relative change in velocity of 67%. The right plot in Figure 2-15 shows the relationship between relative change in lateral velocity variation and static corrections magnitude.
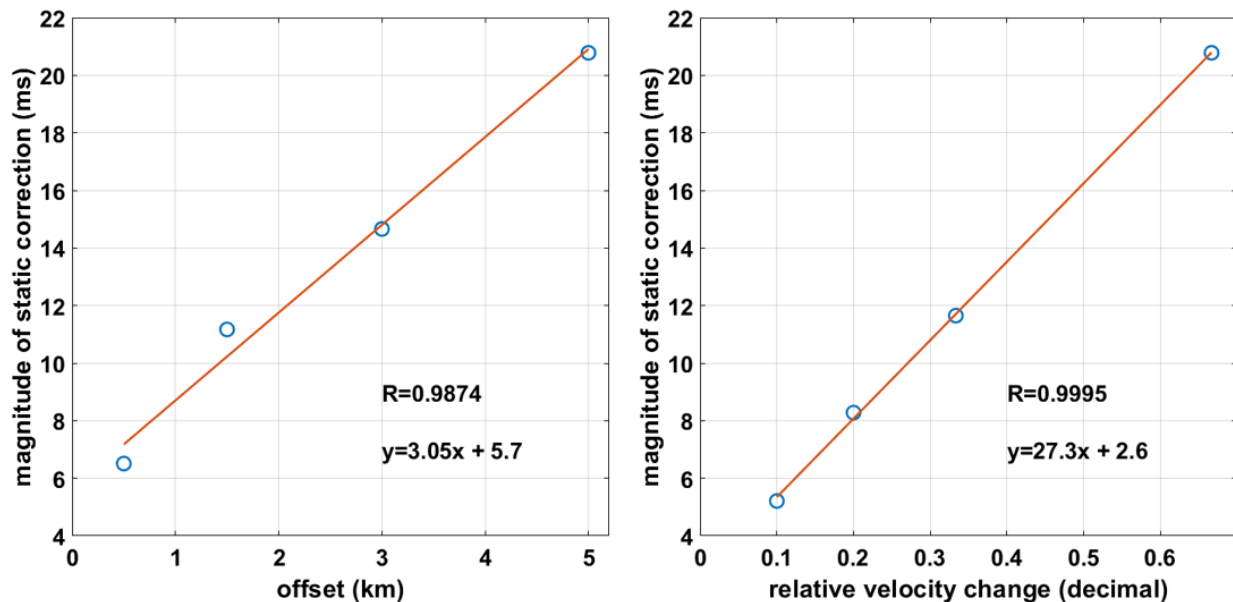
Figure 2-15 Plots comparing the magnitude of static correction with offset (Left) and the magnitude of static correction with relative changes in velocity (Right).

Although the range of testing is limited and if the thrust model, which should not have static corrections, is appropriate to test NMO theory error, then static corrections generated representative of NMO theory error. Figure 2-15 shows a very convincing correlation between NMO theory error with offset (left) and the correlation of NMO theory error with a relative lateral change in velocity. The correlation coefficient with offset is 0.9874 and with relative

changes in velocity is 0.9995. Both correlation coefficients suggest a direct and linear correlation to NMO theory error and dependence on offset and relative change in lateral velocity variation. Given the second term is only dependent on offset and V_{RMS}, a correlation was expected. However, such a strong linear correlation was not expected. The linear regression indicates that a 10% increase in relative velocity contrast or 1 km increase in offset will add approximately 3 ms static shift due to NMO theory error. It should also be noted that the correlation coefficient is the same regardless of how the lateral velocity variation is represented.

2.7 Conclusions

The assumption that the moveout is near hyperbolic enough in shape to be corrected by NMO is insufficient when strong lateral heterogeneity of velocity is present. Based on velocity testing, a strong lateral variation in velocity is approximately a relative lateral change in velocity of 25%, and an offset of 5 km can cause anomalous events to be created due to NMO assumptions. Velocity contrasts less than 25% will have associated static corrections to compensate but not create events that are not truly present in the subsurface.

Offset distance could also bring out false subsurface events in very strong lateral velocity variations. Using a model that had 66% relative in velocity laterally offsets of 1.5 km or larger could generate events that are not representative of the true subsurface. It was seen during velocity testing that an offset of 5 km did not have a negative impact on the stack when the relative velocity change was 20%.

Using static corrections as a measurable proxy for NMO theory error shows that there is a very strong correlation between offset and NMO theory error, and relative change in lateral velocity variation and NMO theory error. The linear regression indicates that a 10% increase in relative velocity contrast or 1 km increase in offset will add approximately 3 ms static shift due to NMO theory error. Static corrections will still be present due to NMO theory error in areas with weak lateral variations in velocity (25% or less), but false reflections will not be created.

Chapter 3: Synthetic Data Testing

3.1 Introduction

I used Acceleware's acoustic modelling software AxWave for the forward modelling of both the Wedge Thrust Model (Figure 3-2) and the 1994 BP Statics Benchmark model (Figure 3-3). AxWave uses the finite-difference method to write the wave-equation in a discrete form. Because of the hyperbolic nature of the wave equation, the edges of the model become reflecting boundaries and do not inherently resemble the infinite half-space of the earth. As such, absorbing boundary conditions are applied to the model edges. This will be discussed in further detail in the modelling section of this introduction.

3.1.1 Geometry.

The geometry of these two lines is different. The wedge thrust model (Figure 3-2) is 20 m x 20 m cell grid that is 10 km long, and the BP 94 model (Figure 3-3) is a 5 m x 5 m grid that is 20 km in length. The acquisition geometry for the wedge thrust model was 80 m source spacing and 40 m receiver spacing equating a max fold of 63, while the BP 94 model was 40 m source spacing and a 10 m receiver spacing producing a max fold of 126.

3.1.2 Modelling.

The finite-difference method in AxWave numerically solves the wave-equation in a discrete form. The 8th spatial order approximation and a 2nd temporal order approximation of the Taylor series expansion were chosen for the centred finite-difference coefficients. When applying this method to the wave equation, the edges of the synthetic model behave as an acoustic and elastic boundary for the seismic wave and is reflected (Engquist & Majda, 1977). This presents a problem when the model is supposed to represent a smaller portion of a semi-infinite half-space such as the subsurface of the earth. The boundaries of the model cause the energy to interfere with the areas of interest and must be minimized as these artificial boundaries are not descriptive of the Earth's subsurface. Boundary conditions allow for the dampening of energy at the model edges so that they will have negligible interference on the boundaries of interest within the model. As such, a sophisticated Convolutional Perfectly Matched Layer

(CPML) boundary is used. The CPML reflectivity is a function of incident angle and frequency and is shown in Figure 3-1 for large – 20 cell – boundaries. The absorbing boundary performs best for normal-incidence wavefield and between 0-10% of the maximum recommended spatial frequencies (AxWave, 2014). CPML boundary conditions were also applied to the surface to avoid surface related multiple in the modelling.
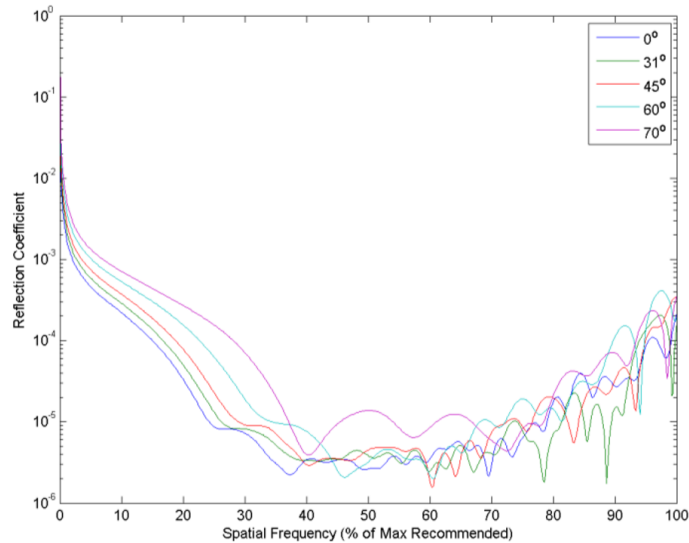
Figure 3-1 Convolutional Perfectly Matched Layers (CPML) reflectivity for large absorbing boundary – 20 cells. From AxWave (2014).

Another precaution was taken in forward modelling. The velocity models used for the forward modelling had a smaller sample interval than the velocity model used for the depth migration. If this were not done, the reflectors would have a blocky appearance because both the forward modelling and the depth migration velocity models would have had the same cell grid.

Using a forward modelling program, every fourth receiver station had a shot location using a 30 Hz source Ricker wavelet for each synthetic.

3.2 Methodology

3.2.1 Synthetic Data.

Three isotropic synthetic datasets were used for modelling and testing MMO. In one model, a wedge thrust model with multiple layers in the footwall (Figure 3-2), another model is a

synthetic acoustic dataset which was created at Amoco in 1994 and has since been publicly released in 2008 by BP (Figure 3-3). The SEG open data website has quoted that this 'model is so detailed that with the noticeable exception of lacking ground roll (since it's acoustic) it looks very much like "real data."' The third model is an interpretive or 'blocky' model of the BP 94 model (Figure 3-4).
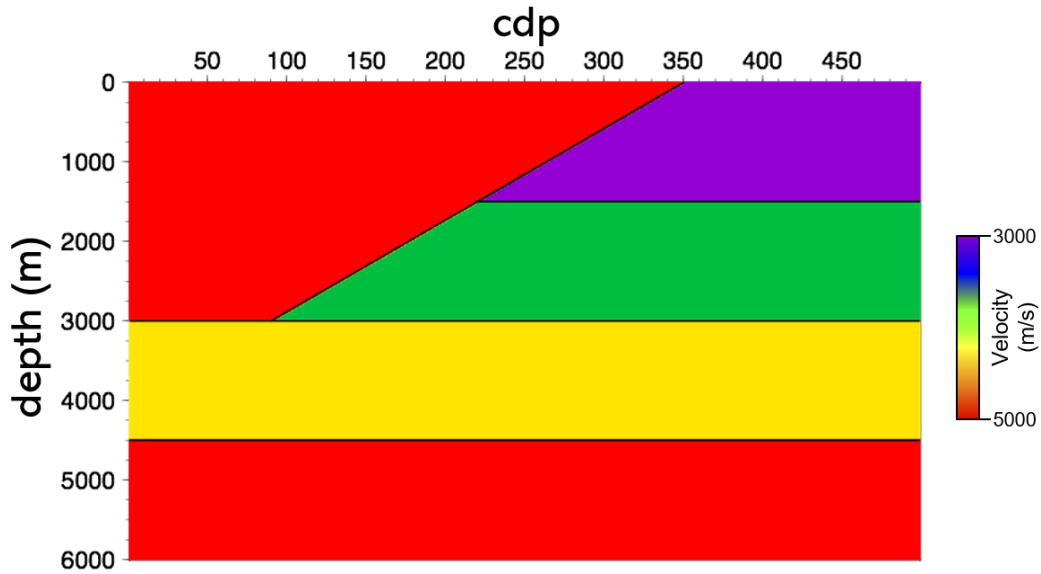
Figure 3-2 Wedge thrust model.

The wedge thrust velocity model is a 20 m x 20 m grid that is 10 km. This idealized model is used to determine the effectiveness of MMO on a synthetic thrust environment with a strong lateral velocity variation but theoretically required no static corrections. Due to the simplicity of the model, theoretical errors and inconsistencies can be readily identified.

The BP 94 velocity model and the interpretive model have a 5 m x 5 m grid that is 60 km line in total length. The BP 94 velocity model not only contains low-velocity layers but is also a suitable example for classic complex foothills environments. The interpretive model is representative of a velocity model that would be generated through the depth migration workflow using a real dataset. The purpose of this interpretive model is to understand the impact of a poorly understood velocity model on MMO statics and whether applying them may have

any value during the intermediate steps of the depth imaging process. Table 2-1 and Table 3-1 shows the velocities used to create the constant velocity panels to pick the NMO velocity field.
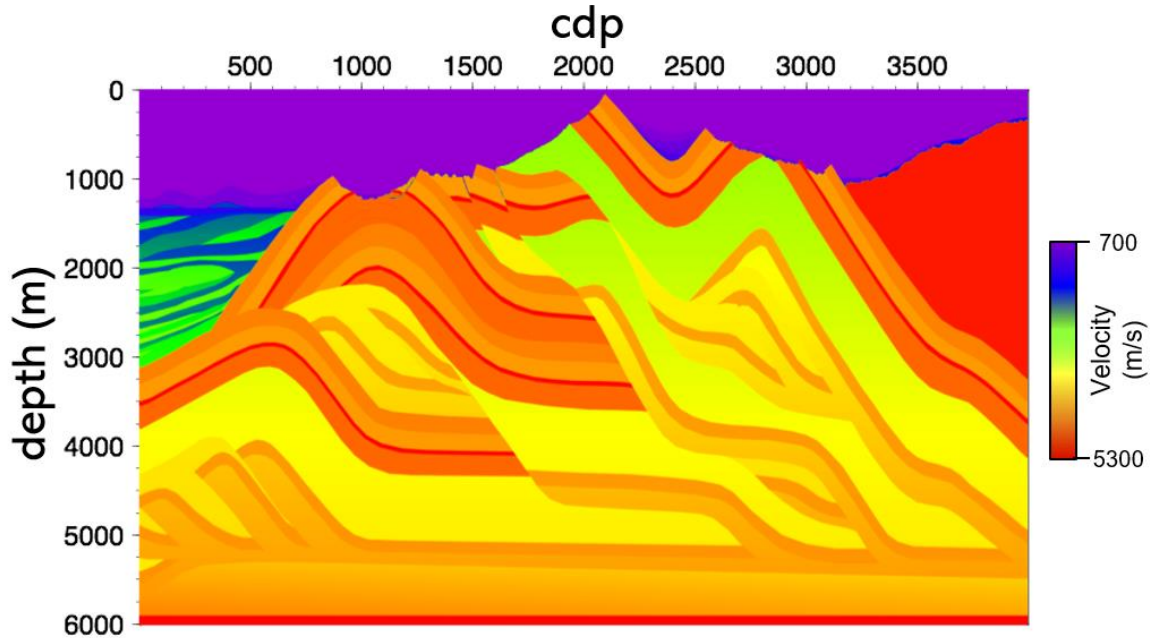
Figure 3-3 1994 BP statics benchmark model, created by O'Brien (1994).
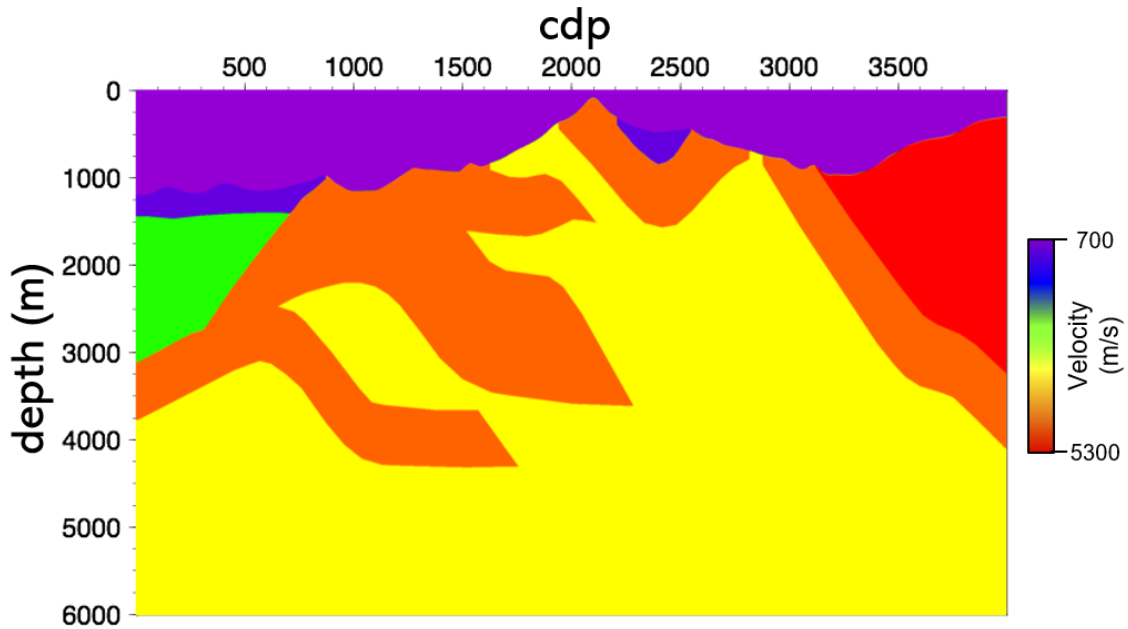
Figure 3-4 A representation of a poorly understood velocity model based on Figure 3-3.

Panel	Velocity (m/s)	Panel	Velocity (m/s)	Panel	Velocity (m/s)	Panel	Velocity (m/s)	Panel	Velocity (m/s)
1	700	16	1200	31	1950	46	3000	61	4500
2	725	17	1250	32	2000	47	3100	62	4600
3	750	18	1300	33	2050	48	3200	63	4700
4	775	19	1350	34	2100	49	3300	64	4800
5	800	20	1400	35	2150	50	3400	65	4900
6	825	21	1450	36	2200	51	3500	66	5000
7	850	22	1500	37	2250	52	3600	67	5200
8	875	23	1550	38	2300	53	3700	68	5400
9	900	24	1600	39	2350	54	3800	69	5600
10	925	25	1650	40	2400	55	3900	70	5800
11	950	26	1700	41	2500	56	4000	71	6000
12	1000	27	1750	42	2600	57	4100		
13	1050	28	1800	43	2700	58	4200		
14	1100	29	1850	44	2800	59	4300		
15	1150	30	1900	45	2900	60	4400		

Table 3-1 Values used to create constant velocity panels for velocity analysis for the 1994 BP statics benchmark model. These values are used to create stacking velocities and time migration velocities.

3.2.2 Model-based moveout.

As discussed in Chapter 1, MMO is a moveout velocity field that can be approximated by ray tracing through the depth velocity model. Effectively, the only change being recommended is the how the moveout velocity field is calculated.

As in Chapter 2, the wedge thrust model will be the model for to test the application of MMO and to gain a sense on the benefits and limitations. As there is no elevation change or low-velocity layer, no static corrections should be needed or applied. The BP 94 model has elevation changes and a smoothed elevation was used as the migration surface necessitating elevation statics to shift sources and receivers from topography to the floating datum.
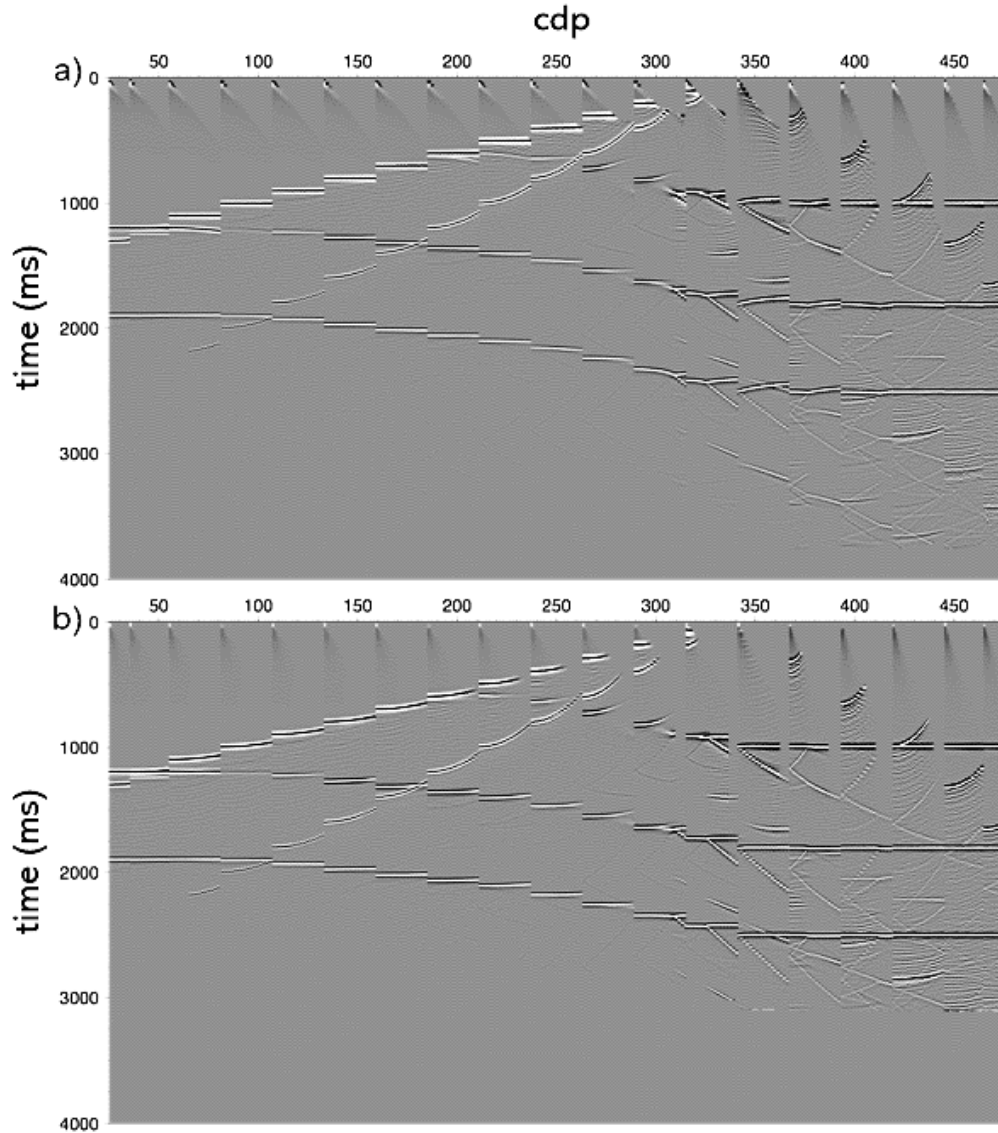
Figure 3-5 (a) NMO gathers, the NMO assumption on flat reflectors below the high-velocity dipping layer cannot flatten the gathers. (b) MMO gathers, MMO can compensate for the high-velocity dipping layer.

The moveout applied to the pre-stack gathers is derived from the depth velocity model. This takes advantage of depth imaging's ability to capture the raypath as it moves through the subsurface which is ignored when using NMO for reflection static corrections. Figure 3-5a illustrates NMO's inability to flatten the gathers under the leading edge of the velocity contrast which cannot flat using a single velocity that assumes lateral homogeneity. This will be compensated for in the reflection static calculations. By using the offset-dependent traveltime

summation, a more appropriate shift for each source and receiver can be determined for the input traces for depth migration. Figure 3-5b illustrates how MMO can flatten the gathers which will limit the magnitude of statics on the traces. This is important to note as the wedge thrust model does not require any statics. The correlation gate for reflection statics calculations is 1850-2700ms (Figure 3-6), with a correlation length of 100ms. These parameters were used for the NMO corrected stack, and the MMO corrected stack to derive the reflection statics.

A caveat to this is that during a typical depth imaging process the true velocity model is unknown. Therefore, an undetermined velocity model will likely produce a moveout velocity that will over or under correct the traces which will lead to greater MMO statics than a correct velocity model.
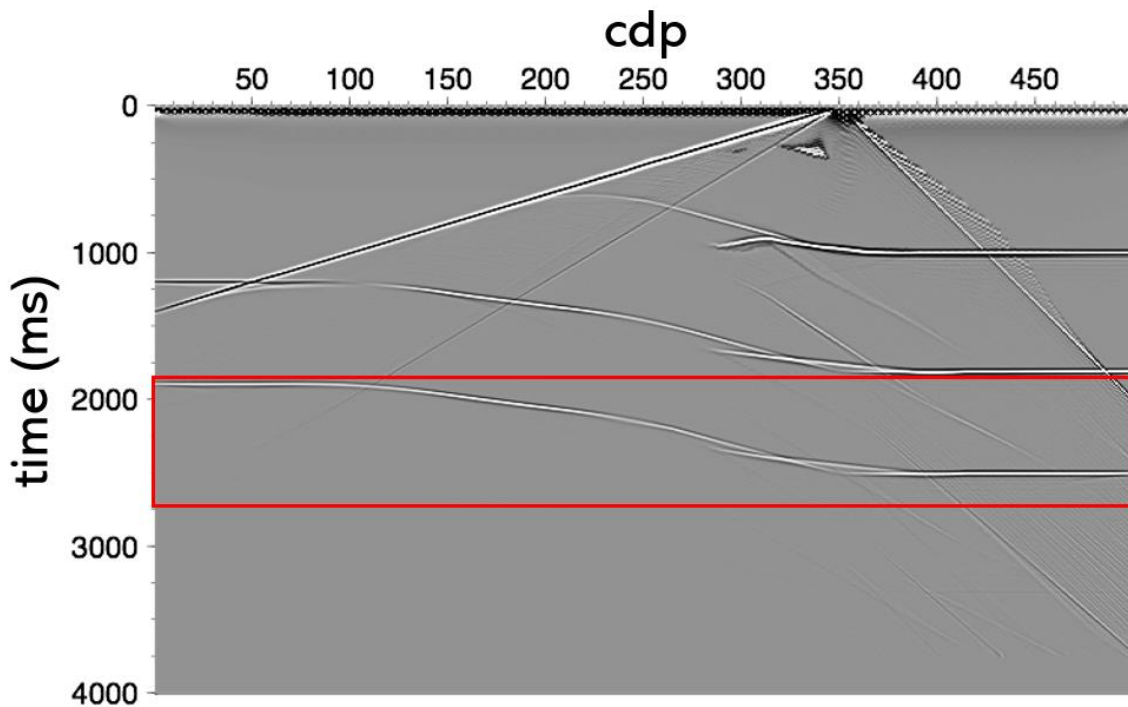
Figure 3-6 NMO stacked gathers in time for the wedge thrust model. The correlation gate is in red.

3.3 Results

Figure 3-7 shows the needed static corrections for the wedge thrust model (Figure 3-2) using the respective moveouts. The most significant static corrections are correlated to where there is a strong velocity contrast in the model. Despite the wedge thrust model not requiring any static corrections, both methods still have statics associated. The MMO statics are likely present due to the smoothing of the interval velocity model before migration which serves to stabilize the Kirchhoff depth migration.

Figure 3-8 shows the results of the BP 94 static corrections for the NMO derived statics, the MMO derived statics using the true velocity model, and the MMO derived statics using the interpretive velocity model. The magnitude of the MMO derived statics using the true velocity model is smaller relative to the other static corrections for the same line. Large NMO static corrections are most dominant near large velocity contrasts in the near-surface. MMO derived statics using the interpretive velocity model have similar magnitudes for statics, but they are unique. It is interesting to note that where there is little to no lateral velocity contrast between CDP 3200 and 4000 that static corrections are nearly identical with each method.
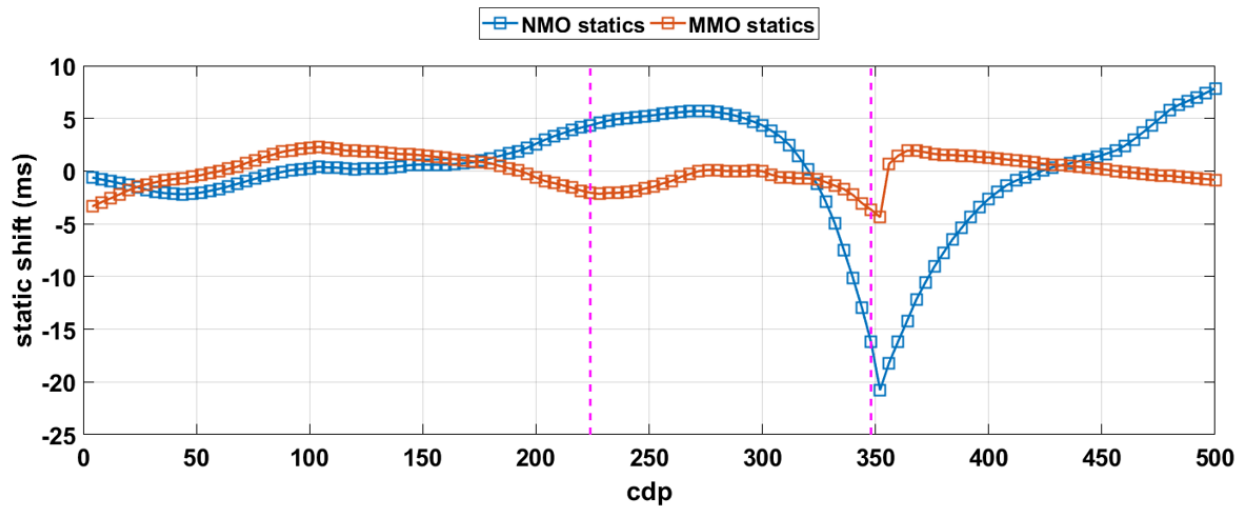
Figure 3-7 The MMO (red) derived statics and the NMO (blue) derived static corrections. The vertical pink lines show where there are strong velocity contrasts in the model. These lines correspond to high magnitudes of NMO derived statics corrections.
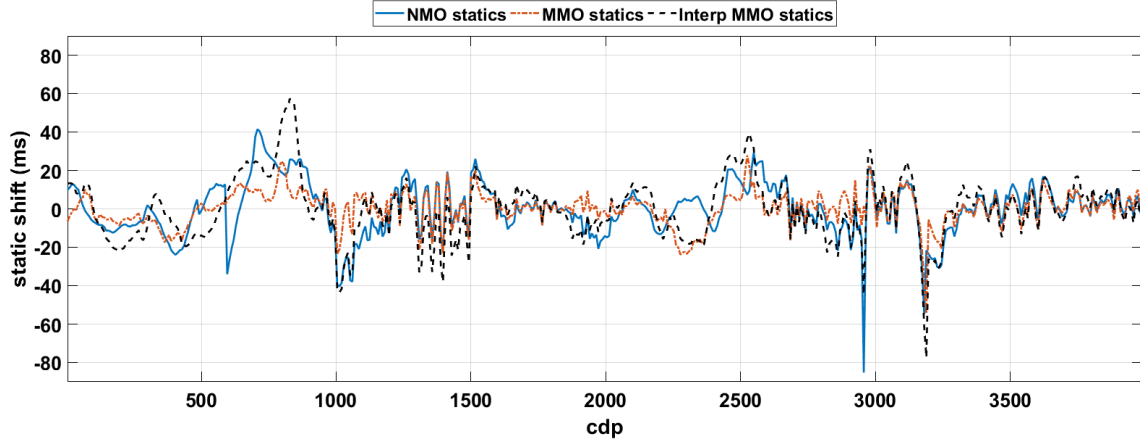
Figure 3-8 NMO (blue) derived statics, MMO derived statics from the true model (red), and MMO derived statics from the interpretive model (black). The magnitude of the MMO derived statics from the true model is the smallest. The MMO interpretive statics and NMO statics are similar in magnitude, yet the static shifts are different.
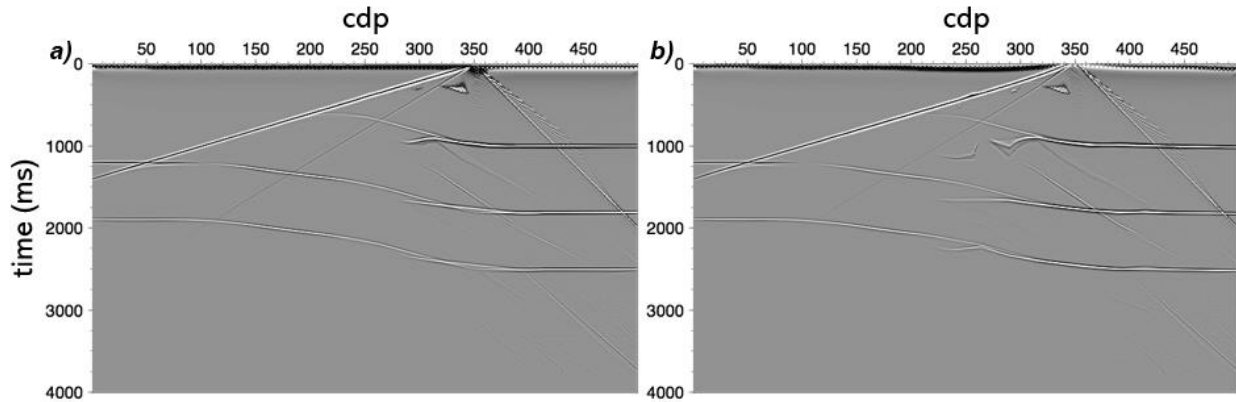
Figure 3-9 Wedge NMO stack in time (a) before and (b) after reflection statics
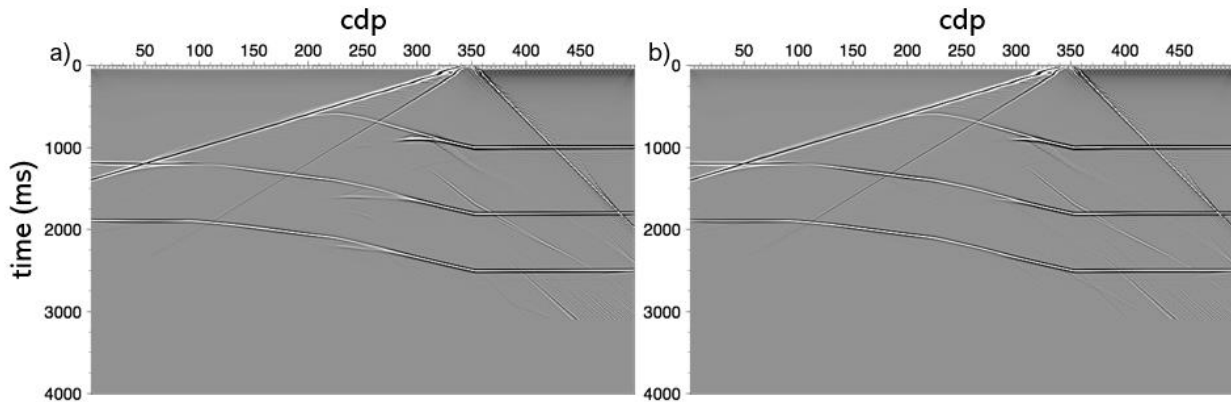
Figure 3-10 Wedge MMO stack in time (a) before and (b) after reflection statics
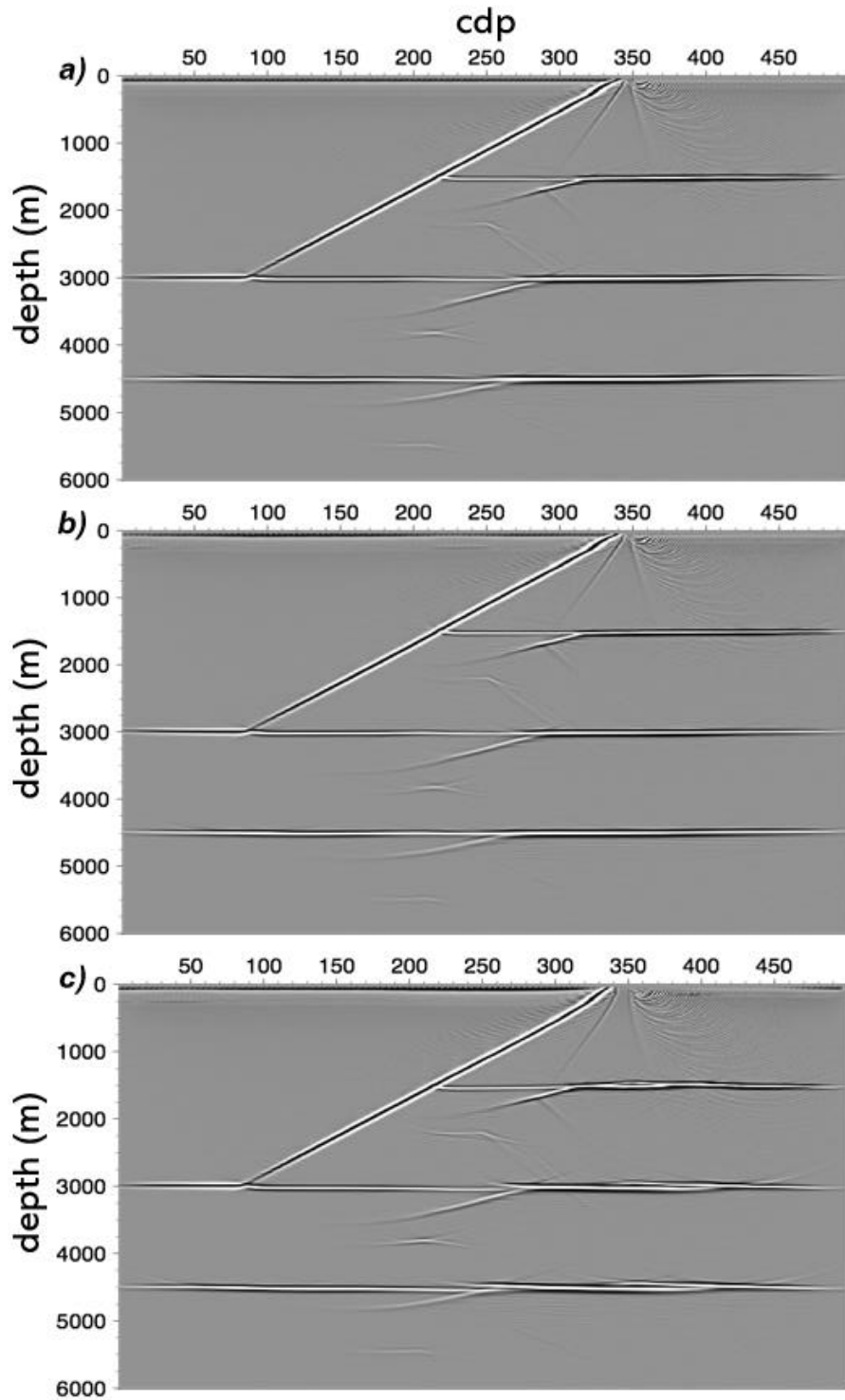
Figure 3-11 Wedge reflection statics comparison (a) no statics, (b) MMO statics, (c) NMO statics. Note the decreased coherency caused by the NMO statics.

The reflection static corrections performed as expected for the time NMO stack in improving reflector continuity within the correlation gate (Figure 3-9). For the time MMO stack, there is a negligible difference before and after static corrections (Figure 3-10). The quality of the reflector continuity on the time NMO stack (Figure 3-9a) versus the MMO stack (Figure 3-10a) prior to the reflection statics calculation is predicative of the required shifts to make a more coherent stack. Regardless of the coherency of the respective input stack, the quality of the output stacks is comparable in the correlation window (Figure 3-9b and Figure 3-10b).

Each of these reflection static corrections was applied to the input traces for depth migration, one with the NMO statics (Figure 3-11c; Figure 3-12c; Figure 3-13c) and another with MMO statics (Figure 3-11b; Figure 3-12b; Figure 3-13b).

The results from this test show that the MMO statics have increased reflector coherency. However, the benefit seems negligible on the wedge thrust model results when compared to the depth image without any static corrections applied. The reflection NMO statics have made the depth image reflections less continuous than when no statics when applied to the input gathers (Figure 3-11c). There is a notable difference in the magnitude of reflection NMO statics required relative to the MMO derived reflection statics, leads one to infer that these reflection NMO statics while effective for time processing, are unfavourable to the final depth image. The MMO derived reflection statics are unnecessary for the wedge thrust model because of the lack elevation and low-velocity layer, but the traveltimes used for MMO and the depth migrations were done on a smoothed velocity which may explain the slight increase in coherency.

Although the wedge thrust model clarifies and illustrates the basic differences between reflection NMO and MMO statics, the BP 94 results are more compelling due to its increased complexity and because of its likeness to real data. The BP 94 model results have a stronger contrast in the data quality between each output. This contrast is also enhanced because the true velocity model is known and used. Figure 3-13, is representative of the interpretive and poorly understood velocity model for the BP 94 solution. It is evident that this is a poorly understood velocity by the velocity pull-ups and push-downs as evident with the smiles and frowns on the stacks (Zhu, Lines, & Gray, 1998).
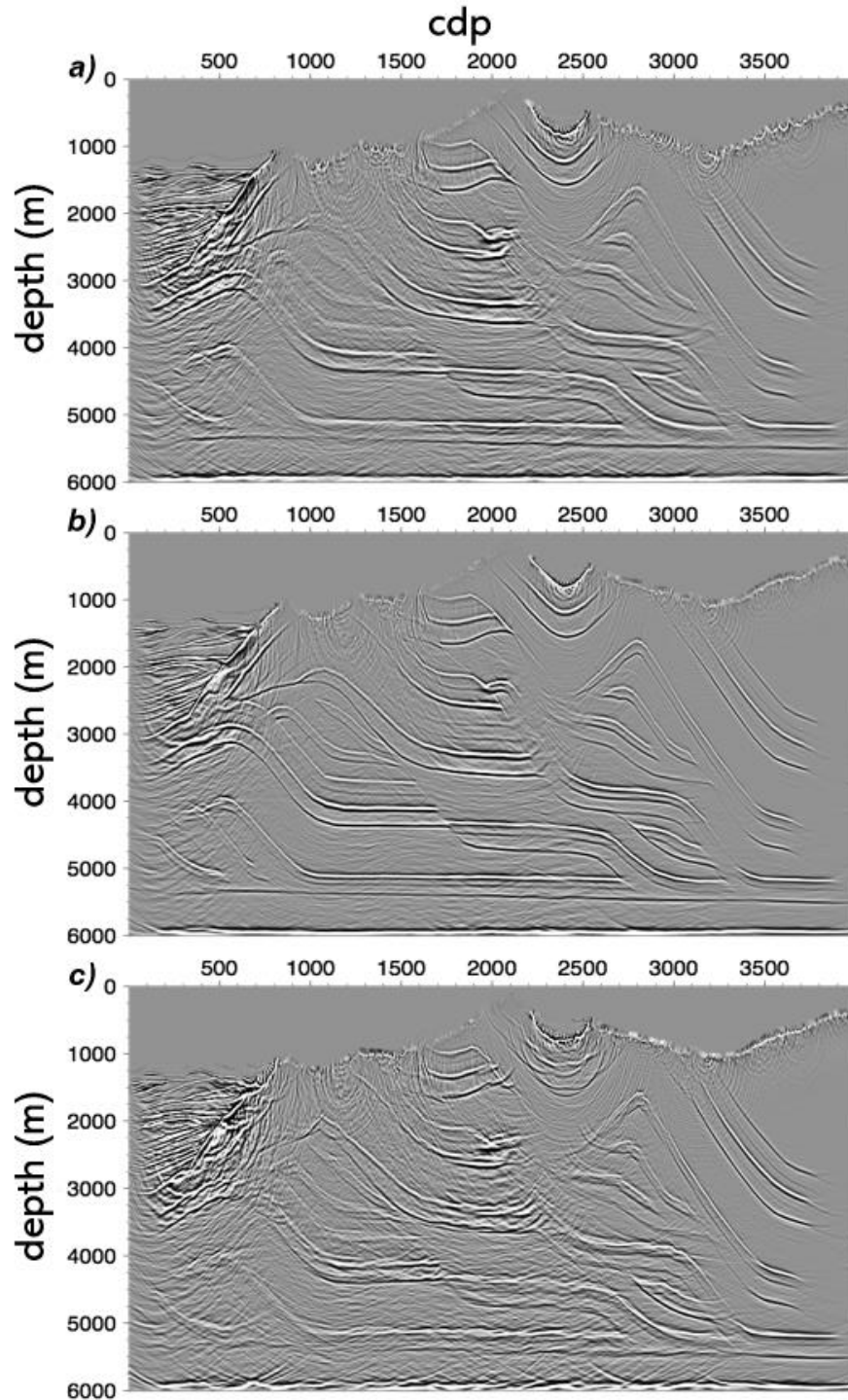
Figure 3-12 BP 94 reflection statics comparison using the model from Figure 3-3. (a) no reflection statics, (b) MMO statics, (c) NMO statics. Note the comparison between CDP 500 and 1500 and 2000 m and 4000 m depth. NMO statics are poor when the velocity model is well understood
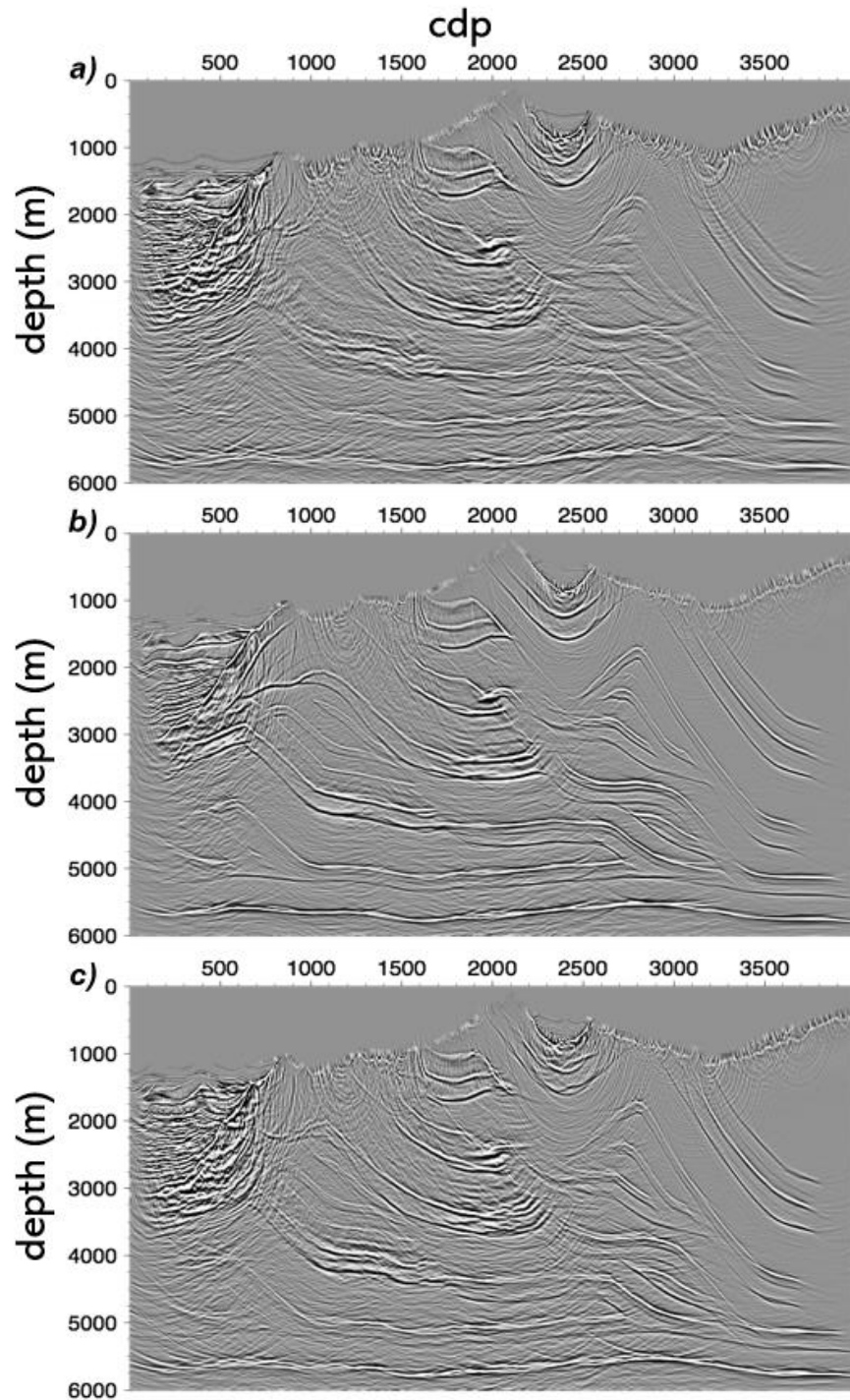
Figure 3-13 BP 94 reflection statics comparison using model the interpretive model from Figure 3-4. (a) no reflection statics, (b) MMO statics, (c) NMO statics. Note the comparison between CDP 500 and 1500 and 2000 m and 4000 m depth. NMO statics result in a better image than no statics.

3.4 Discussion

MMO statics provide a better image as a part of the depth processing workflow than using the reflection NMO statics from time processing. There is increased reflector coherency which allows for more confident interpretations of foothills datasets. The wedge thrust model shows little benefit from using MMO statics compared to no statics, but it does show decreased reflector coherency when the NMO statics are applied to the depth input gathers.

Reflection statics are more closely tied to the time processing workflow and are helpful through to time migration. Weathering corrections in time processing effectively prepares data for reflection statics, so the moveout velocity in near-hyperbolic and can be approximated by the stacking NMO velocity. However, these statics do not correct for the positioning issues related to the time processing of structured data and may add to them (Vestrum, Lawton, & Schmid, 1999).

These same static corrections derived in the time processing workflow are not valid for depth imaging. The NMO assumptions are largely invalid in the foothills data. Knowing that the only differences between Figure 3-11b & Figure 3-11 Wedge reflection statics comparison (a) no statics, (b) MMO statics, (c) NMO statics. Note the decreased coherency caused by the NMO statics.c and Figure 3-12b & Figure 3-12c are the MMO and NMO statics, only firms the thought of the negative effect of reflection NMO statics on the depth input traces.

Both the wedge thrust model (Figure 3-2) and the BP 94 model (Figure 3-3) allow for detailed investigation of the impact of statics on the final image. The resulting statics in Figure 3-7 and Figure 3-8 respectively capture the potential benefit and challenges of determining static corrections that are coupled to depth imaging. Intuitively, if the velocity model is well constrained, more accurate traveltimes will result in better MMO statics and depth image. However, even when the velocity model is poorly understood, MMO derived statics provide greater clarity in the stacked image for interpretation and the identification of subsurface structure.

Overall, MMO provides accurate traveltimes for the moveout velocity field which is dependent on the velocity model rather than how closely moveout can be approximated by a

hyperbola. The ray-tracing for the offset-dependent traveltimes provides a moveout velocity field that is coupled to depth imaging.

3.5 Conclusions

The assumption that the moveout is near hyperbolic enough in shape to be represented by the two-term NMO equation breaks down when the topography is not flat, strong lateral heterogeneity of velocity is present, and when there are variations in the seismic weathering thickness and velocities. It is important to note that the NMO velocity field did increase reflector continuity for the time pre-migration stack. Be that as it may, it did not improve for depth imaging and was more damaging when applied.

Depth migration has a unique algorithm from time migration and can accommodate for lateral velocity variation. Initially with depth imaging, the only difference is the migration algorithms. However, it seems that even the conditioning of the data prior to migration could be an important step as well. The MMO statics appear to be an important step in optimize the depth image as they are coupled to depth migration and the MMO can handle strong lateral velocity variations.

Chapter 4: Time Processing of Field Dataset

4.1 Data Conditioning

The field dataset is from the Canadian foothills and was publicly released in 1995 at the SEG AGM Workshop #6 in Houston as a foothills imaging benchmark. This dataset is known as the 'Husky Structural Dataset' and has a lot of geologic complexity and excellent signal quality (Stork, Welsh, & Skuce, 1995). For time processing, field seismic data needs to be conditioned. This starts with building the seismic geometry of the acquisition survey within the seismic processing software (SeisSpace) so that the acquisition from the field is the same in the software.

4.1.1 Amplitude scaling.
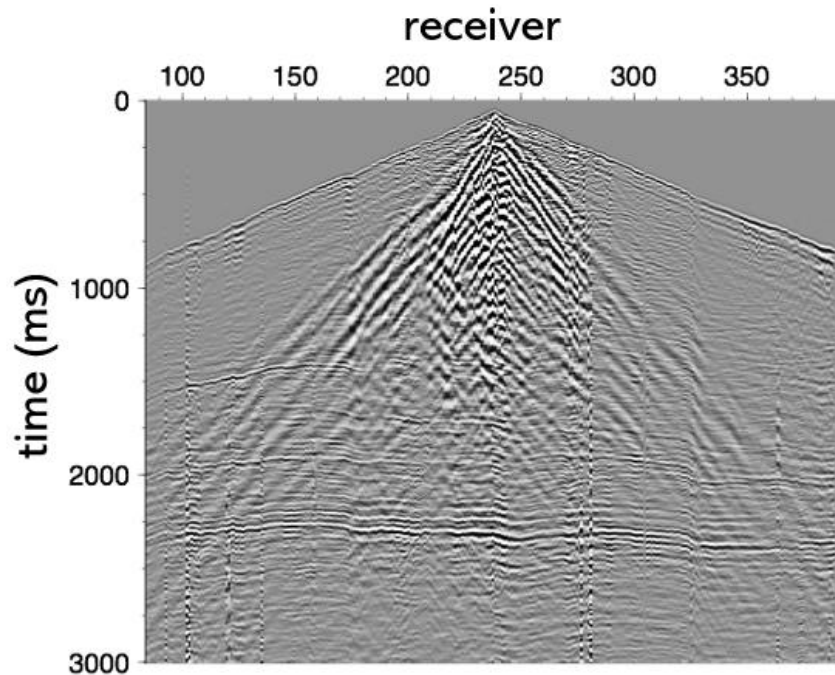
Figure 4-1 This is field shot 43. No processing has been applied and there are many coherent reflection events that can be seen in this gather. There are also dead traces and ground roll that are apparent.

During acquisition, there is a loss of amplitude due to attenuation and variable velocity contrasts from lithologic boundaries (Figure 4-1). Coupling and energy penetration will also vary between shots and between receivers.
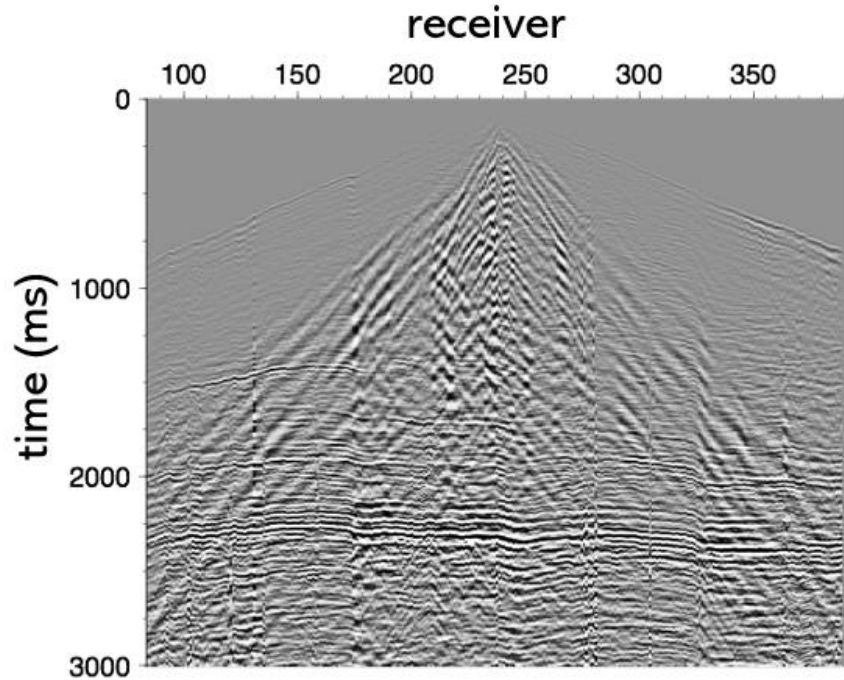
Figure 4-2 Field shot 43 with amplitude scaling. The amplitude scaling has boosted the strength of the signal deeper in the data causing the shallower signal to dim.

As a result, some traces will have stronger or weaker amplitudes relative to others. The time function gain boosts amplitudes of deeper reflectors on a trace by trace basis applying a correction of the time of the signal raised to a constant power (SeisSpace-ProMAX, 2015). These amplitudes on a single trace can also be statistically scaled relative to many traces using a surface consistent amplitude scaling method known as Gauss-Seidel iterative inversion method. This method decomposes the initial amplitude estimates into the source and receiver components. In each component, the mean amplitude of all the traces become the amplitude for all traces. This decreases the effects of amplitude variability on the shot record (Figure 4-2).

4.1.2 Noise attenuation.

The next step in conditioning the data is the noise removal. This is done in two parts, first by removing anomalously high amplitudes, then by removing surface-wave related noise. F-X median noise burst removal which looks for anomalously high amplitudes within a window and at adjacent traces in the frequency domain. The high amplitudes are then replaced with a median value from adjacent traces. Only the portion of the frequency band that seems noisy is replaced within the designated window. Surface wave noise attenuation transforms the data from the time-space domain to the frequency domain.

4.1.3 Deconvolution.

The goal of deconvolution is to recover the earth's reflectivity series from the seismic traces (Figure 4-3). The seismic trace must be separated into the convolutional effects of source, receiver, offset and subsurface response.
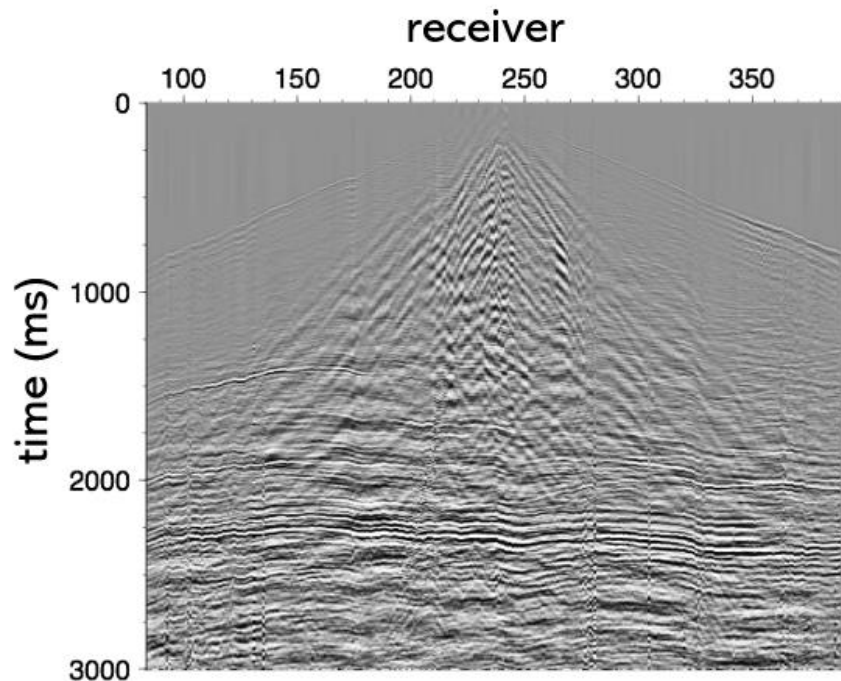
Figure 4-3 Field shot 43 with amplitude scaling and deconvolution. Deconvolution has helped to return some of the higher frequency information but has also introduced stronger low frequency signal. Another pass of noise attention will be applied.

Assuming the data is minimum phase and knowing the amplitude spectrum of each seismic trace, the log-amplitude spectrum for all source, receiver, midpoint, and offset information are computed using a linear system of equations. The error between the observed data and each component must be minimized to build a minimum phase operator and deconvolve each trace in a surface-consistent manner (SeisSpace-ProMAX, 2015).

After deconvolution, another pass of noise attenuation was applied with the same parameters in section 4.1.2.

4.1.4 Time-variant spectral whitening.
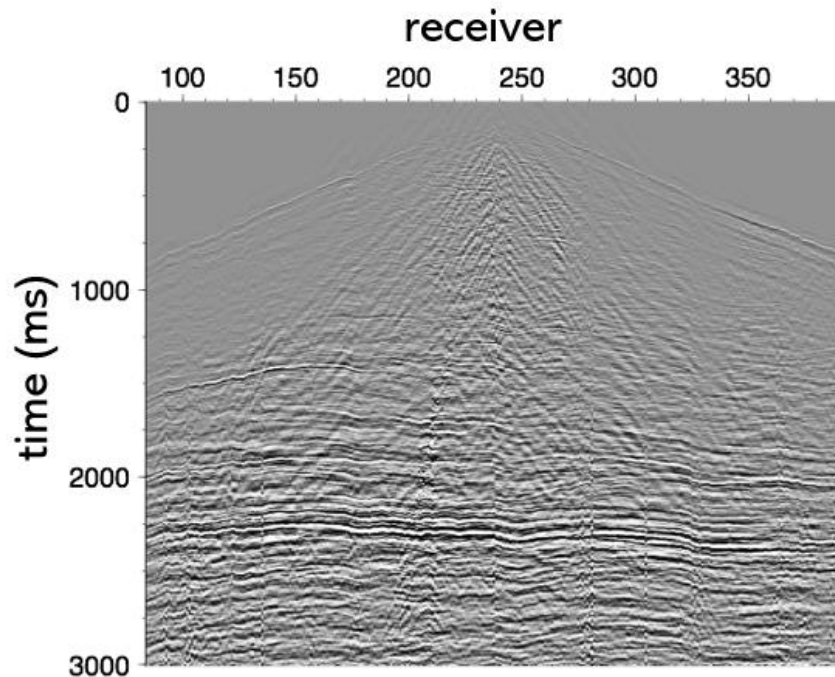
Figure 4-4 Field shot 43 with amplitude scaling and deconvolution and time-variant spectral whitening. The TVSW has increased the strength of the high frequencies in the data in the window below 1000 ms.

Time-variant spectral whitening (TVSW) applies different gains to individual frequency bands as a function of time. The bandwidth is linearly interpolated between desired timing intervals and is constant passed the last interval. Each input trace is transformed to the frequency domain and multiplied by the filter slice spectrum, inverse transformed back to time, and is gained to each narrow bandpass-filtered trace which makes the mean absolute amplitude constant

within the time gate. Both filtered traces and gained filtered traces are then summed to produce the whitened output trace and an average scalar trace (SeisSpace-ProMAX, 2015). The output trace amplitudes are variably scaled over time to match the input trace and ideally restore true amplitude (Figure 4-4).

4.2 Refraction Statics

Tomographic refraction statics are calculated by first picking first-breaks on the refracted arrivals on the shot data. It is assumed that the first arrivals are refracted from the base of seismic weathering or the low-velocity layer, see section 1.3. Once the first-breaks are picked on all the shots and traces (Figure 4-5 First-break picks to estimate near-surface velocity modelling.), the picks and an initial model are inputs in the tomographic inversion algorithm to create the near-surface velocity model (Figure 4-7). After 12 model updates, the error (RMS misfit, Figure 4-7) between the near-surface model data and the field data is minimized and have converged onto a tomographic near-surface velocity model (Figure 4-8).
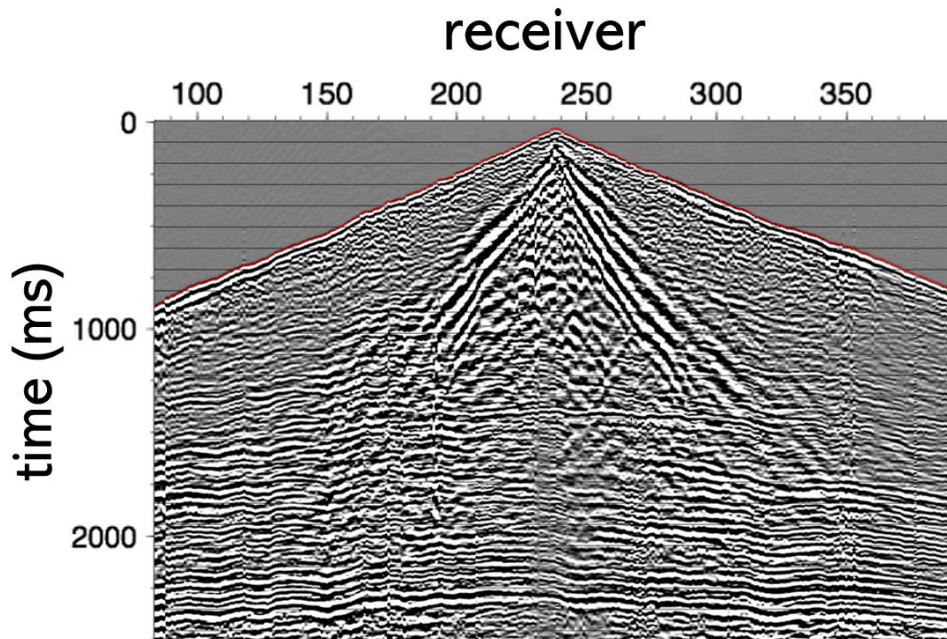
Figure 4-5 First-break picks to estimate near-surface velocity modelling. The red dots are the first-break pick on the first trough of the initial wavelet.

This tomographic near-surface velocity model is then used to calculate refraction static corrections for each source and receiver by calculating the time differences between the final datum and the intermediate datum in the subsurface (Figure 4-9). It is possible to generate an image without applied refraction static corrections (Figure 4-10). However, the diffractions and reflector strength on the stack with refraction statics applied (Figure 4-11) are much more continuous and consistent and will allow for a much more constrained velocity analysis and reflection statics calculations to optimize the final image.
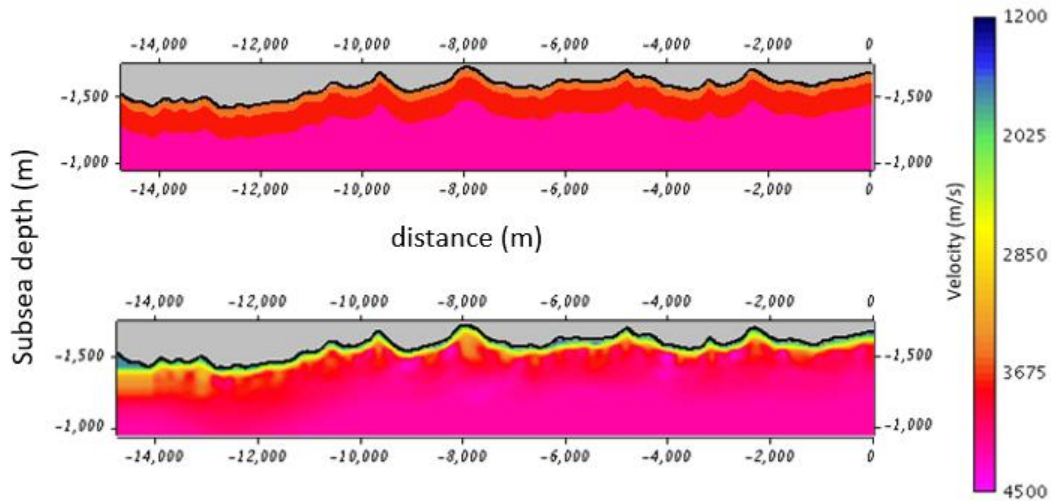
Figure 4-6 Initial (top) and final (bottom) inversion near-surface velocity models. After 12 tomographic iterations there is greater detail in the final inversion model.
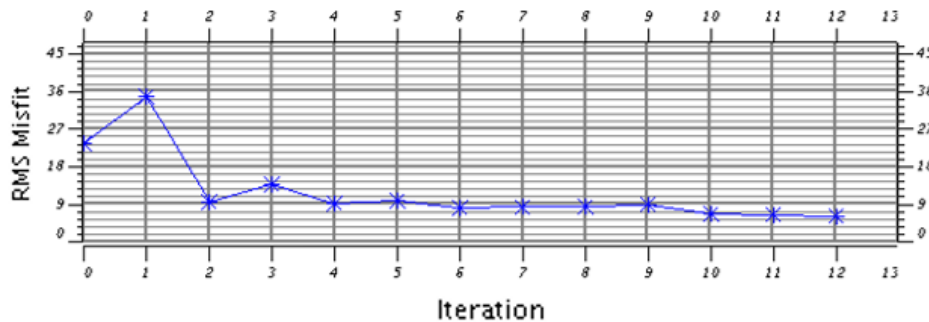
Figure 4-7 Inversion iterations of near-surface modelling to converge on the final model. The largest gain is in the first few model iterations. The remaining iterations are to ensure that the model has converged appropriately. If iteration 4 was the last, I would not be confident in the convergence of that model.
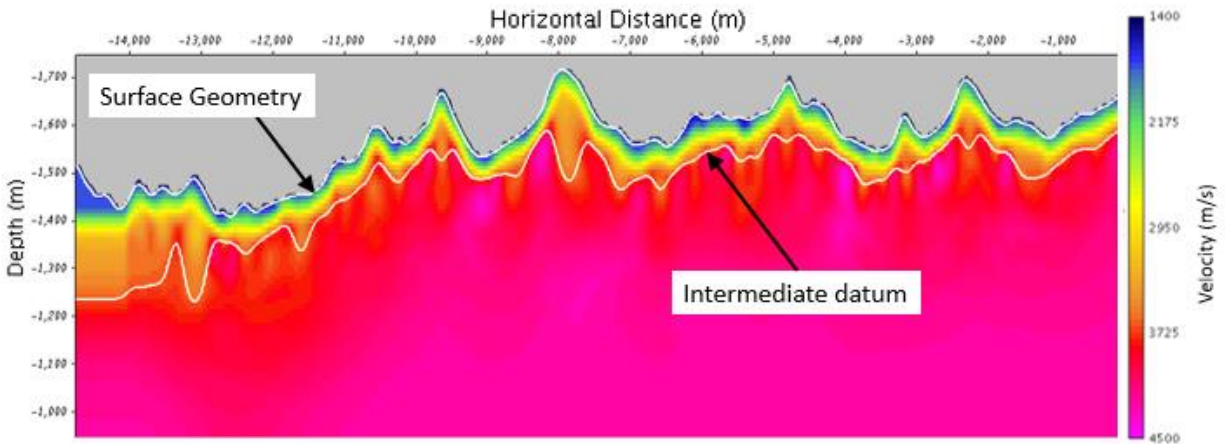
Figure 4-8 Final inversion generated from tomographic inversion of traveltime refraction data based on picks as shown in figure 4-5. The top white line represents the surface geometry. The bottom white line is the intermediate datum which was picked at the 3700 m/s iso-velocity boundary and smoothed to remove sharp changes.
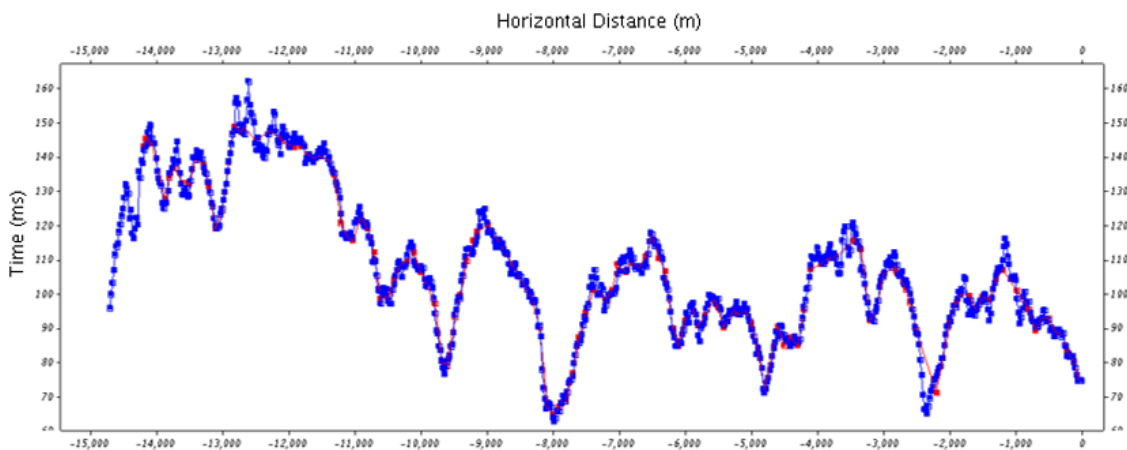
Figure 4-9 Shot (red) and receiver (blue) statics generated from the final tomographic near-surface velocity model.
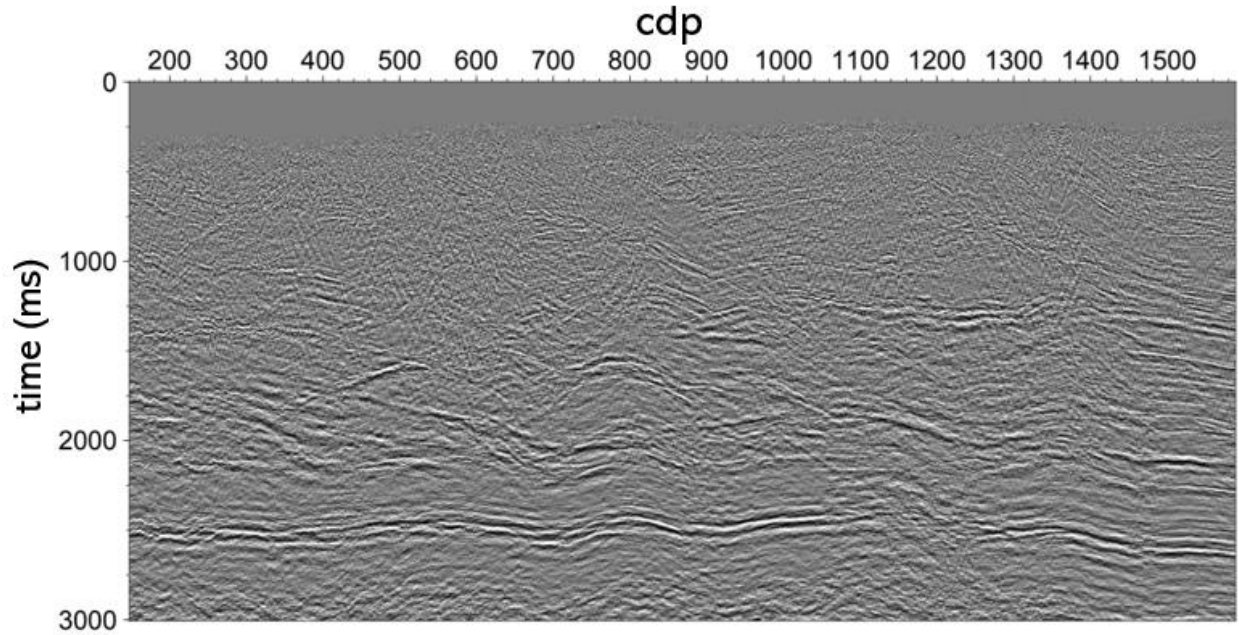
Figure 4-10 Brute stack of the field data using 3500 m/s and 5800 m/s at 1 and 2.2 s respectively, and _no refraction statics applied._
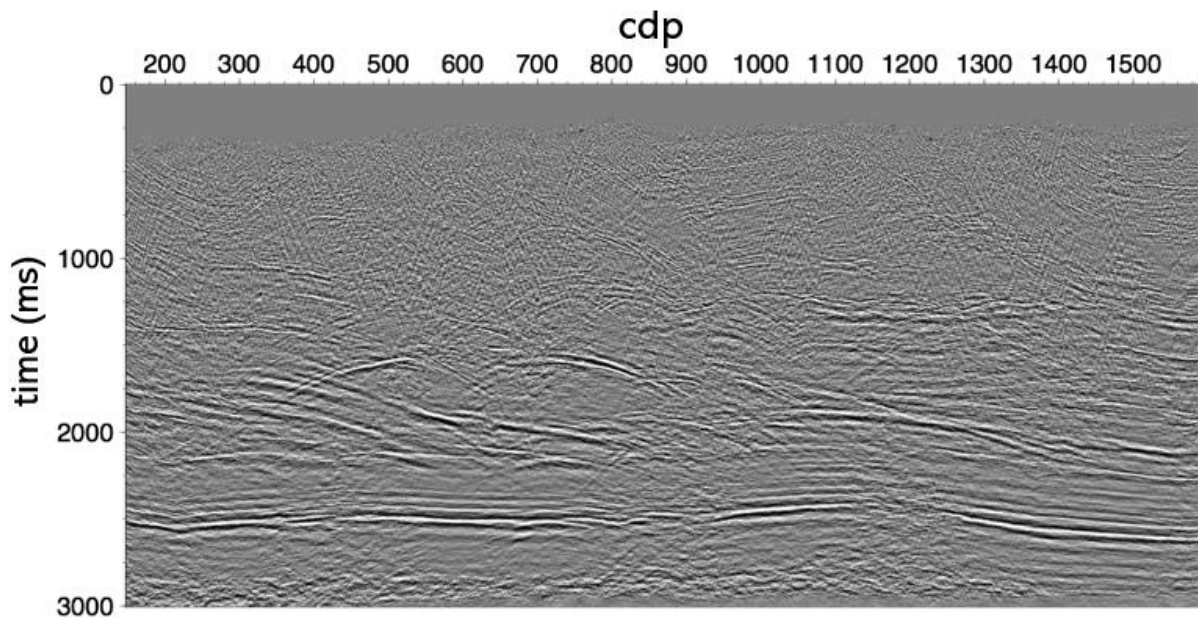
Figure 4-11 Brute stack of the field data using 3500 m/s and 5800 m/s at 1 and 2.2 s respectively with refraction statics applied.

4.3 Reflection Statics

4.3.1 Velocity analysis.

Picking NMO velocities in structured data is difficult. Often there are anomalies and coherency issues with foothills datasets that do not allow for traditional semblance velocity picking. Instead, creating a series of constant velocity stacks from 3000 m/s to 6000 m/s allows for use of the stack summation to enhance the lack of coherency that can often be seen on gathers. This way reflector sharpness, continuity and coherency are used to determine appropriate stacking velocities. In Techco Geophysical's tool VELANAL, control lines are used to assign and lock the velocity of choice that optimizes the stack. A composite stack is also created with the chosen velocities. By switching between viewing the composite stack and the current constant velocity stack, I visually determined which velocities enhanced the image based on reflector sharpness, continuity, and coherency. Once the final NMO velocity field was chosen, I applied it to the data in preparation for reflection statics calculations. The same methodology was implemented for time migration velocities.
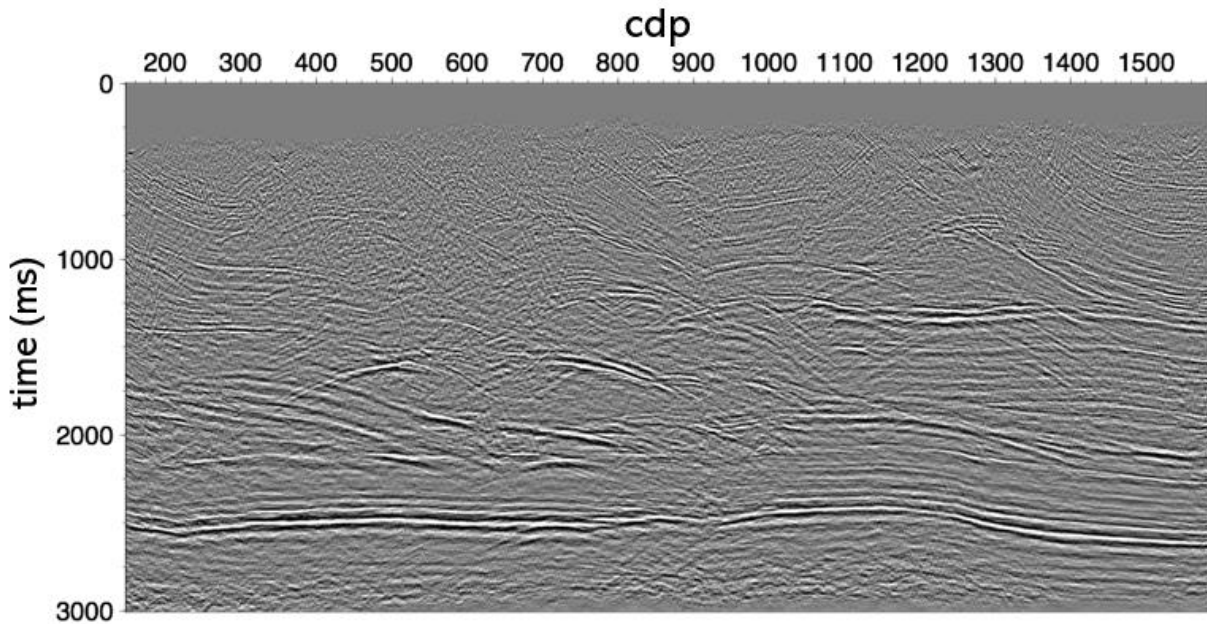
Figure 4-12 NMO stack using velocities from Figure 4-13
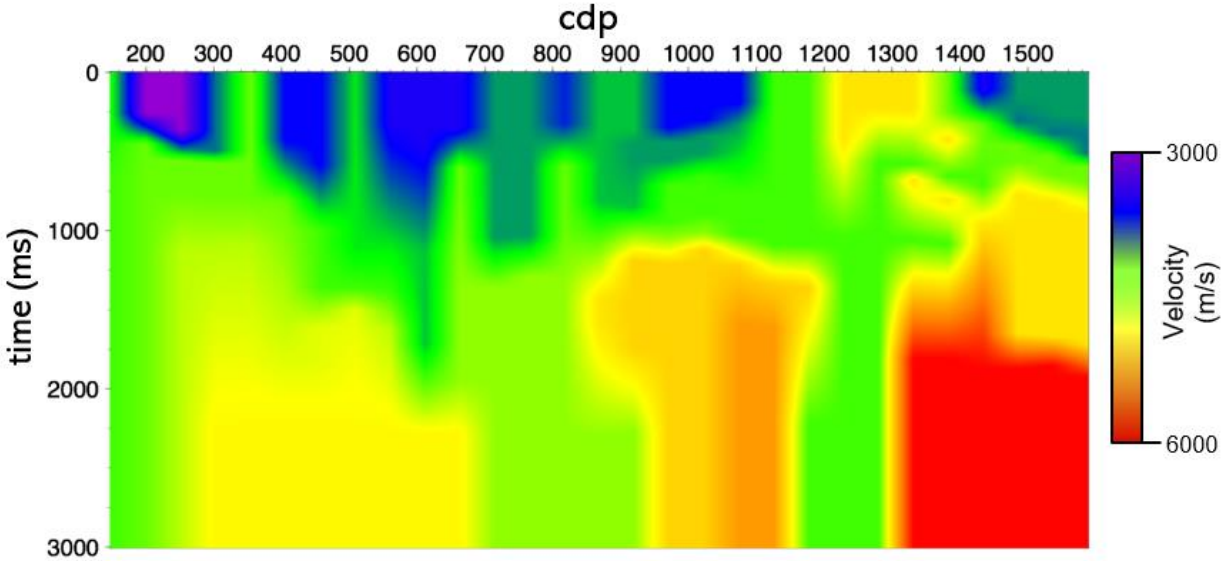
Figure 4-13 NMO stacking velocities used to create Figure 4-12

Panel	Velocity (m/s)	Panel	Velocity (m/s)	Panel	Velocity (m/s)
1	2800	9	3600	17	4400
2	2900	10	3700	18	4500
3	3000	11	3800	19	4600
4	3100	12	3900	20	4700
5	3200	13	4000	21	4800
6	3300	14	4100	22	4900
7	3400	15	4200	23	5000
8	3500	16	4300		

Table 4-1 Values used to create constant velocity panels for velocity analysis for the Canadian foothills dataset. These values are used to create stacking velocities and time migration velocities.

A brute velocity stack (Figure 4-11) was created using a time-variant velocity function with values of 3500 m/s at 1 s and 5800 m/s at 2.2 s. The velocity is linearly interpolated between these values and is constant beyond either side. Often various brute stack velocities are chosen to be applied, and the velocities that create the best brute will be chosen and guide the range of NMO velocities to investigate (Table 4-1). Through velocity analysis the NMO velocities (Figure 4-13) are determined based on the semblance plot and the optimized stack

(Figure 4-12) which has greater coherency and reflectivity than the brute stack (Figure 4-11). At 1 s across the NMO stack, there is a marked improvement in the reflectivity. The basement reflector at 2.5 s also show a marked improvement and most significantly at CDP 400 and 1200.

4.3.2 Static corrections.
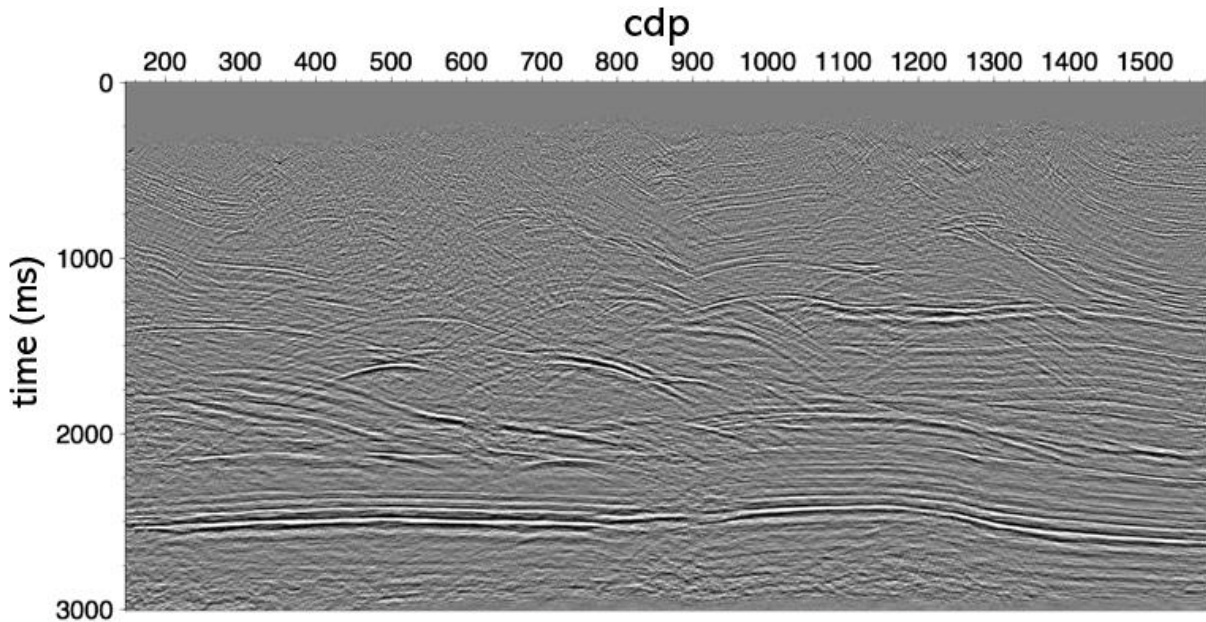
Figure 4-14 NMO stack using velocities from Figure 4-13 after applying reflection statics.

The reflection static corrections were calculated as described in section 1.3 of Chapter 1. Although equation 1-3 has four terms that are involved in static corrections, only two of them are applied to the data, the receiver static (R_j) and source static (S_i). The structure term C_k and residual NMO term M_k are not applied to the data. Figure 4-14 has a significant increase in reflector coherency after reflection statics are applied. To highlight an area, between CDP 800 and 1000 the trace has a shift in time that visibly enhances the coherency of the reflections.

4.4 Kirchhoff Prestack Time Migration

Kirchhoff migration is a method that sums traces from along a predicted diffraction curve of unknown amplitude. This summation is done within a given aperture that applies an analytical diffraction estimate for an assumed subsurface diffractor location. Traveltime calculations from the RMS velocities are used to identify which input sample to scale, and sum Perturbation

Theory gives ground for the assumption of local linearity in reflector behaviour. These small perturbations allow for any reflector to be sufficiently approximated given a series of closely spaced diffractor locations. Kirchhoff migration assumes that the reflected energy is sampled enough to be measured accurately.
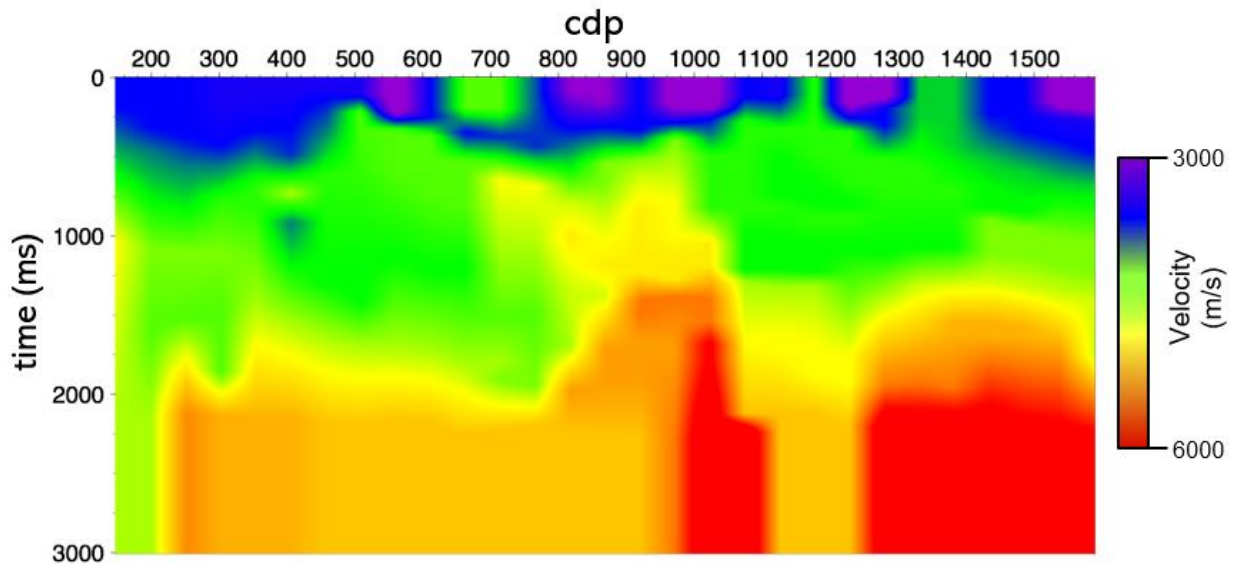
Figure 4-15 Prestack time migration velocities used to create Figure 4-16
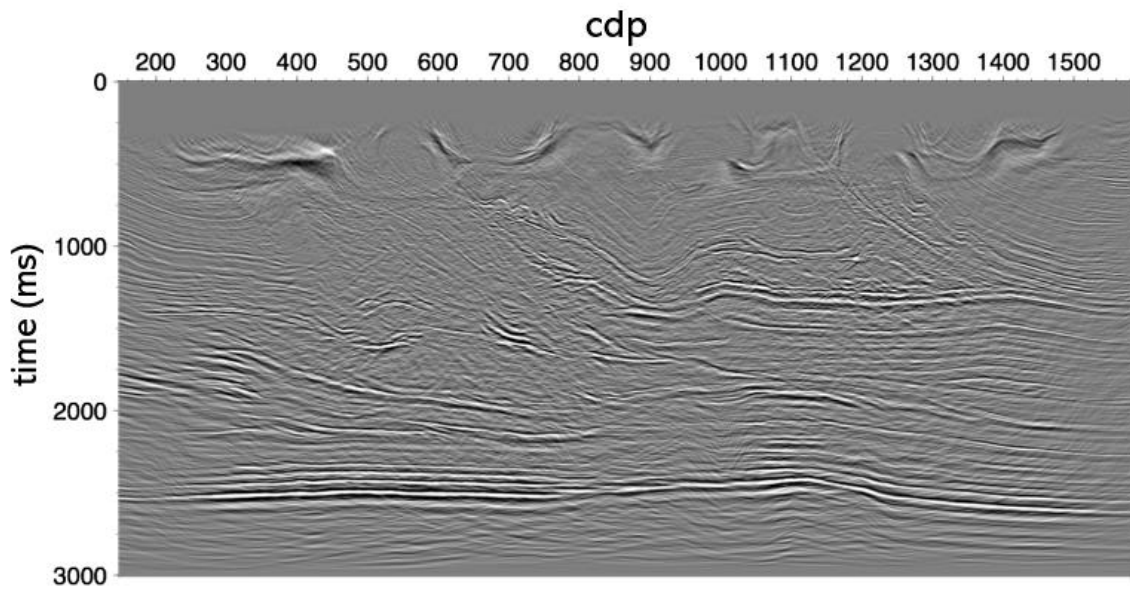
Figure 4-16 Prestack time migration with no post-migration processing.

In determining the appropriate migration velocities, the velocity analysis method described in 4.3.1 is now applied for migration stacks. This is run for 43 panels migrated stacks with constant velocities ranging from 2800 m/s to 7000 m/s and is scanned for the best reflector coherency and sharpness in the composite image, which closely resembles what the final migrated image. A final migration is done using the velocities (Figure 4-15) chosen to optimize the composite image (Figure 4-16).

4.5 Post-Migration Processing

As seen in Figure 4-16, there is a significant amount of low-frequency noise that is related to refractions and direct arrivals. As this noise is generally dominated on the far offsets near the surface, a mute is applied to remove this noise. It is not obvious where the mute should be positioned as the signal-to-noise ratio gradually gets weaker at far offsets. As such, a few mutes are picked and evaluated based on what optimizes the image (Figure 4-17).
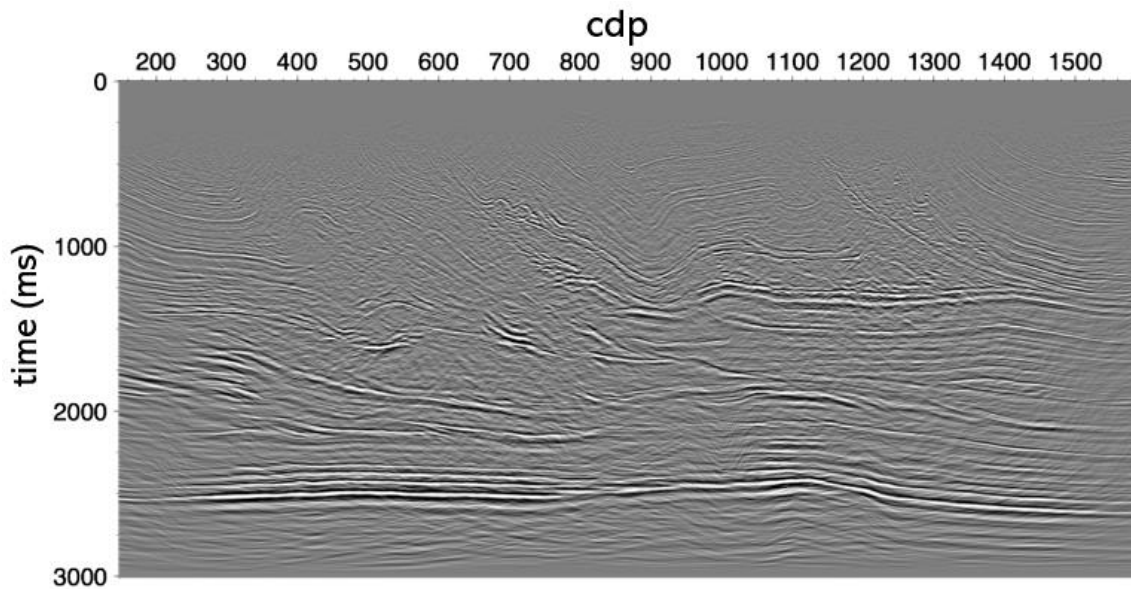
Figure 4-17 Prestack time migration with mute.

Figure 4-18 has and bandpass filter and automatic gain correction (AGC) applied. The bandpass filter is a time-variant Butterworth filter of 3-12-70-80 Hz in the first window, 0-1400 ms, and 3-12-50-60 Hz in the second window, 2200-3000 ms. The first parameter (3-12-70-80 Hz) was constant from the beginning of the trace to the end of the first window (1400 ms)

decreased with a linear taper to the beginning of the second window. The second parameter (3-12-50-60 Hz) increased with a linear taper from the end of the first window to the beginning of the second window (2200 ms) and is constant to the end of the trace. The AGC is applied the mean value of a rolling 600 ms window to normalize the strength of the reflectors in the image.
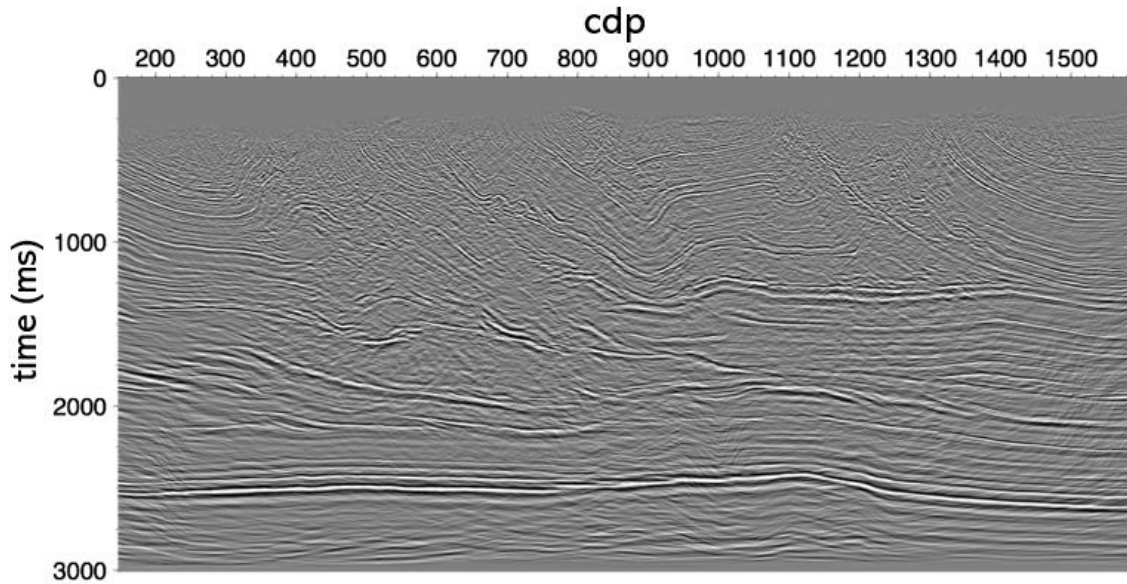
Figure 4-18 Prestack time migration with mute, bandpass filter, and AGC.

4.6 Conclusion

Pre-stack time migration can be valuable where there is increasing structural complexity and conflicting dips in the data, which results in inaccurate velocity analysis. Analysis of statics computation and application also had a large impact on the result and were sensitive to changes in the stacking velocity field.

This seismic dataset was structurally complex, had strong lateral velocity contrasts and has good signal to noise content. An optimal image was achieved through judicious investigation of both the stacking and migration velocities. The work put into deriving sufficient refraction and reflection static corrections helped to enhance the detail of the final image. The goal for the basic time processing was to create the optimal PSTM image. This was done by retaining as much signal as possible in the data conditioning phase to optimize the surface-consistent static corrections and velocity analysis.

Chapter 5: Depth Processing of Field Dataset

5.1 Velocity Model Building

It has been the author's experience that velocity model building highly-structured reflection seismic data benefits the most from an interpretive and geologically constrained approach. Accurately positioning of velocities and bedding planes in complex-structured data with anisotropic parameter allows for non-unique solutions (Newrick, 2004). As such, a velocity model that has been converged upon through an iterative interpretive depth imaging process that is geologically constrained can give greater confidence in the final depth imaging parameters than other automatic tomography methods. This imaging process begins in the depth domain by converting the time stack to depth using the replacement velocity. The velocity model is built interpretatively (Figure 5-1) using the latest image to identify where the velocity magnitudes and boundaries should be until the velocity model is optimized (Murphy & Gray, 1999; Gray, Cheadle, & Law, 2000).
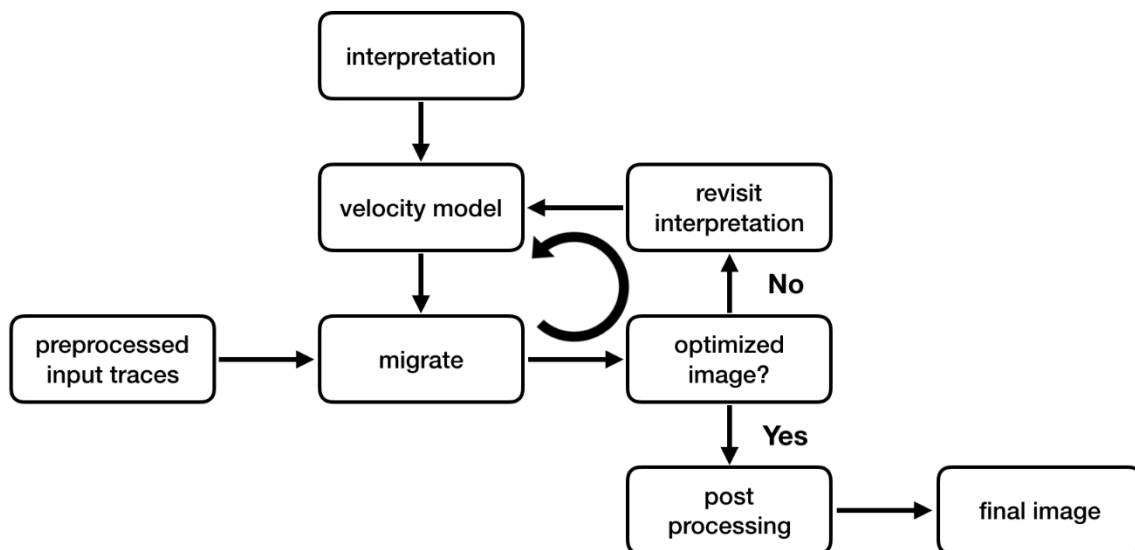
Figure 5-1 The interpretive velocity model building workflow based on conventional preprocessing of the input traces to depth migration. – Courtesy of Rob Vestrum

The initial velocity model is built from available well-log data and the migrated velocities used for prestack time migration (Figure 4-15). It has also been of benefit to the author that this field dataset was released for industry and academic research (Stork, Welsh, & Skuce, 1995). As such, the publication of final depth images and some velocity models have aided in providing a benchmark of results of different processing solutions to overcome common issues with structured land data.

Throughout the depth migration, anisotropic values of $\varepsilon=12\%$ and $\delta=3\%$ have been constant. Vestrum, Lawton, & Schmid (1999) discussed and illustrated the value of using non-zero assumptions of anisotropy despite being difficult to determine analytically. While these values are not correct, they are conservative and are likely to be more correct than assuming no anisotropy, which would yield artificially high isotropic velocity values for depth imaging.

5.2 Depth Statics
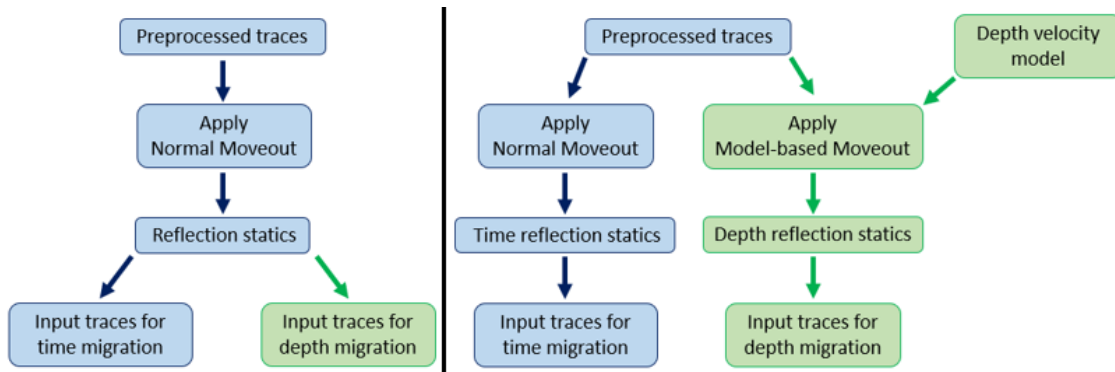
Figure 5-2 (Left) Conventional reflection statics for both time and depth migration. (Right) Depth specific reflection statics. This shows how depth statics derivation can be decoupled from time statics.

The reflection static corrections were calculated as described in section 1.3 of Chapter 1. Although equation 1-3 has four terms that are involved in static corrections, only two of them are applied to the data, the receiver static (R_j) and source static (S_i). The structure term C_k and residual moveout term M_k are not applied to the data.

To fully use the advantages of depth imaging, the assumptions with the static corrections should also be tailored to the depth migration algorithm (Figure 5-2). Taner, Koehler, & Alhilali (1974) discussed assumptions that are appropriate for the time-domain but lack application in depth: the effect of the near-surface is purely a time delay, and the time-delay is the same regardless of reflection time. These assumptions justify using a time shift that is constant or 'static' for the entire trace.

Applying static corrections created derived from MMO is still a constant shift, but it is a dynamic moveout that allows for asymmetric non-hyperbolic moveout and is kinematically related to depth imaging. MMO is employed using the reciprocity assumption for the relative source and receiver positions (Taner & Koehler, 1981) which allows a consistent method in applying the traveltimes to the respective source and receiver trace.

5.3 Kirchhoff Depth Migration

Depth migration differs from time migration in how it uses velocity models. Depth imaging is the process of making velocity structures well understood using seismically constrained inferences. Time migration and ignores ray bending at velocity boundaries. Depth migration is sensitive to velocity boundaries and the resulting image is dependent on the accuracy of the velocity model with respect to the subsurface (Etgen & Kumar, 2012). Depth imaging migrates along the diffraction shape derived from the velocity model. This diffraction shape that is not always hyperbolic like in time migration but is sensitive to poorly understood velocity models and may require many iterations which further increases run time. However, when the velocity model is incorrect then the migration will be incorrect. Prestack depth migration can provide an error estimate and vector for determining the next appropriate step (smiles and frowns) that will converge on a geologically meaningful velocity model (Charles, Mitchell, Holt, Lin, & Matheson, 2008; Gray & Marfurt, 1995; Gray, Cheadle, & Law, 2000; Gray S. , et al., 2002; Zhu, Lines, & Gray, 1998). Figure 5-3 the resulting velocity model that began with information from Wu et al (1995) at the 1995 SEG workshop and converge upon using manual tomography (Murphy & Gray, 1999; Gray, Cheadle, & Law, 2000).

As shown in Chapter 3, if the velocity model is very well understood, NMO derived reflection statics corrections are unnecessary. However, given the complexities, uncertainties, and obstacles of land seismic data, it is unlikely that enough noise removed, and signal preserved to enable a sufficient convergence on a velocity model with enough detail.
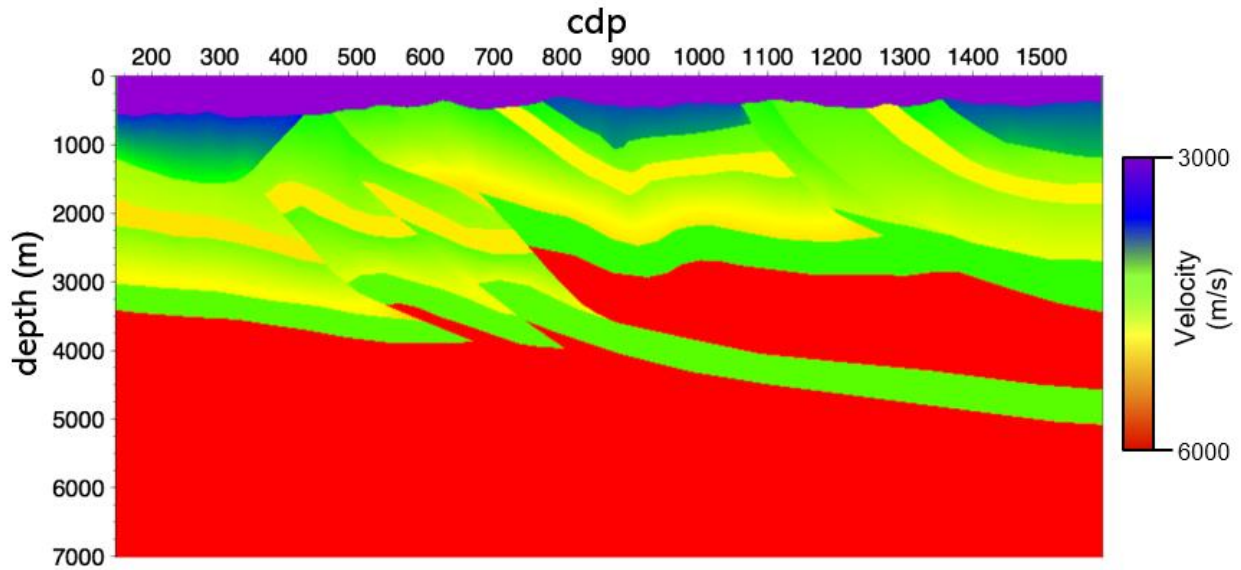
Figure 5-3 Canadian foothills depth velocity model derived from the conventional model building workflow

5.3.1 Prestack depth migration with refraction statics applied.

Two prestack depth migrations were done using the velocity model shown in Figure 5-3. The first was done using conventional methods for static correction derivations from NMO corrected data. Through this method manual tomography and conventional static corrections, the author converged on Figure 5-3. Overall this image seems sufficient, and any limitation in the quality of the imaged reflector can be explained as significant geologic complexity that is not able to be resolved using current methods. The other depth migration was done using MMO derived static corrections (Figure 5-5). Both methods have refraction statics (Figure 4-9) applied which were created from the tomographic near-surface velocity model (Figure 4-8).
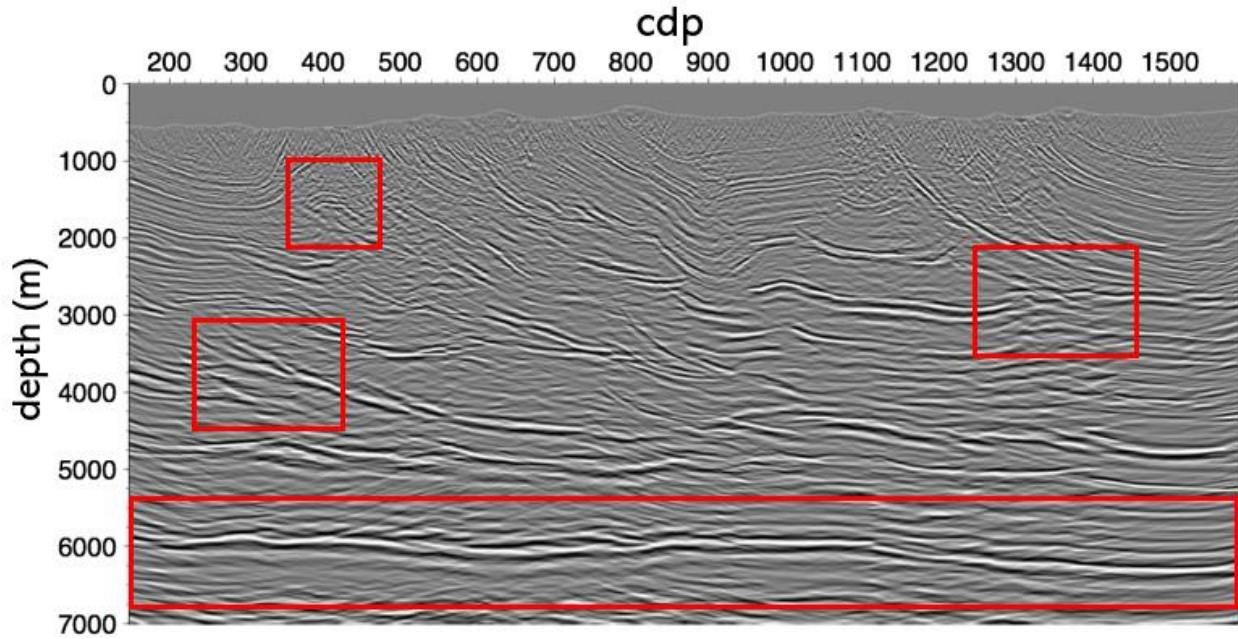
Figure 5-4 Prestack Depth Migration with Conventional statics applied. (Tomographic refraction statics and reflections statics derived from NMO corrected data)
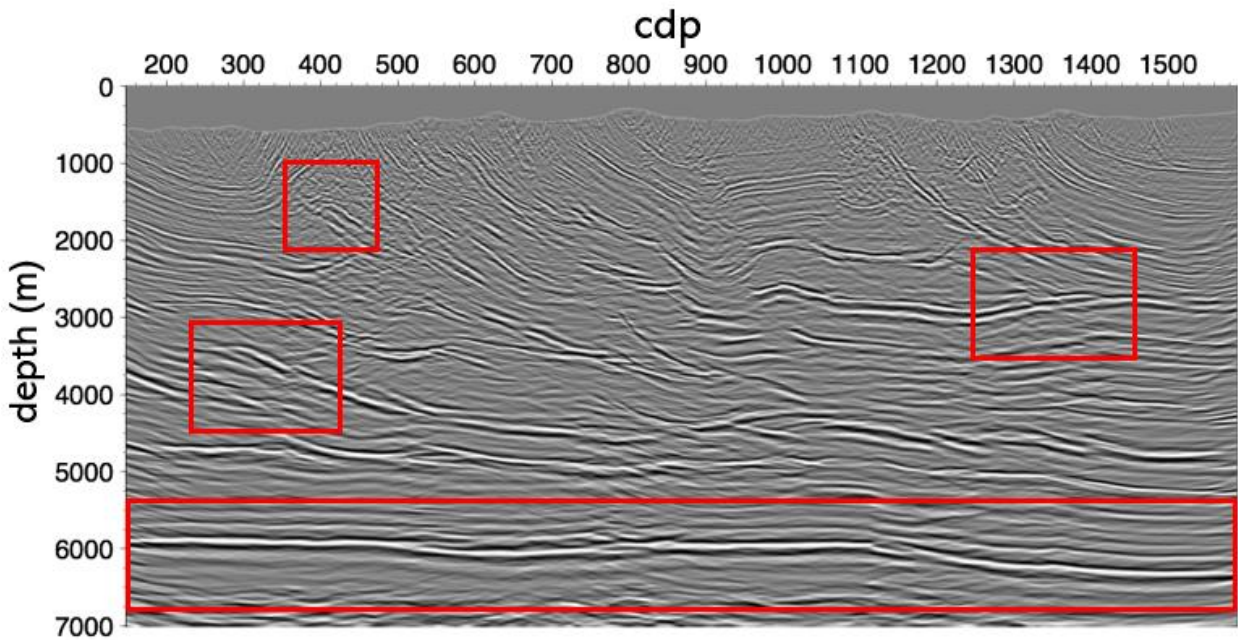
Figure 5-5 Prestack Depth Migration with tomographic refraction statics and reflections statics derived MMO corrected data.

These refraction statics, while they are necessary for time migration, create a migration surface that is, ideally, a smoothed version of the topography. However, lateral velocity variation

in the near-surface makes this difficult. Where the migration surface is above topography shows where the replacement velocity was too fast and where it is below, shows where the replacement velocity is too slow (Figure 5-6). Using this migration surface can be beneficial, but it can also inhibit the ability to understand and converge on the true geologic velocity model of the Earth. Further discussion on the comparison will be done later in this chapter. Some initial observations concerning these results are that MMO derived (Figure 5-5) reflection statics enhance the coherency of the reflectors and shows some defined fault terminations as well as better reflector continuity beneath some zones of lateral velocity variation. The major differences are highlighted in the red rectangles. These red rectangles will be the focus of comparison between each method tested.
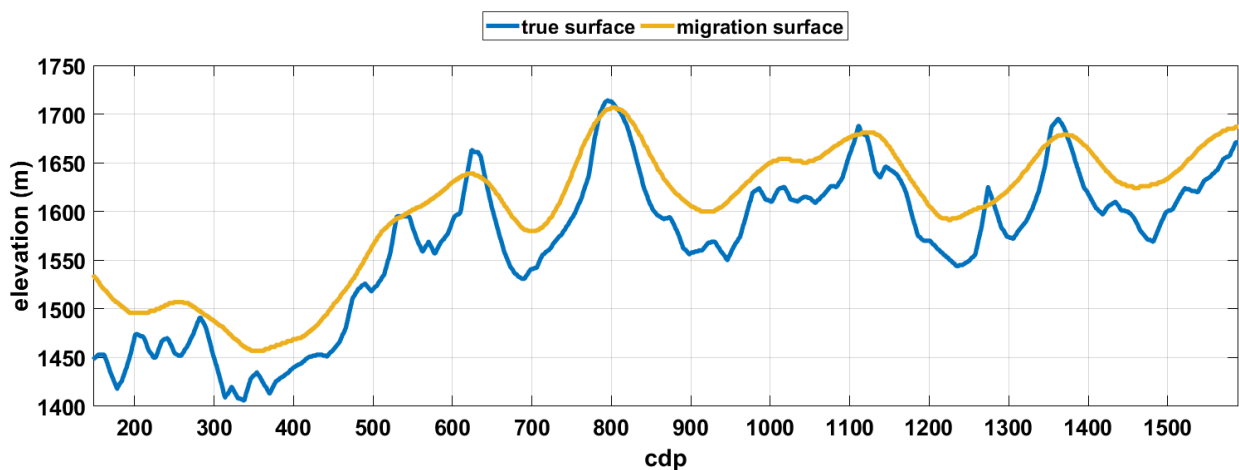
Figure 5-6 The migration surface (yellow) is calculated from the during the refraction statics process and is ideally a smoothed version of the topography (blue). However, this is difficult to achieve as a single replacement velocity is chosen across the entire line. Where the migration surface is above the true surface shows where the replacement velocity was too fast and where it is below, shows where the replacement velocity is too slow.

5.3.2 Prestack depth migration without refraction statics applied.

The refraction statics derived from the tomographic near-surface velocity model are suitable for time migration as an imperfect way of circumventing the issue of lateral velocity variation in the near-surface. However, these static corrections are not coupled to depth imaging. To navigate this issue, Wiggins (1984) introduced a method of migrating from topography. Other authors (Gray & Marfurt, 1995; Lines, Wu, Lu, Burton, & Zhu, 1996) have reinforced this

method as generating superior results for depth imaging, while some (Charles, Mitchell, Holt, Lin, & Matheson, 2008) have been more cautious about its benefits.
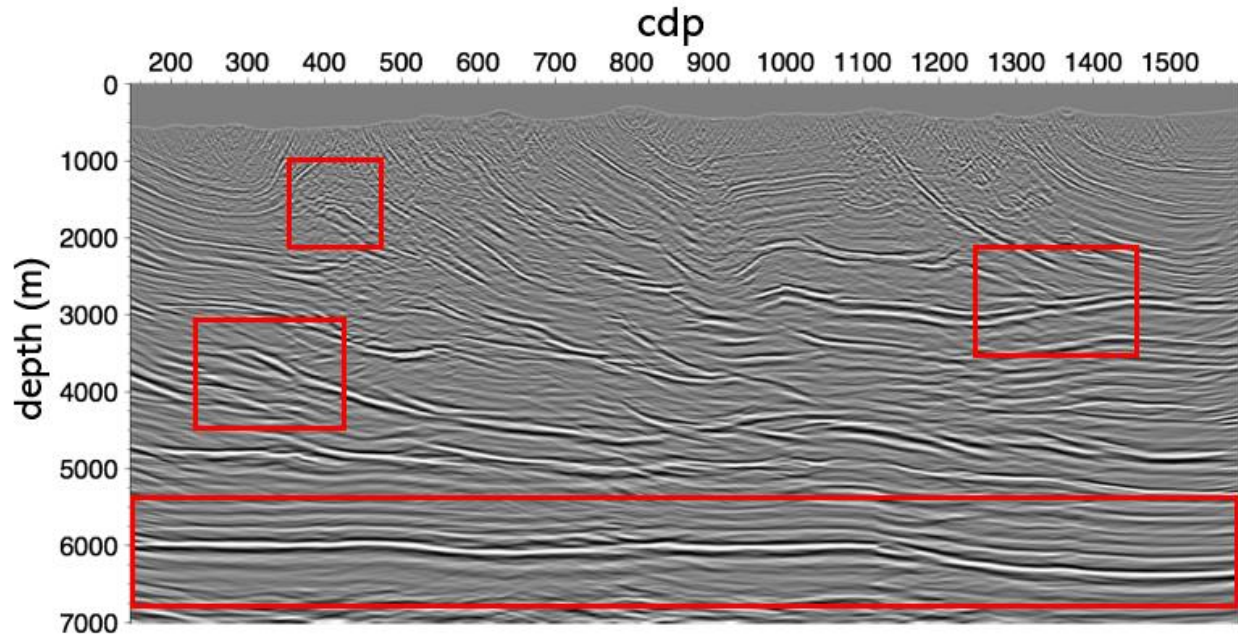
Figure 5-7 Prestack Depth Migration without tomographic refraction statics and with MMO reflections statics. Data is migrated from a smoothed topography

After removing the refraction statics from the input gathers for depth imaging, the topography was smoothed to generate a migration surface that would resemble the topography (Figure 5-8). An 11-point smoother was applied to the topography to generate the migration surface from the smooth surface. This smoothing was applied to remove rapid variation in topography that could be presented in the subsurface data. Minor elevation statics are applied to the source and receivers to move them from the true surface to the migration surface. Figure 5-7 was created using the depth velocity model in Figure 5-3.

Although the depth velocity model being optimized based on the input traces for depth migration that had both refraction statics and NMO derived reflection static corrections, Figure 5-7 still shows that the depth migration was able to generate a comparable image. This depth image with no refraction statics and with MMO derived reflection static corrections only has minor changes compared to the depth image with refraction statics and MMO derived reflections

static corrections (Figure 5-5). The most dominant changes are structural as can be seen in some of the reflectors highlighted in the red rectangles.
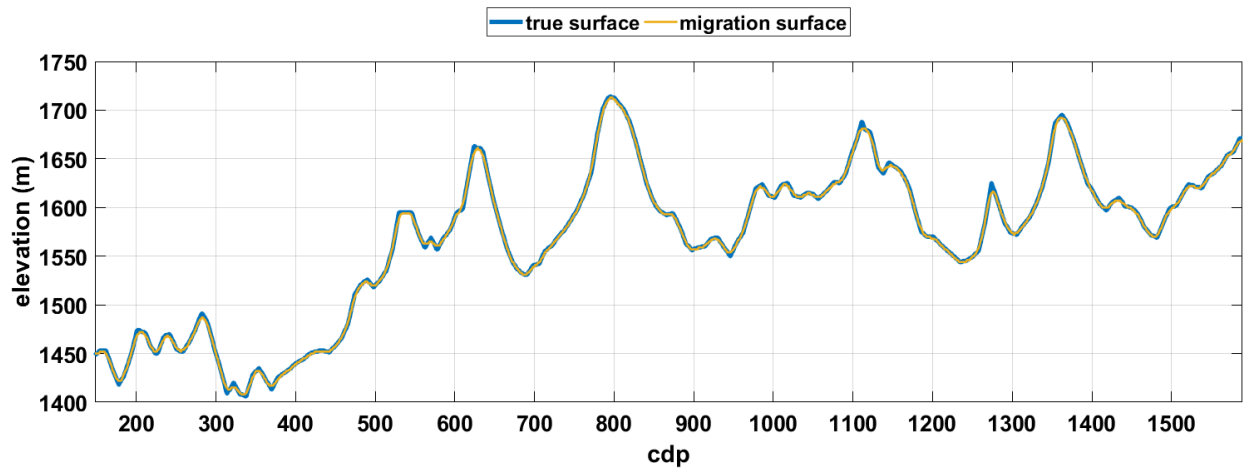
Figure 5-8 The migration surface (yellow) is a smoothed version of the topography (blue). An 11-point smoother was applied to the topography to generate the migration surface from the smooth surface. This smoothing was applied to remove rapid variation in topography that could be presented in the subsurface data.

5.3.3 Prestack depth migration with near-surface tomographic model applied.
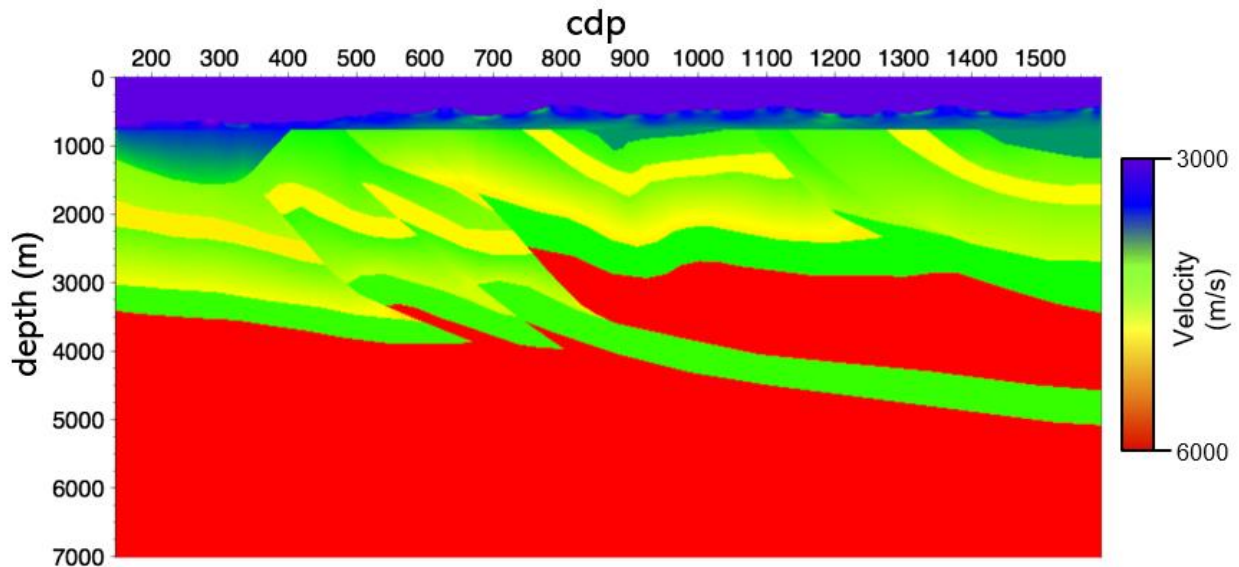
Figure 5-9 Canadian foothills depth velocity model with near-surface tomographic refraction model merged with the depth velocity model.

In regions of complex velocity, the tomographic approach of using diving rays generally produce a near-surface model that is capable of handling lateral velocity variations (Zhu, Cheadle, Petrella, & Gray, 2000). The data derived from the near-surface tomographic modelling can be useful information.
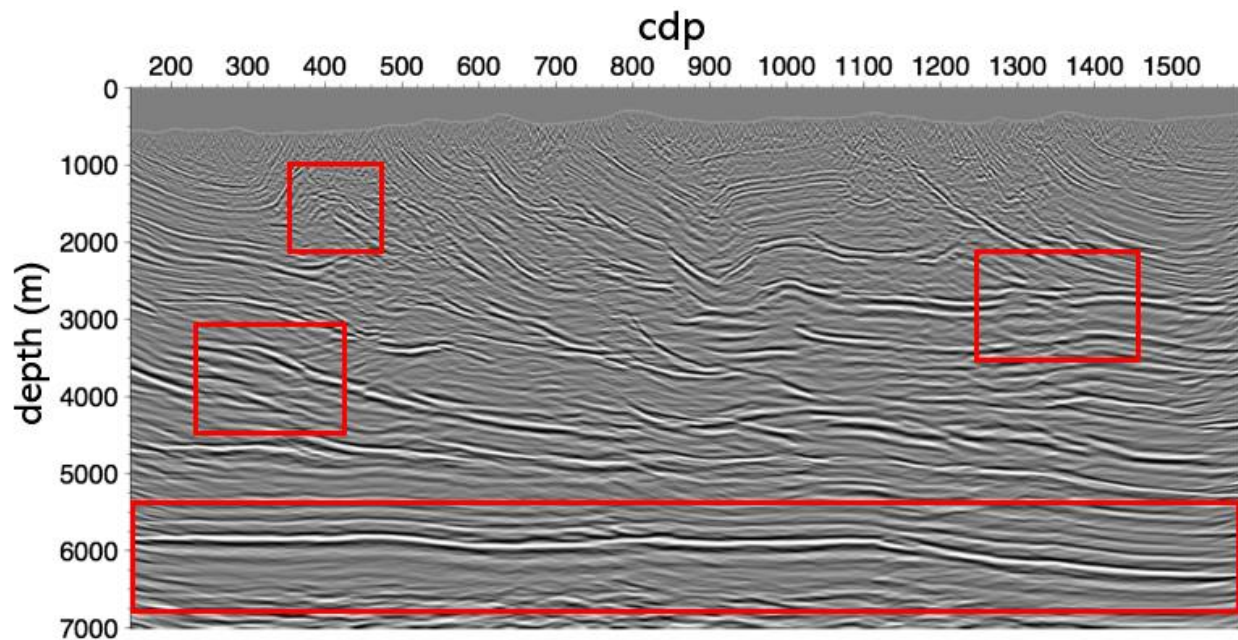
Figure 5-10 Prestack Depth Migration with refraction statics removed and the tomographic near-surface velocity model merged with the depth velocity. This model also has reflections static corrections derived from MMO.

As discussed in the previous section, migration from topography has been shown to generate superior results. However, there is a general agreement with the authors that if the refraction statics are removed for depth imaging, the near-surface velocity model should be inserted into the depth velocity model. To merge the near-surface tomographic model with the depth velocity model, the refraction static corrections derived for time migration must be removed. With the refraction statics removed and the near-surface model merged with the depth velocity model, there is now have a blended depth velocity with no static corrections that are coupled to time migration (Figure 5-9). The top 750 m from the seismic datum of the tomographic near-surface model was chosen as the ray density in the tomographic inversion severely decayed after this depth. By merging the tomographic near-surface with the depth velocity, the migration traveltimes will be different, and MMO needs to be reapplied for the new

model (Figure 5-12). Even though the model may be a low-frequency version of the true near-surface would be, if it is accurate enough it can be helpful (Gray S. , et al., 2002).

5.4 Discussion

5.4.1 Prestack depth migration with refraction statics applied.

Figure 5-4 and Figure 5-5 illustrate the impact of NMO derived reflection static corrections (Figure 5-4) and MMO derived reflection static corrections (Figure 5-5) on data with refraction statics applied. Improvements using the MMO derived statics can be seen primarily in the basement reflector where there is an increase in coherency and sharpness between Figure 5-4 and Figure 5-5. Other improvements can be seen in the fault imaging at CDP 900 and depth of 3500 m, reflectors near CDP 250 and 2000 m depth, and the continuity of the reflectors at CDP 1300 and 2800 m depth.

Figure 5-6 shows that the migration surface can be as high as 75 m above the true surface and as low 25 m below it. This means that the raypath for traveltime calculations and depth imaging are not starting at the surface, and the velocity model that optimizes the image with these corrections diverges from geologic velocities. Even though the migration surface deviates from the true surface, the NMO and MMO derived static corrections are both able to determine a reasonable shift for the sources and receivers to enhance the image.

5.4.2 Prestack depth migration without refraction statics applied.

Figure 5-7 is a stack that was migrated from topography with no refraction statics or reflection statics applied and with MMO derived reflections statics applied. This MMO was created from the traveltimes that were calculated from the migration surface in Figure 5-8 and the velocity model in Figure 5-3.

What is interesting about this is the methodology in which the velocity model was created. The velocity model was converged upon using input traces for depth migration that had conventional static corrections applied. A plausible explanation is that even though the conventional statics may not be able to optimize an image, they do not impede the determination of large velocity structures in the subsurface. Figure 5-7 has the MMO derived reflection static

corrections applied and demonstrates the value of these static shifts. The image overall has better reflector continuity and sharpness. The areas with the largest benefit can be seen where there are large velocity contrasts, primarily near CDP 600 and the basement reflector at 6000 m depth. Another location is near CDP 1200 and the same basement reflector at 6000 m depth. While the improvements in the basement reflector are the most noticeable, the reflectors above it in the same CDP locations previously mentioned show improvement as well.

5.4.3   Prestack depth migration with near-surface tomographic model applied.

Figure 5-10 is a stack that was migrated from topography with the tomographic near-surface velocity model applied and with MMO derived reflections statics applied. This MMO was created from the traveltimes that were calculated from the migration surface in Figure 5-8 and the velocity model in Figure 5-9.

By replacing the near-surface tomographic model for refraction static corrections and the deriving reflections static corrections with MMO corrected gathers instead NMO corrected, the assumptions couple to time migration have been removed from depth imaging. An improvement that can be seen from this update are at CDP 900 and a depth of 2500 m where the syncline is now more convincingly connected from the image with MMO and especially the image with time statics. Another improvement is the fault plane reflector at CDP 650 and 1500 m depth. The coherency of this structure is visible, but it was difficult to image. Some post-migration processing methods could enhance this structures clarity but depth imaging itself using time static corrections was limited.

The method of applying the near-surface tomographic model causes a sharp contrast where the two models merge (Figure 5-9). Initially, there were sharp velocity inversions and increases, but the inversions were removed to restore image quality underneath the inversions at the edge of the seismic line. The sharp velocity increases are still present from the tomographic merge. However, initial results are convincing with the improvements in the section around 2 km depth and above. As this is still a working model, improving the velocity model merged with the near-surface tomographic model will take further consideration.

Another consideration is that this velocity model was built using refractions statics and NMO derived reflections statics and would need to be updated to reflect the new near-surface correction methods employed using this model.

5.4.4 Static correction comparison
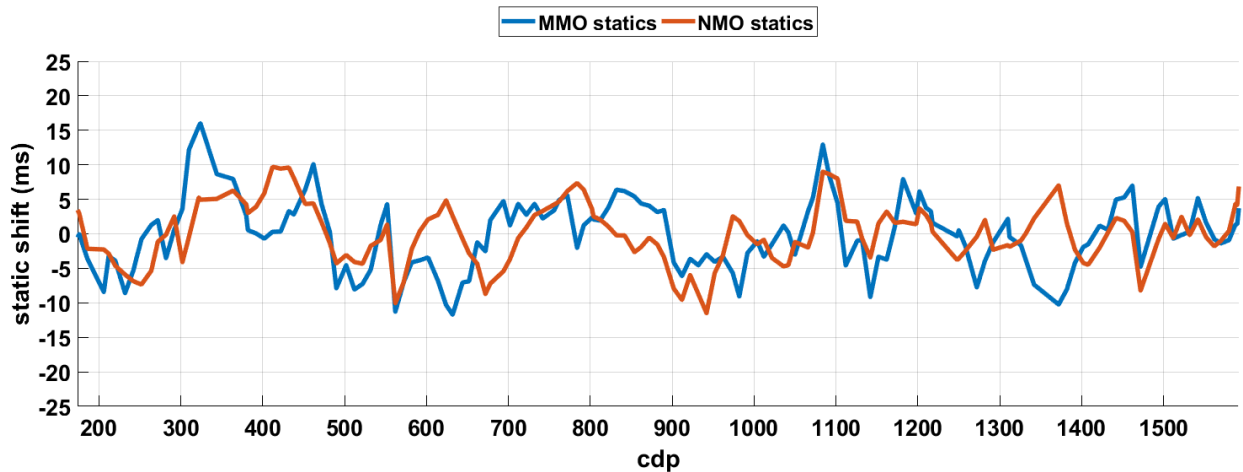
Figure 5-11 Husky Structural Dataset reflection static corrections derived from MMO (blue) and NMO (red). The largest differences between these corrections are in zones where there are strong lateral velocity variations. E.g. near CDP 425 and CDP 1375.
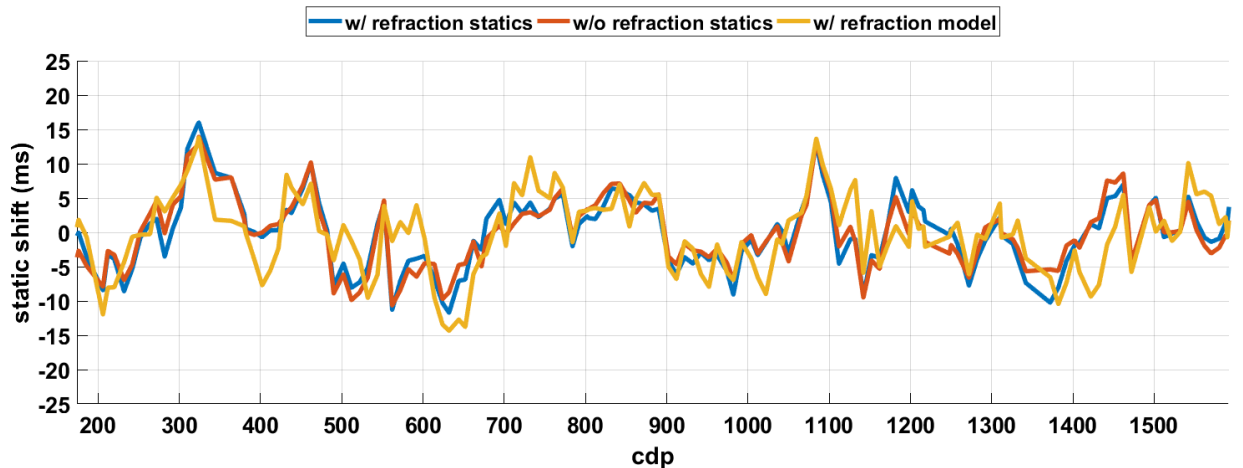
Figure 5-12 Husky Structural Dataset reflection static corrections with MMO derived reflection source static corrections. The different applications of the refraction solution are: statics derived from the tomographic near-surface velocity model and migrating from the surface shown in Figure 5-6 (blue); no statics or model and migrated from the smoothed topography surface shown in Figure 5-8 (red); and the near-surface model merged with the depth velocity model and migrated from the smooth topography.

Figure 5-11 illustrates the differences in the static corrections necessary with each NMO and MMO derived solutions. The areas with the largest differences between these static corrections are in zones where there are strong lateral velocity variations in the velocity model at the near surface. Consequently, there are also the areas that have the some of the largest improvement in the depth image. By using reflection static corrections derived from MMO calculated from the current depth velocity model, the assumptions of the NMO velocities that are irrespective to the model or the kinematics of depth imaging are no longer imbedded in the statics solution.

Figure 5-12 shows the MMO derived reflection static corrections from the three tests of near-surface solutions. The three test were: using the refraction statics derived from the tomographic near-surface velocity model and migrating from the surface shown in Figure 5-6; using no statics or near-surface model and migrated from the smoothed topography surface shown in Figure 5-8; and using the tomographic near-surface model merged with the depth velocity model and migrated from the smoothed topography surface.

It is interesting to note that the MMO statics calculated using refraction statics and the associated migration surface and no refraction statics and the smooth topography determine remarkably similar corrections. However, the corresponding stacks (Figure 5-4 and Figure 5-5 respectively) do show subtle structure changes and a slight bulk shift in the depth of the reflectors. The MMO statics that were generated with the near-surface velocity merged with the depth velocity model are the more unique from the other two. Yet, they still follow a similar trend. For all three MMO static solutions, the greatest static shifts are near CDPs 320 and 1080. There may be a few plausible explanations for these magnitudes. Two of them, as seen from the modelling examples, may be that this may be an area were either the location of the velocity contrast is poorly determined or has a high relative change in velocity that will be difficult to resolve with the traveltime and migration techniques applied.

5.5 Conclusion

The Husky Structural Dataset is a good quality foothills dataset from the Canadian foothills. The assumption that the moveout is near hyperbolic enough in shape to be represented

by the two-term NMO equation for reflection static corrections is inappropriate for foothills data and when there are variations in the seismic weathering thickness and velocities. Applying a model-based moveout for reflection static corrections is coupled with the depth migration algorithm and provides better static solutions for depth imaging the Husky Structural Dataset.

Removing the refraction static corrections and merging the near-surface tomographic model with the depth velocity model also enhanced the coherency of the depth image. The assumption that near-surface layer has a much lower-velocity than the next layer is not suitable for the geologic complexity of foothills seismic data. Through replacing static corrections derived for time migration with MMO reflection static corrections and merging the near-surface tomographic model with the depth velocity model the depth image is improved.

However, the velocity model is coupled to the data that refraction statics and NMO reflection statics applied. The new depth velocity should be updated to reflect the new refraction model being merged with it and then calculate new reflection statics derived from MMO to couple the static corrections to depth imaging.

Chapter 6: Conclusions

6.1 Normal Moveout Theory Error

The assumption that the moveout is sufficiently hyperbolic in shape to be corrected by NMO is invalid when strong lateral heterogeneity of velocity is present. Based on velocity testing, a strong lateral variation in velocity is approximately a relative lateral change in velocity of 25%, and an offset of 5 km can cause anomalous events to be created due to NMO assumptions. Velocity contrasts less than 25% will have associated static corrections to compensate but not create events that are not truly present in the subsurface.

Offset distance could also bring out false subsurface events in very strong lateral velocity variations. Using a model that had 66% relative in velocity laterally offsets of 1.5 km or larger could generate events that are not representative of the true subsurface. It was seen during velocity testing that an offset of 5 km did not have a negative impact on the stack when the relative velocity change was 20%.

Using static corrections to quantify NMO theory error show that there is a very strong correlation between offset and NMO theory error as well relative change in lateral variation in velocity and NMO theory error. The linear regression indicates that a 10% increase in relative velocity contrast or 1 km increase in offset will add approximately 3 ms static shift due to NMO theory error. Static corrections will still be present due to NMO theory error in areas with weak lateral variations in velocity (25% or less), but false reflections will not be created.

6.2 Synthetic Data Testing

MMO statics provide a better image as a part of the depth processing workflow than using the reflection NMO statics from time processing. There is increased reflector coherency which allows for more confident interpretations of foothills datasets. The wedge thrust model shows little benefit from using MMO statics compared to no statics, but it does show decreased reflector coherency when the NMO statics are applied to the depth input gathers.

Reflection statics are more closely tied to the time processing workflow and are helpful through to time migration. Weathering corrections in time processing effectively prepares data for NMO reflection statics, so the moveout velocity in near-hyperbolic and can be approximated by the stacking NMO velocity. MMO, on the other hand, provides accurate traveltimes for a moveout velocity field that is coupled to depth imaging.

The assumption that the moveout is near hyperbolic enough in shape to be represented by the two-term NMO equation breaks down when the topography is not flat, strong lateral heterogeneity of velocity is present, and when there are variations in the seismic weathering thickness and velocities. It is important to note that the NMO velocity field did increase reflector continuity for the time pre-migration stack. Be that as it may, it did not improve for depth imaging and was more damaging when applied.

Depth migration has a unique algorithm from time migration and can accommodate for lateral velocity variation. Initially with depth imaging, the only difference is the migration algorithms. However, it seems that even the conditioning of the data prior to migration could be an important step as well. The MMO statics appear to be an important step in optimize the depth image as they are couple to depth migration and the MMO can handle strong lateral velocity variations.

6.3 Canadian Foothills Field Dataset

This seismic data was structurally complex, had strong lateral velocity contrasts and has good signal to noise content. The data pre-conditoning for amplitude scaling, noise attenuation, deconvolution, an spectral-whitening helped to ensure good signal-to-noise content and optimize the stacked image.

The assumption that the moveout is near hyperbolic enough in shape to be represented by the two-term NMO equation for reflection static corrections is inappropriate for foothills data and when there are variations in the seismic weathering thickness and velocities. Applying a model-based moveout for reflection static corrections is coupled with the depth migration algorithm and provides better static solutions for depth imaging the Husky Structural Dataset.

Removing the refraction static corrections and merging the near-surface tomographic model with the depth velocity model also enhanced the coherency of the depth image. The assumption that near-surface layer has a much lower-velocity than the next layer is not suitable for the geologic complexity of foothills seismic data. Through replacing static corrections derived for time migration with MMO reflection static corrections and merging the near-surface tomographic model with the depth velocity model the depth image is improved.

However, the velocity model is coupled to the data that refraction statics and NMO reflection statics applied. The new depth velocity should be updated to reflect the new refraction model being merged with it and then calculate new reflection statics derived from MMO to couple the static corrections to depth imaging.

6.4 Future Work

Future work to be done with MMO and statics coupled to depth imaging would incorporate iterative tomographic velocity analysis rather than manual tomography. This could allow for velocity convergence with greater accuracy in areas with strong lateral velocity variation or other areas where depth coupled statics would allow greater uplift to imaging.

Other areas to investigate would be applications to other migration types. Kirchhoff is a robust and well-studied method for migration, but others are becoming more prominent such as reverse time migration, wave equation migration, and full waveform inversion on land datasets.

References

AxWave. (2014). *AxWave Seismic Modelling User Interface Document.* Acceleware AxWave (6.5.0).

Charles, S., Mitchell, D. W., Holt, R. A., Lin, J., & Matheson, J. (2008). Data-driven tomographic velocity analysis in tilted transversely isotropic media: A 3D case history from the Canadian Foothills. *Geophysics, 73*(5), VE261-VE268.

Cox, M. (1999). *Static Corrections for Seismic Reflection Surveys.* Tulsa, OK: SEG.

Dix, C. H. (1955). Seismic velocities from surface measurements. *Geophysics, 20*(1), 68-86.

Engquist, B., & Majda, A. (1977). Absorbing boundary conditions for numerical simulation of waves. *Mathematics of Computation, 31*(139), 629-651.

Etgen, J. T., & Kumar, C. (2012). What is the difference between Time and Depth Migration? A tutorial. *Society of Exploration Geophysicists, Annual General Meeting, Technical Abstract.* SEG.

Fomel, S., & Kazinnik, R. (2013). Non-hyperbolic comon reflection surface. *Geophysical Prospecting, 61*, 21-27.

Gray, S. H., Cheadle, S., & Law, B. (2000). Depth model building by interactive manual tomography. *Society of Exploration Geophysicists, Annual General Meeting, Technical Abstracts*, (pp. 914-917).

Gray, S., & Marfurt, K. (1995). Migration from topography: Improving the near-surface image. *Canadian Journal of Exploration Geophysics, 31*, 18-24.

Gray, S., Cheadle, S., Vestrum, R., Gittins, J., Zhu, T., & Nanan, H. (2002). Using Advanced Seismic Imaging Tools to See the Invisible Beneath Foothills Structures. *CSEG Recorder, 27*(3).

Green, C. H. (1938). Velocity determinations by means of reflection profiles. *Geophysics, 3*(4), 295-305.

Knopoff, L., & Gangi, A. F. (1959). Seismic Reciprocity. *Geophysics, 24*(4), 681-691.

Koren, Z., & Ravve, I. (2018). Slowness domain offset and travelltime approximations in layed vertical transversely isotropic media. *66*, 1070-1096.

Landa, E., Thore, E., & Reshef, M. (1993). Model-based stack: a method for constructing an accurate zero-offset section for complex overburdens. *Geophysical Prospecting, 41*(6), 661-670.

Larner, K., & Tjan, T. (1995). Simultaneous estimation of statics and velocity for data from structurally-complex areas. *Society of Exploration Geophysicists, Annual General Meeting, Technical Abstract* (pp. 1401-1404). SEG.

Lines, L., Wu, W.-J., Lu, H.-X., Burton, A., & Zhu, J. (1996). Migration from topography: Experience with an Alberta Foothills data set. *Canadian Journal of Exploration Geophysics, 32*, 24-30.

Marsden, D. (1993). Static corrections—a review, Part III. *The Leading Edge, 12*(3), 210-216.

Murphy, G., & Gray, S. (1999). Manual seismic reflection tomography. *Geophysics, 64*(5), 1546-1552.

Newrick, R. T. (2004). *Vεδθ Models for Pre-Stack Depth Migration.* PhD Thesis, University of Calgary.

O'Brien, M. (1994). *1994 BP Statics Benchmark Model.* (Amoco Tulsa Research Lab, Tulsa, OK) Retrieved from SEG Wiki: https://wiki.seg.org/wiki/1994_BP_statics_benchmark_model

Schmid, R. (1995). Use of Model Based NMO with Prestack Depth Migration - Foothills Example (Benjamin). *Workshop #6, Society of Exploration Geophysicists, Annual General Meeting.* Houston.

SeisSpace-ProMAX. (2015). *SeisSpace-ProMAX reference guide.* Halliburton-Landmark (5000.8.5.1).

Sheriff, R. E. (2002). *Encyclopedic Dictionary of Applied Geophysics* (4th ed.). Tulsa, OK: SEG.

Sherwood, J. W., Adams, H., Blum, C., Judson, D. R., Lin, J., & Meadours, B. (1976). Developments in filtering seismic data. *Society of Exploration Geophysicists, Annual General Meeting.* Houston.

Sherwood, J. W., Chen, K. C., & Wood, M. (1986). Depths and Interval Velocities from Seismic Reflection Data for Low Relief Structures. *Society of Exploration Geophysicists, Annual General Meeting, Technical Abstract* (pp. 553-557). SEG.

Stork, C., Welsh, C., & Skuce, A. (1995). Proceedings in Workshop #6: Demonstration of processing and model building methods on a real complex structure data set. *Workshop #6, Society of Exploration Geophysicists, Annual General Meeting.* Houston.

Taner, M. T., & Koehler, F. (1969). Velocity spectra-digital computer derivation and applications of velocity functions. *Geophysics, 34*(6), 859-881.

Taner, M. T., & Koehler, F. (1981). Surface Consistent Corrections. *Geophysics, 46*(1), 17-22.

Taner, M. T., Koehler, F., & Alhilali, K. A. (1974). Estimation and correction of near surface time anomalies. *Geophysics, 39*(4), 441-463.

Tjan, T., Larner, K., & Audebert, F. (1994). Prestack migration for residual statics estimation in complex media. *Society of Exploration Geophysicists, Annual General Meeting, Technical Abstract* (pp. 1513-1516). SEG.

Vestrum, R., Lawton, D., & Schmid, R. (1999). Imaging structures below dipping TI media. *Geophysics, 64*(4), 1239-1246.

Widess, M. B. (1952). Salt solution, a seismic velocity problem in western Anadarko Basin, Kansas-Oklahoma-Texas. *Geophysics, 17*(3), 481-504.

Wiggins, J. W. (1984). Kirchhoff intergral extrapolation and migration of nonplanar data:. *Geophysics, 49*(8), 1239-1248.

Wu, W.-J., Lines, L., Burton, A., Lu, E.-X., Jamison, W., Zhu, J., & Bording, R. P. (1995). Prestack Depth Migration of an Alberta Foothills Data Set - The Husky Experience. *Workshop #6, Society of Exploration Geophysicists, Annual General Meeting.* Houston.

Yilmaz, O. (2001). *Seismic data analysis: processing, inversion and interpretation of seismic data* (2nd ed.). Tulsa, OK: Society of Exploration Geophysicists.

Zhu, J., Lines, L., & Gray, S. (1998). Smiles and frowns in migration/velocity analysis. *Geophysics, 63*(4), 1200-1209.

Zhu, T., Cheadle, S., Petrella, A., & Gray, S. (2000). First-arrival tomography: Method and application. *Society of Exploration Geophysicists, Annual General Meeting Technical Abstract*, (pp. 2028-2031).